Canadian Nuclear Laboratories | Laboratoires Nucléaires Canadiens

Supplier Document

Groundwater Modelling at the Site of the Decommissioned Rolphton Nuclear Power Demonstration (NPD) Reactor

64-508760-REPT-012

Revision 1.0

Accepted by:	Kathryn Shorter	2024/02/28
	Manager, NPD Regulatory Approv	Date

ARCADIS

With Support From:

Quintessa **And,**

GEOFIRMA ENGINEERING

Canadian Nuclear Laboratories

2023 Groundwater Modelling at the Site of the Proposed Decommissioned Rolphton Nuclear Power Demonstration (NPD) Reactor

June 2023

2023 UPDATE TO GROUNDWATER MODELLING AT THE SITE OF THE PROPOSED DECOMMISSIONED ROLPHTON NUCLEAR POWER DEMONSTRATION (NPD) REACTOR

CNL Acceptance:

Katie Shorter
Manager, NPD Regulatory Approvals, CNL

Arcadis Project Director; Approver:

Nava Garisto, Ph.D
Vice President, Radioactive Waste Management & Decommissioning, Arcadis

Author:

Nicola Calder, M.Sc., P.Eng.
Senior Numeric Modeller; Geofirma Engineering Ltd.

Technical Reviewers:

Nicholas Sgro, M.A.Sc., P.Eng.
Numeric Modeller; Geofirma Engineering Ltd.

Frank Garisto, Ph.D
Senior Scientist, Arcadis

Prepared for:
Canadian Nuclear Laboratories Ltd.
Chalk River Laboratories
286 Plant Road, Building 457
Chalk River, ON
K0J 1J0

Prepared by:
Arcadis Canada Inc.
121 Granton Drive, Suite 12
Richmond Hill, ON L4B 3N4
Tel 905.764.9380

Our Ref.:
351240

Date:
June 2023

CONTENTS

TABLES

FIGURES

1 INTRODUCTION

Safety Assessment (SA) of the proposed decommissioning of the Nuclear Power Demonstration (NPD) reactor site in Rolphton, in the town of Laurentian Hills, Ontario, requires estimates of volumetric flow and velocity of the groundwater that would come into contact with the proposed decommissioned reactor building and surrounding engineered facilities (referred to herein as NPD facility). Site data indicate that the average water table position is just above the top of the bedrock, with overlying sands and gravels being largely unsaturated. Natural groundwater flow will be over the surface of the bedrock. Flow directions are expected to reflect topography, with recharge upgradient of the NPD facility and discharge to the river. However, the NPD facility, including tile drains and construction backfill, are expected to collect and control groundwater flow. These features are of sufficient geometric complexity to require numeric assessment.

A steady-state groundwater flow model of the site was initially developed and reported in Calder (2016), and has since undergone several updates to reflect additional data and improve the model calibration. Companion models have also been developed, a resaturation model developed in 2017 and a near-field transport model in 2019. The initial 2016 groundwater flow model provided a good estimation of measured water elevations, but it was unable to reproduce the high flows observed in the tile drains. The difficulty in modelling tile drain flow rates is that the amount of water required to obtain such high flow rates in the tile drains requires a catchment area much larger than suggested by recharge estimates and the catchment area defined by topography and the expected bedrock surface. In the spring of 2017, a resaturation model was completed that describes the water saturation of the grout filling the NPD facility post-decommissioning (Calder 2017a). The resaturation model considers only a small section of the groundwater flow model, obtaining boundary conditions from the groundwater flow model. In the fall of 2017, an update of the groundwater flow model (Calder 2017b) was conducted to (a) include additional data that had become available since the first groundwater flow model (and was included in the 2017 resaturation model), and (b) attempt to reproduce tile drain flow rates. The groundwater flow model update was still unable to reproduce tile drain flow rates. A third update to the model was conducted in 2018 (Calder 2018) to address external comments to the groundwater flow modelling. This groundwater model, while not calibrated to the tile drain flows, was able to illustrate the discrepancy between water flowing into the groundwater system and water flowing through the tile drains.

Subsequent to the 2018 groundwater model, detailed site characterization was conducted at the NPD site. The data from this site characterization was synthesized in a geosynthesis report (Raven *et al*. 2021). The geosynthesis report provides a detailed description of the geological and hydrogeological framework of the site, including conceptualization of the groundwater flow systems. The steady-state groundwater model and resaturation model were both updated in 2019 to reflect the new data obtained during site characterization. In particular, this groundwater flow model was able to obtain a satisfactory calibration by extending the model domain to the west and including permeable overburden features parallel to the river consistent with the geology at the site and some of the features observed in site characterization boreholes. A near-field groundwater flow and transport model was also developed in 2019, to provide detailed flow and transport information within and in the vicinity of the NPD facility. The near-field model considers only a small section of the groundwater flow model, obtaining boundary conditions from the groundwater flow model.

In 2021 through 2023, the groundwater model, resaturation model, and near-field model were updated and are documented in this report and two companion reports. This update to the detailed groundwater flow models considers the following:

- Inclusion of a deep section of tile drain 2, identified under the pressure-relief pit and connecting to the tile drain 2 discharge pipe to the north-east of the building, downstream of manhole 3. This information was missing from previous groundwater flow models.
- Updates to the concrete cap and engineered cover design.
- Updates to the measured tile drain flow data.
- After the model is calibrated, the models are modified to include grouted pipes in the pipe trench between the facility and the river.

The three detailed models are each described in separate reports, for a total of three reports. The present report is the primary report, detailing the connections between data detailed in the geosynthesis, and measured data specific to the groundwater flow regime and the groundwater flow models, as well as reporting the model approach and results of the groundwater flow model. The reports for the resaturation model and near-field model are companion reports to this report; background and common information is not repeated, and each companion report focuses on the approach and results of the subject model.

The groundwater flow model report is organized as follows:

- Section 2 summarizes background data for the Rolphton NPD site, including descriptions of the hydrogeologic setting, water elevation and hydraulic conductivity measurements, and measured tile drain flows.
- Section 3 describes the calibrated model, integrating the data described in Section 2 into the numeric model, and includes the modelling and calibration approach and a summary of model calibration results.
- Section 4 provides model results and groundwater flows for scenario cases, including the Normal Evolution Scenario (NES) cases, and includes particle tracks for the NES current conditions case.
- Section 5 provides sensitivity cases that investigate calibrated model uncertainties.
- Section 6 summarizes and concludes the report.

2 BACKGROUND

2.1 NPD Setting

The NPD is located between Ontario Highway 17 and the Ottawa River, approximately 100 m south-west of the river, and approximately 3 km east of the Des-Joachims hydroelectric station. The NPD was constructed between 1956 and 1961, and was operational from 1962 to 1987 (MacLarentech 1990, Killey and Munch 1988).

Prior to building excavation, ground surface elevation ranged from 132.6 m (435 ft) at the south-west corner of the building to 123.4 m (405 ft) along the northern edge of the building (drawing NA25-f-2201 1958). Bedrock elevation is 123.3 m (404.6 ft) in the south-western corner of the building, and 123.1 m (404 ft) along the northern edge of the building. Groundwater elevations prior to building excavation were reported at 128.6 m (422 ft) (Hydro Electric Power Commission of Ontario, 1961), and given ground surface elevations, this value must be representative of the upgradient side of the building. The ground surface slopes sharply down north of the building towards the river, with river elevations at approximately 111 m. Numerous springs were observed on the slope towards the river (Hydro Electric Power Commission of Ontario, 1961, Canadian General Electric Company Ltd. 1962), prior to building excavation. These springs are no longer observed at the site, likely due to the tile drains (described below) lowering the water table in the vicinity of the facility.

The geologic and hydrogeologic setting at the NPD site is described in detail in Raven *et al*. (2021). The bedrock at the NPD site is described as migmatitic biotite gneiss. The major structural geologic feature at the site is the Mattawa Fault, which defines the course of the Ottawa River. Groundwater, both shallow and deep, discharges into this fault and the river. While historical documents (Canadian General Electric Company Ltd. 1962) suggest the presence of a shear zone near the building, the presence of a shear zone is not corroborated by any other evidence, including recent bedrock boreholes at the site and photographs of the NPD bedrock excavation (Raven *et al*. 2021). While this shear zone was considered in a sensitivity case of a previous version of the groundwater model, the current version of the model bases the bedrock conceptualization on the latest evidence and data describing the bedrock which does not support the presence of a shear zone as described historically.

Overburden at the site consists of fluvial sands and gravels, a silt to cobble glacial till unit, and a boulder glacial till unit (Raven *et al*. 2021). Surficial geology from Ontario Geologic Survey (2010) is shown in Figure 2-1. The till units extend below the fluvial sand and gravels, but does not exist throughout the site, as Killey (2014) notes that fluvial sands and gravel lie directly over bedrock in some areas. Near the river, the till is more permeable than upgradient of the site (Raven *et al*. 2021). MacLarentech (1990) identifies mainly till in the overburden of several wells near the shoreline, however, these are identified as native glacial till used as fill. Fill is present surrounding the facility, and other areas subject to excavation for construction. For the most part, the fill is similar to the sand overburden at the site, but with a more consistent size of gravel and boulders and the presence of debris.

Figure 2-1 Surficial Sediments (surficial geology data from Ontario Geological Survey 2010)

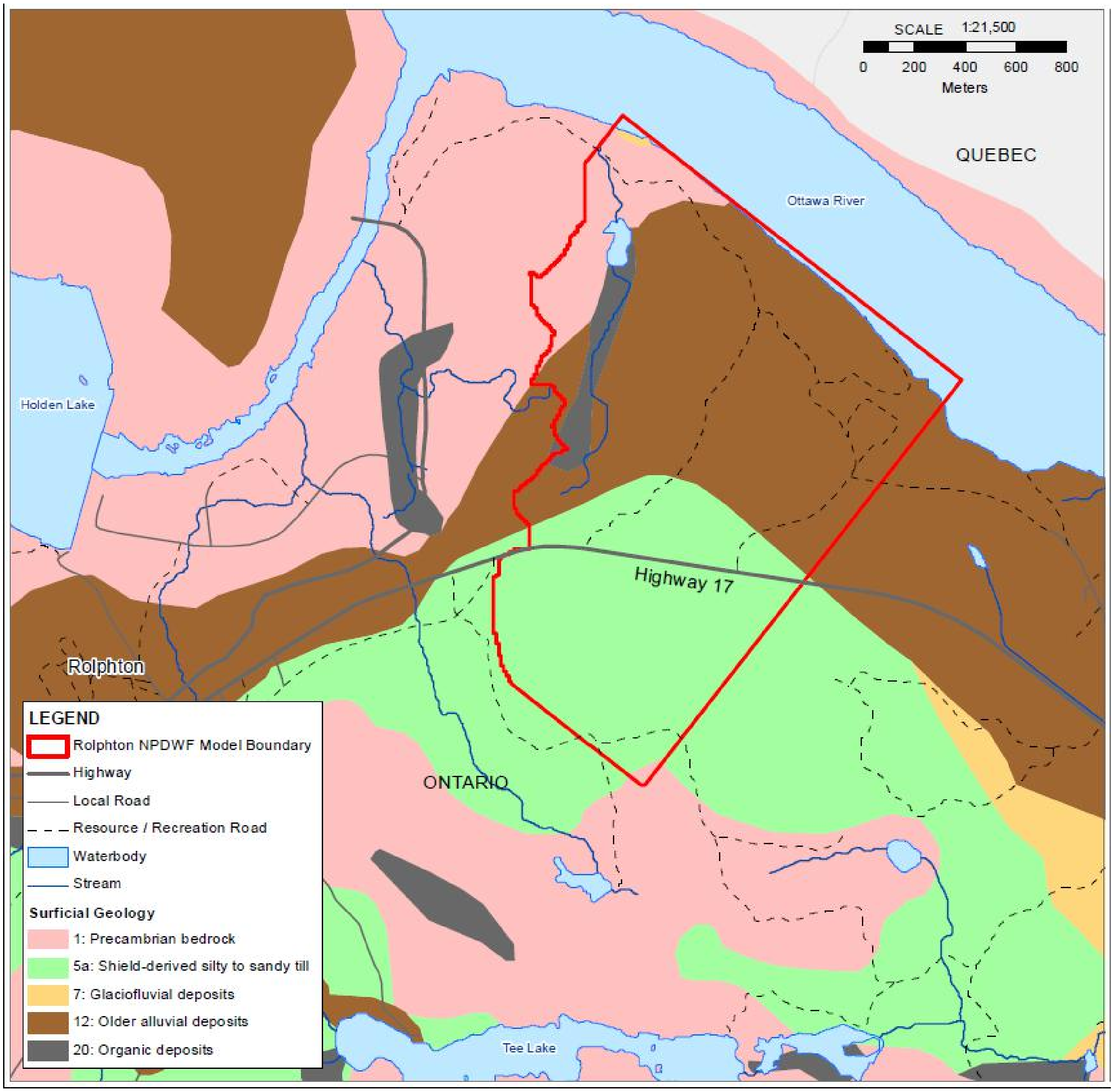

Note: Surficial geology descriptions are obtained from Ontario Geologic Survey (2010). Gadd (1963) provides the following descriptions for the same units:

5a: glacial till: chiefly non-calcareous sandy grey till comprising material from silt to boulder size in a heterogeneous mixture; includes thick deposits of lag gravel or rubble

7: sand: uniform fine-grained grey to yellow-buff sand; mainly deltaic, includes dunes; some gravel, and minor banded silt deposits

12: fluvial gravel: medium to coarse gravel in abandoned river terraces; includes some sand and minor banded silt deposit

20: bog deposits: mainly peat, some muck

Raven *et al*. (2021) also provides a detailed description of the conceptual model of groundwater flow at the site. In summary, local groundwater flow systems will be the dominant groundwater flow system at the NPD site, with recharge occurring near Highway 17 and discharge to the Ottawa River. The majority of flow occurs within permeable sandy deposits, with some flow occurring in underlying shallow bedrock. Intermediate groundwater flow systems likely exist between the topographic highs south of Highway 17 near Tee Lake and discharge to the Mattawa Fault and the Ottawa River.

The NPD facility was excavated into the bedrock. Man-made terraces were formed around the building, significantly altering the local landscape. During construction of the building, the water table dropped due to dewatering to 123.4 m (405 ft) along the south and west edges of the excavation (Hydro Electric Power Commission of Ontario, 1961). This water table elevation is near the bedrock surface, slightly above bedrock surface on the north-west edge of the excavation. During construction, flows into the excavation were initially approximately 99 L/s (3.5 cfs), and dropped to 14 L/s (0.5 cfs) once the adjacent swamp areas had dried up (Hydro Electric Power Commission of Ontario, 1961). The swamp areas are noted by Killey and Munch (1988) to be previously located west of the site. A 1955 drawing shows that the sandpit that became landfill 1 was occupied by a pond 1-1.5 m deep (Killey and Munch 1988), and this is another potential source of water that was drained during construction.

Current ground surface elevation at the facility is approximately 128 m, and the elevation at the bottom of the facility is approximately 104 m. (NPD Facility Rooms and Areas drawings 201-E-279 through 201-E-279 and 201-E-301, 2013 and Building Arrangement Reactor Process Area drawing 201-E-302, 1960). Bedrock elevation is approximately 123 m at the facility (drawing NA25-f-2201 1958).

The space between the bedrock and the concrete walls of the NPD facility is filled with concrete (Powerhouse Waterproofing and Backfilling drawings NA25-f-2206 through NA25-f-2208, 1958), and the space between the overburden and the concrete walls is filled with a high-permeability fill (MacLarentech 1990). Waterproofing was applied to the exterior of the concrete walls and floors upon construction, consisting of six layers of a waterproofing membrane and an asphalt emulsion. Based on Design Manual 211.2 (Canadian General Electric Company Ltd., 1961), waterproofing was not installed to expectations, and was subjected to accidental damage and displacement of asphalt emulsion by groundwater flows. Waterproofing was designed to minimize heavy water loss from the facility (rather than prevent seepage), and counter measures for the poorly installed waterproofing included additional drains, the use of steel liners in the reactor vault and dump pipe room, and an epoxy-coating on the walls of the boiler room.

A tile drain system, trenched into the surface of the bedrock, surrounds the building and drains into the Ottawa River. The tile drain system is divided into two separate systems, one draining the western side of the building, referred to as Tile Drain 1, and the second draining the eastern side of the building, referred to as Tile Drain 2, as shown in Figure 2-2. Only the shallow section of tile drain 2 is shown in Figure 2-2. The deep section of tile drain 2 is described further below.

Figure 2-2 Tile Drains (Shkarupin and Miller 2016)

Note: for tile drain 2, only the shallow portion is depicted on this figure.

Manhole 3, the collection point for the shallow portion of tile drain 2, has always been observed to be dry. This tile drain is therefore assumed to be non-functional likely due to the location of the shallow portion of tile drain 2 above the water table. Bedrock elevations on the south-eastern side of the building are elevated relative to the western side, and the tile drain invert elevations are correspondingly higher on the south-eastern side of the building. Invert elevation refers to the elevation at the inside of the bottom of the pipe. Invert elevations are the same at manhole 2 and manhole 3 (the tile drain outlets for tile drain 1 and 2, respectively), but are above water table elevations at nearby wells. For modelling purposes, the shallow portion of tile drain 2 is ignored.

The deep section of tile drain 2, not shown in Figure 2-2, is located under the pressure relief duct on the eastern side of the building. It is deeper than either tile drain 1 or the shallow section of tile drain 2, and it connects to the tile drain 2 discharge pipe between manhole 3 and the river. This deep section of tile drain 2 is documented in 492D218 REV1 (1960). No flow measurements are available for this portion of the tile drain, as it is downstream of manhole 3 and the outflow to the river is below the river elevation. Recent observations have indicated water in the discharge pipe of tile drain 2, and while the flow was qualitatively judged by CNL to be less than tile drain 1, flow measurements have not yet been conducted (CNL 2022). Despite the lack of flow measurements, the location of this deep section of tile drain 2 below the water table ensures that it will collect groundwater. Throughout this report, the deep section of tile drain 2 under the pressure relief duct will be referred to as the deep section of tile drain 2 and it does not include any portion of the shallow section of tile drain 2, which is considered effectively inactive as discussed above.

The tile drains around the building are constructed of a corrugated galvanized steel coated with hot asphaltum, perforated in the bottom half of the pipe with 3/8 inch perforations at a density of 40 per foot. The tile drain pipe is surrounded by approximately 2 ft of gravel or crushed stone, which is then surrounded by 2 ft of sand. Based on video inspection of tile drain 1 (Drain All 2017), the tile drains show surface wear due to corrosion, the presence of significant flow, and the presence of debris sand and gravel. The coating on the pipe was still observable. The video inspection of tile drain 1, starting at manhole 1 and headed west, found a large increase in flow along this portion of the drain (Drain All 2017). This may be indicative of preferential flow, or it may simply be that the tile drain dips below the water table along this stretch of the tile drain.

Once the tile drains leave the building and drain towards the river (at manhole 2), the pipe is no longer perforated. Video inspection (Drain All 2017) is limited due to significant flows, although large pockets of debris sand, gravel and boulders were observed. Corrosion of the top of the pipe has occurred at approximately three-quarters of the way between the building and the river, referred to as the “break” in the tile drain. Breaks or leaks in the tile drain along this stretch may result in leaks out of the tile drain or increases in the flow along this tile drain.

Groundwater seepage into the building, and water vapour condensation, is collected by a sump, which is periodically pumped and sent to Chalk River Laboratories (CRL for treatment.

2.2 Water Elevations and Hydraulic Conductivities

Fifty-five wells have been drilled near the NPD site for various site investigations:

- NPD-1 through NPD-14 were drilled as part of AECL hydrogeologic investigations of landfill 1 and 2 (Killey and Munch 1988 and 1989).
- MT-1 through MT-10 were drilled by MacLarentech (1990) for site characterization purposes.
- BH-06-01 through BH-16-01 were drilled by J.D Paterson and Associates in 1993 (BH-14-01 through BH-16-01 are dry).
- BH16-01 through BH16-04 were drilled by Golder (2017) for hydraulic conductivity testing.

- MW18-01 through MW18-10 were drilled by Geofirma (Sterling *et al*. 2019) for characterization of the shallow bedrock (top 50 m of bedrock) and the till upgradient of the facility.

The locations of these wells are shown in Figure 2-3.

Figure 2-3 Wells Near the NPD Site

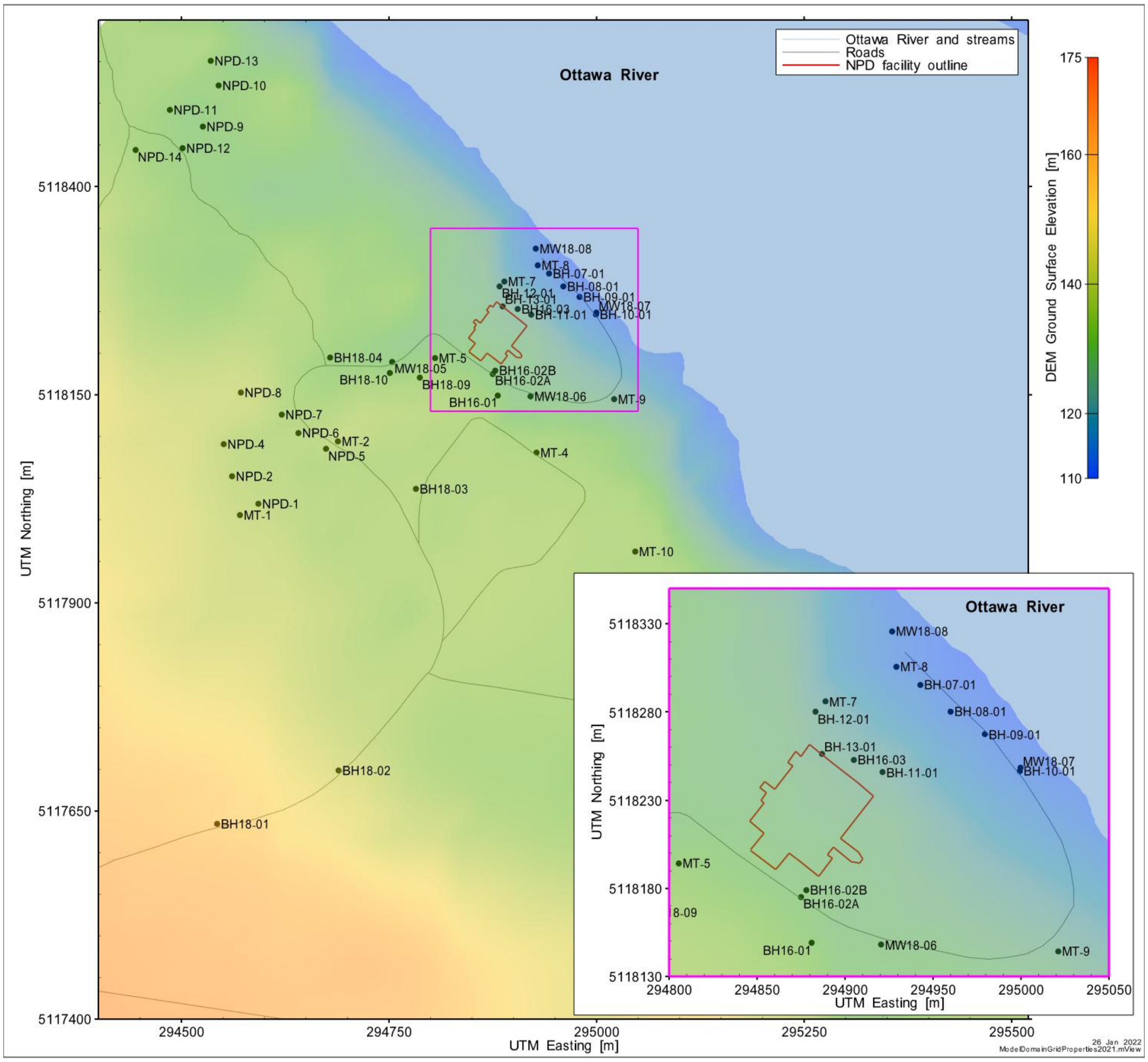

Measured water levels are illustrated in Figure 2-4 and Figure 2-5, and tabulated in Appendix A. Figure 2-4 excludes water levels in the Geofirma bedrock wells, which are provided in Figure 2-5. In some wells with multiple water level measurements, winter water level measurements are lower than spring and summer measurements of water levels. In other wells, the variation between water level measurements at a single well is not seasonal. The variation in water levels at a single well can be considerable, a maximum of 3.4 m and an average of 1.4 m difference, excluding bedrock wells. Bedrock water levels (Figure 2-5) from hydraulic testing are less reliable than those from CMTs (continuous multi-channel tubing for multilevel groundwater monitoring), due to the influence of open borehole water levels prior to packer inflation (Raven *et al*. 2021). Note that Figure 2-4 identifies the water levels used in model calibration (July 2014, December 2018 and January 2019), and the selection of water levels for model calibration is discussed in more detail in Section 3.1.6.

Figure 2-4 Measured Water Levels

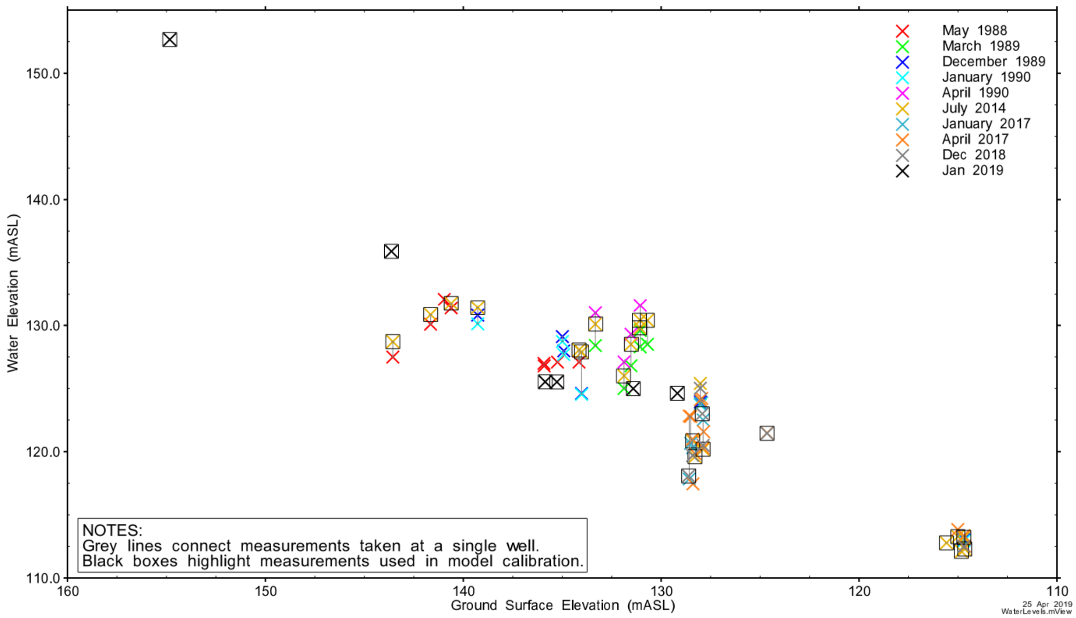

Figure 2-5 Measured Bedrock Water Levels

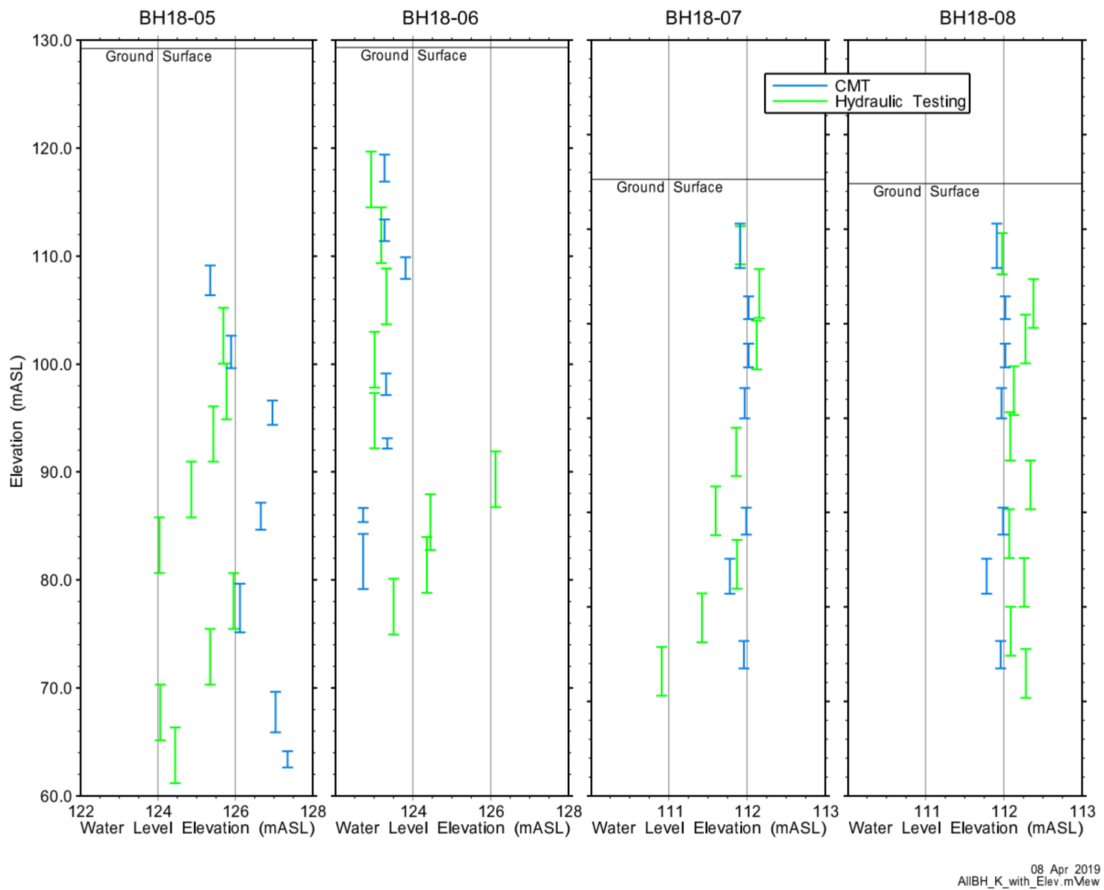

Hydraulic conductivities at the NPD site were measured by Killey and Munch (1988), Golder (2017) and Geofirma (Sterling *et al*. 2019). Overburden hydraulic conductivities are summarized in Table 2-1 and Figure 2-6. Figure 2-6 also displays the hydraulic conductivity measurements in the bedrock. All measurements that span both sand and shallow bedrock are assumed to be reflective of the higher sand conductivity, and the hydraulic conductivity values for these boreholes were corrected to represent only the sand. Hydraulic conductivity measured in the fill is low, and represents a small interval at the bottom of the borehole (BH-16-03). There is considerable heterogeneity in the fluvial sand and gravels with no particular spatial pattern, as shown in Figure 2-7, and so fluvial sand and gravels is represented by a single hydrogeologic unit in the groundwater model. The hydraulic conductivities of the native and fill materials in the groundwater flow model are calibrated, and fall within the range of these measurements.

Table 2-1 Measured Overburden Hydraulic Conductivities

Hydrogeologic Unit	Borehole ID	Hydraulic Conductivity (m/s)
Killey and Munch (1988)		
sand and gravel	NPD-1	7.0E-06
coarse sand	NPD-4	4.0E-05 (minimum)
silty sand and gravel	NPD-7	6.0E-07 (OM estimate)
glacial till	NPD-5	8.2E-08
Golder (2017) Winter 2017		
Sand	MT-5	7.0E-04
Sand / Shallow Bedrock	BH12-01	1.0E-03
Sand	BH16-01	5.0E-04
Golder (2017) Spring 2017		
Fill	BH16-03	1.0E-06
Till	MT-8	2.0E-05
Sand	MT-5	2.0E-04
Sand / Shallow Bedrock	BH7-01	1.0E-04
Sand / Shallow Bedrock	BH9-01	3.0E-07
Sand / Shallow Bedrock	BH11-01	3.0E-05
Sand / Shallow Bedrock	BH12-01	2.0E-04
Sand / Shallow Bedrock	BH13-01	1.0E-05
Sand	BH16-01	5.0E-05
Geofirma (Sterling *et al*. 2019) December 2019		
Till	MW18-01	7.61E-08
Till	MW18-02	3.25E-08
Till	MW18-03	6.56E-09
Till	MW18-04	3.18E-08
Till	MW18-09	1.12E-05
Till	MW18-10	2.47E-05

Figure 2-6 Measured Hydraulic Conductivities

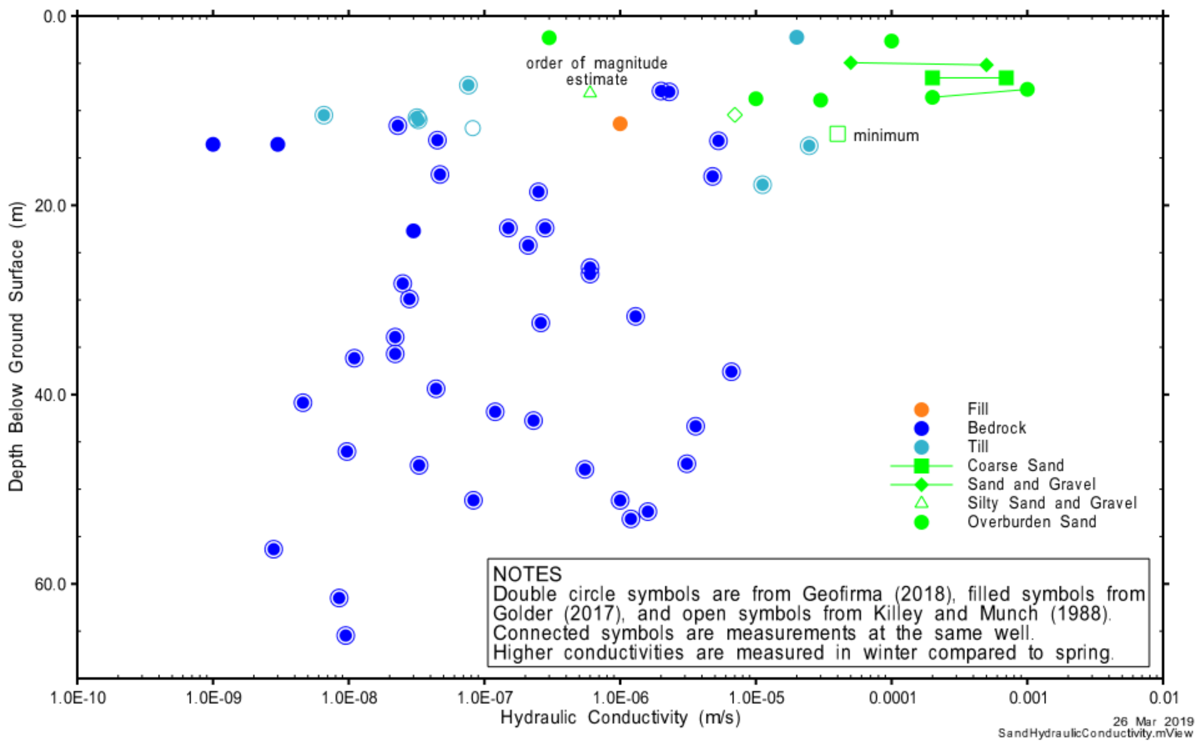

Figure 2-7 Spatial Distribution of Sand Hydraulic Conductivity

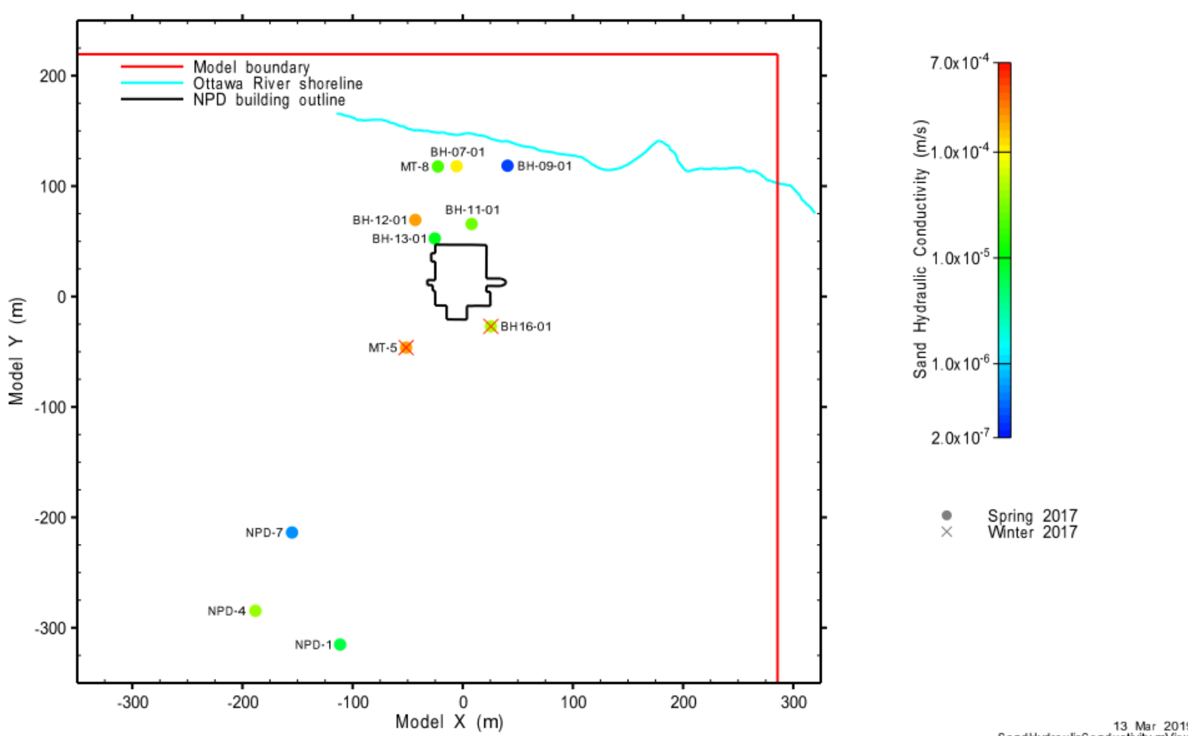

2.3 Tile Drain Flows

Tile drain flows have been measured in tile drain 1 using a dilution gauging approach (Killey and Benz, 2009). All discussion of tile drain flow rates refers to flow measurements in this tile drain (tile drain #1), and not in the deep section of tile drain 2. Dilution gauging consists of injecting a known quantity and concentration of the tracer Fluorescein at a constant flow rate, and measuring the concentration of the tracer at a location downstream that ensures sufficient mixing has occurred. At the NPD tile drain (see Figure 2-2), the tracer is injected at Manhole 2, and the concentration typically measured at the break in the tile drain. The break is located approximately three-quarters of the way between manhole 2 and the river. The concentration is measured by taking a sample at defined time intervals and using a handheld fluorometer, which establishes concentration based on a calibration curve. Two calculation methods were typically used, both steady-state and integrated methods, and similar results are obtained for both methods for reliable measurements. Appendix B provides the tile drain flow measurements using the dilution gauging approach.

Dilution gauge measurements assume complete mixing of the tracer within the water, and no losses of tracer or water between injection and measurement. Incomplete mixing would be expected to result in erratic measurements, and concentration curves are generally smooth, based on available curves in 2009 and 2019. Losses due to sorption are considered unlikely, due to previous experience that has shown Fluoroscein to be unreactive with local sediments at Chalk River (Killey and Benz, 2009). Uncertainty in the dilution gauging method is most likely to arise at the NPD tile drain due to the assumption that the tile drain is intact between Manhole 2 and the break. Any leaks from the tile drain could result in additional water flowing into the tile drain, resulting in incomplete mixing, or water and tracer leaking out of the tile drain. Video footage of the tile drain shows substantial boulders and sediment within the pipe (Drain All Ltd, 2017), and the lining within the pipe has been observed to have eroded away (Geofirma 2019). Consequently, an intact pipe is unlikely, however the extent of any leakage or additional flow is unknown. Small leaks or small additional flow will be inconsequential.

A second method of measuring tile drain flow has also been conducted by Geofirma in the winter of 2019, consisting of an ultrasonic MACE FloPro XCi flow meter that measures the height of water and average velocity in the tile drain, from which a flow rate is calculated. The sensor was installed at the break in the tile drain, and the installation details are described in Geofirma (2019). The velocity meter assumes a smooth pipe upstream of the sensor, whereas the tile drain pipe is a corrugated pipe 21 inches in diameter. The strong velocity profile is indicative that the pipe corrugations are not an issue for calculating velocity. The flowing area of water is calculated by assuming a level depth of water across the pipe, and a pipe of 21 inches in diameter. Observations in early March and April 2019 during installation of the meter suggested that there was some mounding of water above the sensor, due to the turbulent nature of the water and perhaps the corrugated pipe, and the assumption of a level depth of water is inaccurate. The advantage of the ultrasonic flowmeter is continuous measurement of the flowrate.

Figure 2-8 shows the ultrasonic flowrate in comparison to the dilution gauge flow measurements over the time period of ultrasonic flowrate measurement. Dilution gauge measurements were taken at increased frequency during this time period, providing a good comparison to the ultrasonic flowrate measurement.

The ultrasonic flowrate measurement is consistently twice that of the dilution gauge measurements. This large discrepancy is not easily understood; given the large uncertainties in the ultrasonic flow measurement due to the corrugated pipe and turbulent flow, and the successful use of the dilution gauging approach at other CNL locations, the dilution gauge measurements are assumed to be correct. The ultrasonic measurements, however, provide a continuous measurement, describing the seasonal shape of flow in the tile drains. It also highlights a potential for error in the dilution gauge measurements, such as those in December 2019 and May 2020. The dilution gauge measurement in May 2020 is considered a poor test, due to large differences between the steady-state and integration methods.

Figure 2-8 2019 and 2020 Tile Drain Flow Measurements

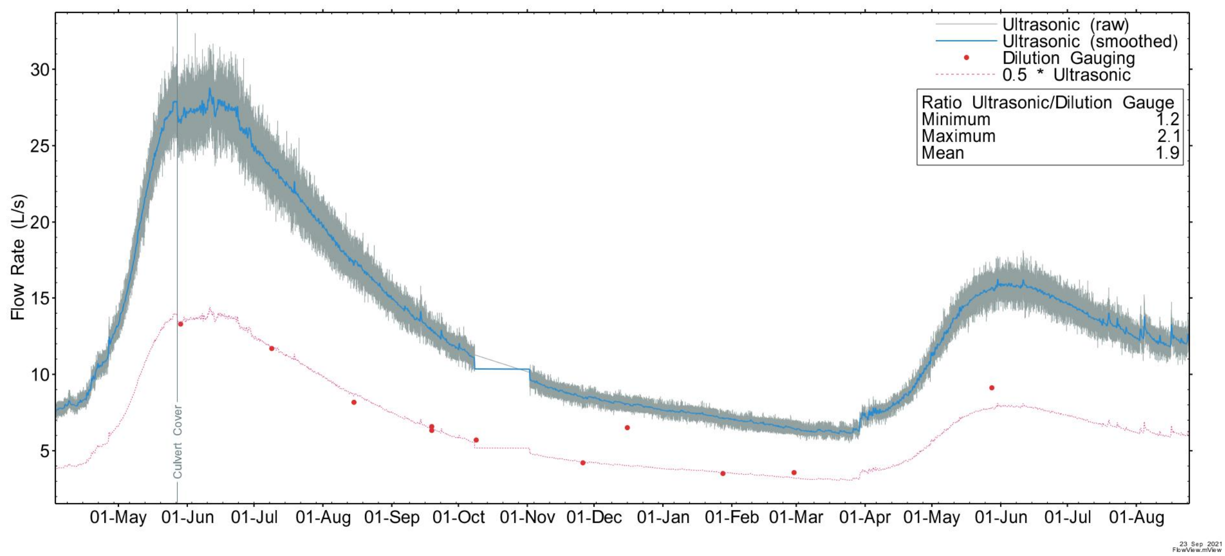

The arithmetic average of the dilution gauge tile drain flows is 7.5 L/s. This average is calculated without any suspect measurements, and only for those measurements taken between Manhole 2 (MH2) and the river. However, an arithmetic average does not take into consideration the seasonal nature of the tile drain flow measurement. In some years, only one or two measurements are taken. A more comprehensive annual steady-state average tile drain flow rate, calculated using a correlation between annual precipitation and an estimated maximum peak tile drain flow rate, results in an annual steady-state average of **7.0 L/s ± 1.4.** Calculation of this steady-state average is presented in Appendix C. The steady-state average is used for calibration of the groundwater model, as described in Section 3.1.6.

The observed tile drain flow rates are generally consistent with the flow observed during construction of the NPD facility, estimated to be 14 L/s. During construction, some draining of wetland areas was also observed. The tile drain flow rates are very high when considering the catchment area required to obtain these rates. Raven *et al*. (2021) notes that most of the flow in the tile drains originates from the overburden, based on an assessment of geochemistry, indicating that the high tile drain flowrates do not occur due to discharge from bedrock or bedrock fractures. The large overburden catchment area required to obtain these tile drain flowrates is much larger than the surface water catchment area defined for the NPD building, as will be discussed in Section 3.1.6, and explains why early groundwater flow models were unable to obtain these high flowrates.

3 CALIBRATED MODEL

3.1 Modelling Approach

3.1.1 Quality Assurance

All modelling work was conducted under Geofirma's ISO 9001:2015 compliant quality management system (QMS). Software control and use is also covered under Geofirma's QMS system.

The Geofirma ISO QMS system is subject to independent external and internal semi-annual audits to confirm adherence to the ISO 9001:2015 Standard requirements, with the most recent external audit and recertification in December 2021 (recertification audits occur every 2 years). Our QMS system is also compliant with the CSA N286.7 standard, as required by CNL, and has undergone an external audit from CNL in 2018 and 2023.

3.1.2 Model Code

All groundwater flow simulations are performed with the FRAC3DVS_OPG V1.3.0 code. FRAC3DVS_OPG is a 3D finite-element / finite-difference code (Therrien *et al*. 2010) for groundwater flow and solute transport. The groundwater flow model presented here uses FRAC3DVS's ability to represent variably saturated groundwater flow above the groundwater table. mView version 4.2X, developed by Geofirma Engineering, is used for all model pre- and post-processing.

PEST++ version 5.0.0 (Welter *et al*. 2015) was used as a parameter estimation tool to obtain a numeric calibration of the groundwater flow model.

Particle tracks are executed using MODPATH version 7.1.000 (Pollock 2016). MODPATH calculates the analytic flow path of a particle within each model grid block, and tracks the particle from one grid block to the next until the particle reaches a boundary or satisfies another termination criterion. mView converts the FRAC3DVS groundwater flow output to a MODPATH compatible form.

3.1.3 Model Domain and Discretization

The watersheds near the facility were delineated using Arc Hydro Tools, which uses a digital elevation model (DEM) to determine flow directions and catchment boundaries. Arc Hydro Tools (version 2) is part of ESRI's ArcGIS. Using a 20 m resolution DEM (Ontario Ministry of Natural Resources 2013), the resulting watershed boundary is complicated, divided into the several magenta sub-catchments shown in Figure 3-1. Upgradient of highway 17, the dashed line sub-catchments drain into the wetland immediately south of the highway. Flow from the wetland appears to drain into two catchments, the catchment containing the NPD facility, as well as the catchment east of the NPD facility catchment (not shown). It should be emphasized that these catchments reflect surface water flow, and not groundwater flow. However, groundwater flow is currently assumed to follow a similar flow path to surface water, except where permeable overburden features parallel to the river are defined. This assumption is reasonable given that groundwater in the overburden is expected to mainly flow along the top of the bedrock surface. The bedrock surface follows the trends in elevation at ground surface, generally sloping towards the river.

The current model domain, shown in Figure 3-1, is a reasonable approximation of the delineated surface water catchment area of the facility, as well as the catchment areas west of the facility. The southern edge of the model domain corresponds to the top edge of the surface water catchment. The surface water catchment containing the NPD facility is also generally narrower than the model domain, except at the south-eastern corner of the surface water catchment boundary, which extends considerably beyond the current model domain but the water within which, both surface and ground, is also highly likely to drain into the adjacent catchment area. Previous topographically-driven groundwater models had shown that groundwater generally flows towards the river, along the top of the bedrock surface, and expanding the domain either east or west of the facility had negligible impact on groundwater flows near the facility. The model domain was extended to the west to allow consideration of a hydrogeologic conceptual model that increases the catchment area of the NPD tile drains, which exhibit high flows that could not be explained by topographically-driven groundwater flows alone. The specifics of this conceptual model are discussed further in Section 3.1.4. A sensitivity case also examines the extension of the model domain to the east, discussed in Section 5.1, finding this extension to have negligible impacts on geosphere flows in the vicinity of the facility.

Figure 3-1 3D Groundwater Flow Model Domain

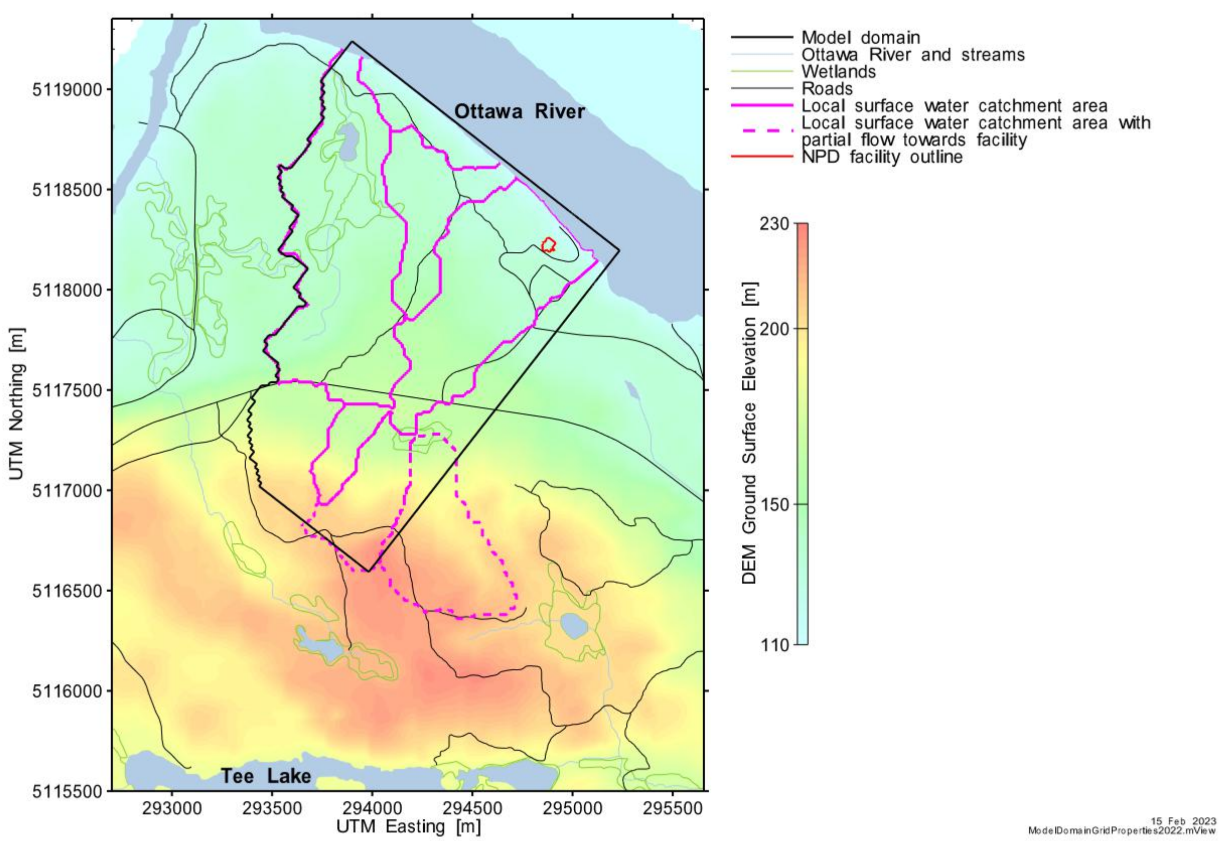

Figure 3-2 shows the model's plan and vertical discretization. The domain was horizontally discretized to provide a higher level of detail in the vicinity of the NPD, the area of interest. Building dimensions were obtained from the NPD Facility Rooms and Areas drawings (201-E-279 through 201-E-284 and 201-E-301, 2013) and Building Arrangement Reactor Process Area drawings (201-E-302, 1960). Vertical discretization was informed by building dimensions, the topography and bedrock elevation. Topography was obtained from a 20 m resolution DEM (Ontario Ministry of Natural Resources 2013), and adjusted near the building based on excavation plans and building drawings. Surfaces were developed for the top of bedrock based on existing boreholes and other available data, as will be described below. Shallow tile drains were trenched into the bedrock, and consequently the bedrock elevation was adjusted to ensure that the tile drains, located at bedrock surface, sloped toward the river, with elevations similar to the invert elevations of the tile drains (invert elevation refers to the elevation at the inside bottom of the pipe). The model also includes a deep section of tile drain 2 under the pressure relief building (492D218 REV1, 1960), not considered in previous versions of the model. The model grid has 701 676 active nodes and 667 290 elements, divided into 27 layers.

Figure 3-2 Horizontal and Vertical Discretization, Full and Detailed Views

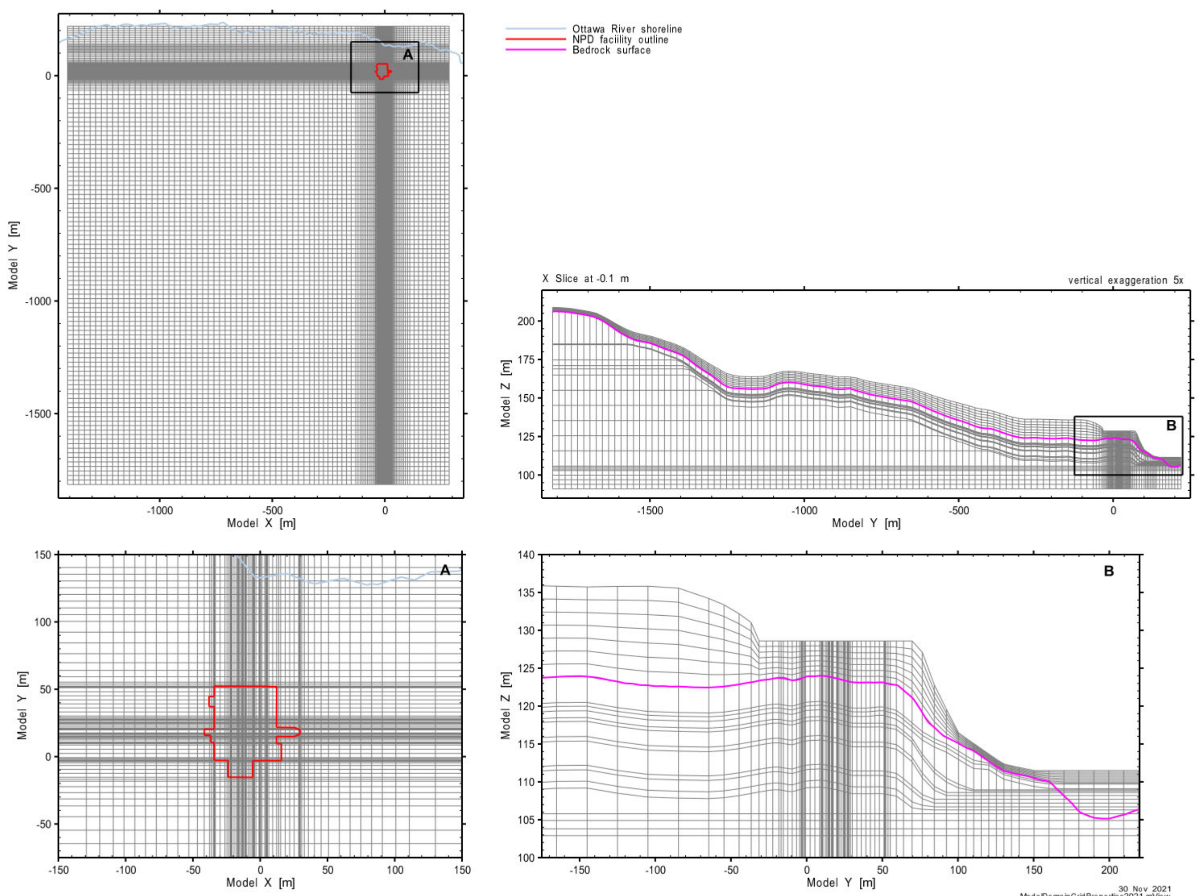

The bedrock surface was developed using a kriging algorithm that took into consideration:

- Bedrock top elevations from boreholes drilled by Geofirma (Sterling *et al*. 2019) and Golder (2017). Other boreholes either had limited or uncertain data about the top of bedrock, and did not provide additional spatial representation.
- Bedrock contours detailed in the powerhouse excavation plan (drawing NA25-f-2201 1958).
- S-borings under the river (drawing NA-25-EG-120-1 R0 1958). Note that other s-boring elevations are considered in the bedrock contours of the powerhouse excavation plan.
- Shallow bedrock based on bedrock surficial geology in Figure 2-1 (both south and west of the facility). Bedrock was assumed to be 1 m below ground surface in the areas delineated with bedrock surface geology. The assumption is made for 1 m, acknowledging that (1) bedrock surficial geology is not all exposed bedrock but bedrock very near the surface, (2) areas with bedrock near surface are small, and far from the area of interest, and (3) the presence of some overburden improves gridding and numeric performance.
- Bedrock depth between 9 and 12 m upgradient of the facility, based on bedrock elevations from Geofirma boreholes, reducing to 1 m depth at the southern boundary of the model domain based on surficial geology as described in the previous point.
- Bedrock depth along the shoreline, based on borehole bedrock elevations from Geofirma and s-borings (drawing NA-25-EG-120-1 R0 1958).
- Artificial points immediately west of the facility to provide a relatively flat bedrock surface. Kriging algorithms would create a bedrock valley in this area, due to the low bedrock surface at borehole BH18-05, BH18-09 and BH18-10 relative to the bedrock elevation in the vicinity of the facility. Such a bedrock valley would encourage groundwater flow towards the river rather than towards the tile drains. This flattening was therefore undergone to increase flows into the tile drain. Note that there is no bedrock elevation data in this area to support or refute this adjustment, but was conducted for calibration purposes. Without this adjustment, the high tile drain flow rates observed would be unattainable in the groundwater model.

The resulting bedrock surface is shown in Figure 3-3.

Figure 3-3 Bedrock Surface used for Gridding and Property Assignment

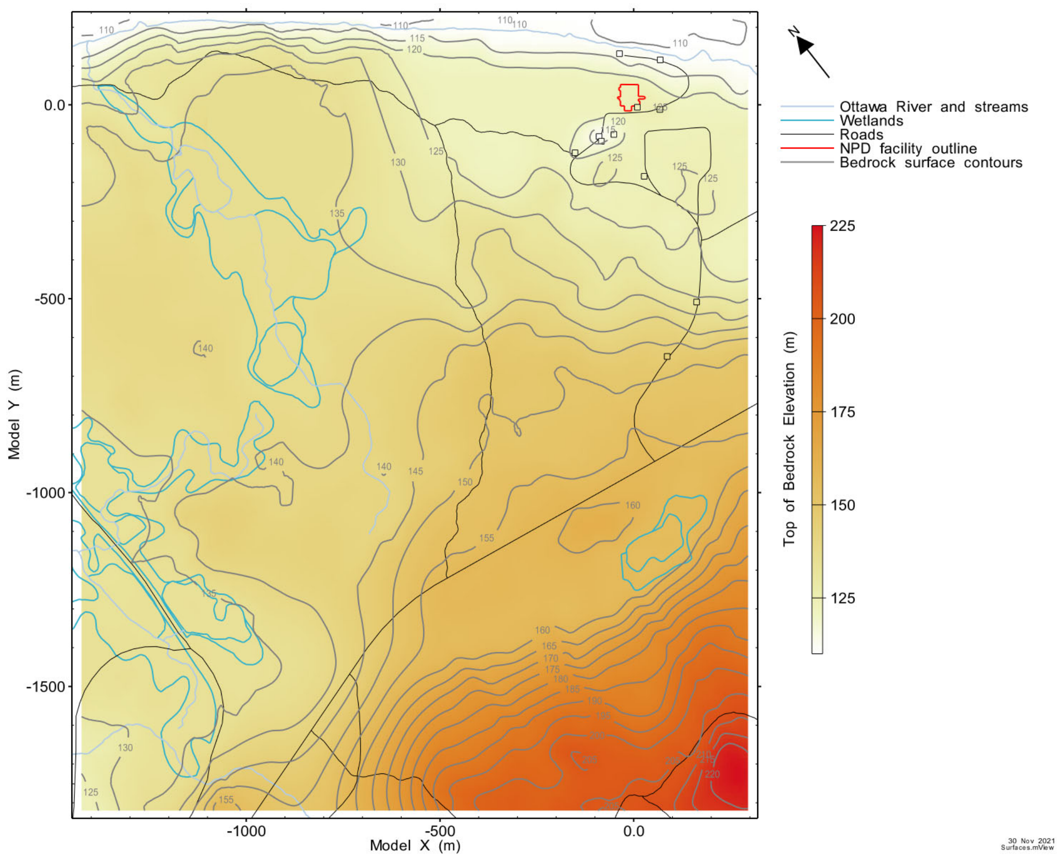

3.1.4 Material Properties

There is a reasonable amount of data describing hydraulic conductivities of the materials at the site. Hydraulic conductivity is the main parameter required for the steady-state flow model. The geosynthesis report (Raven *et al*. 2021) describes the hydraulic conductivity and porosity data used in this model with some detail; two-phase flow parameters are provided in this document. Some model parameter values are based on published data. Some of this published data is for Chalk River Laboratories (CRL), which is located near Deep River, Ontario, approximately 20 km from the NPD site. Located within the same geologic region, with similar hydrogeologic materials, data from the CRL site is a reasonable approximation for the NPD site, where available.

It is important to note that the companion geosynthesis report (Raven et al., 2021) contains considerable and detailed discussions of the site's characteristics; it is relied upon as a key source of information on site materials and their properties.

3.1.4.1 Bedrock

Site-specific shallow bedrock characterization synthesized by Raven *et al*. (2021) recommends a bedrock hydraulic conductivity of 7.3E-8 m/s near the facility, and 3.6E-7 m/s near the river. The bedrock in the groundwater model was simply divided halfway between the measurement points near the facility (BH-18-05 and BH-18-06) and near the river (BH-18-07and BH-18-08). These hydraulic conductivity estimates take into consideration the fractured nature of the bedrock, assuming the bedrock to be an equivalent porous medium. Specific fractures are not modelled due to the lack of correlation in the fracture sets between bedrock boreholes. Both bedrock units are assumed to have a porosity of 0.005 (RBEL 1994), a specific storage value of 1.2E-6 m^{-1} (Raven *et al*. 2021) and two-phase flow parameters estimated based on values used in flow modelling at the Chalk River Laboratories (Acsion 2014 and Calder and Walsh 2016).

3.1.4.2 Sand

All overburden in the model was designated sand, if it was not otherwise designated as till or fill. The surface sediments are generally consistent with the surficial geology map (Figure 2-1). MacLarentech (1990) describes the overburden near the NPD facility to be predominantly sand, divided into four classifications of sand with various amounts of gravel, boulders and trace amounts of silt. Based on hydraulic conductivity measurements (Section 2.2), the sand is heterogeneous, with a wide range of conductivity and no particular spatial pattern. The sand is represented by a single homogenous unit. Based on a cumulative distribution function of the sand hydraulic conductivity (Figure 3-4), the median horizontal hydraulic conductivity of the sand is expected to be near $5x10^{-5}$ m/s, and the range of hydraulic conductivity is between $3x10^{-7}$ and $1x10^{-3}$ m/s. The sand is also assumed to be anisotropic. Sand at CRL has an anisotropy ratio (horizontal/vertical) between 2 to 10 depending on the degree of silt lamination (RBEL 1994). Sand porosity is assumed the same as CRL, at 0.4. This is consistent with previous estimates by Killey and Munch (1988) of sand porosity between 0.3 and 0.4. Two-phase flow parameters for sand were estimated based on samples with similar hydraulic conductivities in the Rosetta model database (USDA 1990). Previous groundwater flow modelling (Calder 2016) found the model to be insensitive to the two-phase flow parameters in the sand, as expected for a steady-state model in a permeable material where capillarity will have little impact on the water table.

Figure 3-4 Cumulative Distribution of Measured Sand Hydraulic Conductivity

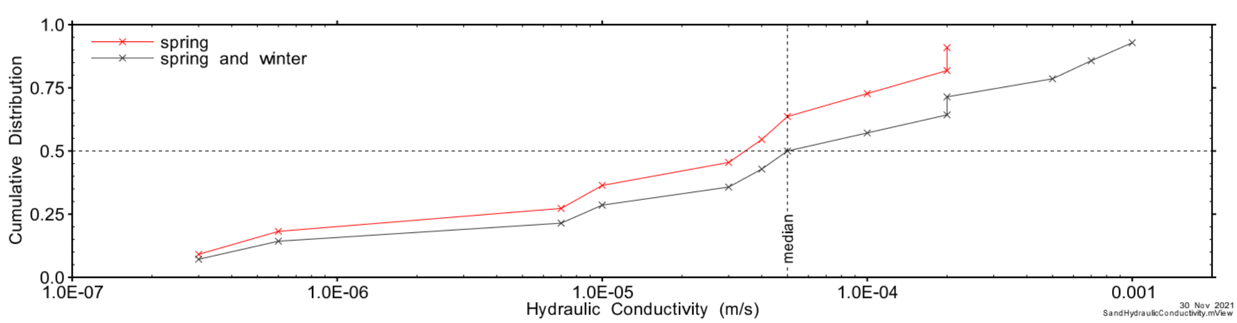

3.1.4.3 Till

Site-specific till characterization synthesized by Raven *et al*. (2021) recommends a till conductivity of 3.3×10^{-8} m/s upgradient of the facility, and a range between 2×10^{-5} and 2×10^{-4} m/s near the river. The till in the groundwater model was simply divided halfway between the nearest conductivity measurement points in the two till units (BH-18-04 and BH-18-10). Till porosity is 0.3 (RBEL 1994). Two-phase flow parameters for till were estimated based on samples with similar hydraulic conductivities in the Rosetta model database (USDA 1990).

3.1.4.4 Boulder Till

Raven *et al*. (2021) identified a boulder till at the site, in the vicinity of the facility, and recommends a hydraulic conductivity for this unit of 1.7E-5 m/s. Porosity and storage are assumed to be the same as the till (Raven *et al*., 2021). Two-phase flow parameters were also assumed to be the same as the till.

3.1.4.5 Fill

The fill above the bedrock used at the NPD was described by MacLarentech (1990) as a bouldery sand, similar to the sand overburden found at the site, but with a more consistent size of gravel and boulders and the presence of debris such as rock and construction rubble. A single measurement of the hydraulic conductivity of the fill of 1×10^{-6} m/s is low compared to the values of sand and till near the river. The measurement is for a small interval at the bottom of the borehole, and is expected to represent the lower end of the range of potential values. For calibration purposes, the upper estimate of the fill conductivity is the same as the upper estimate for sand. Two phase flow properties were assumed similar to the sand overburden, with the alpha parameter scaled by permeability and porosity using the Leverett J-function (Leverett 1941).

3.1.4.6 Building Materials

The fill surrounding the building and below bedrock is a concrete. This concrete fill is assumed to have a moderate conductivity of 10^{-10} m/s, which is within the wide range of conductivities for concrete that are reported: Quintessa and Geofirma (2011) propose a range of 10^{-9} and 10^{-11} m/s for structural concrete, and 2×10^{-11} and 2×10^{-12} m/s for high performance concrete, based on a compilation of seven different references including Garisto *et al*. (2004), Guo (2004), Hurtado *et al*. (1997), NAGRA (1994), NAGRA (2008), Russell and Simmons (2003), and WIPP (2009); Dixon *et al.* (2008) reports concrete conductivity values between 3.1×10^{-10} and 9.3×10^{-11} m/s; and Rockhold *et al*. (1993) reports a concrete conductivity of 3.8×10^{-12} m/s. The concrete porosity of 0.125 is consistent with the value used in the Postclosure Safety Analysis (Penfold *et al.* 2017).

Numeric grid elements on the exterior of the NPD facility were assumed to be concrete walls and floors. Concrete wall and floor hydraulic conductivity of 3×10^{-11} m/s is based on calibration of this material property with the resaturation modelling, as reported in the companion resaturation model (Sgro, 2023). The calibration of the concrete wall and floor hydraulic conductivity is conducted on an empty building version of the restauration model (i.e. no grout), with flows into the building compared to measured sump pump values. The concrete conductivity calibrated by this resaturation model takes into consideration the membrane waterproofing or asphalt emulsion damp-proofing on the exterior of the concrete walls and floors (Powerhouse Waterproofing and Backfilling drawings NA25-f-2206 through NA25-f-2208, 1958). The design manual 211.2 (Canadian General Electric Company Limited, 1961) indicates that the waterproofing did not meet expectations during construction, with damage occurring to the membrane and displacement of the asphalt emulsion by groundwater flows. The calibrated value is also consistent with hydraulic conductivities measured from cores taken from the concrete walls, between $1.4x10^{-11}$ and $2.4x10^{-11}$ m/s (Kinetrics, 2018).

Numeric grid elements within the building were assumed to be a low permeability grout. Grout conductivity was modelled as $6.3\ x10^{-11}$ m/s below bedrock and $6.3x10^{-10}$ m/s above bedrock, consistent with the Post SA model (Arcadis 2018). These conductivities are based on a grout testing program (CNL, 2018) which estimated an undegraded grout in laboratory conditions to have a conductivity of $6.3x10^{-12}$ m/s. The more permeable values used in the model is intended to represent in situ conditions, and takes into consideration the decommissioning plan (CNL, 2020) measures to ensure uniformity in the grout material properties, including removing equipment, sealing penetrations, filling pipes and penetrations, and continuous inspection during emplacement. The porosity of the grout was calculated as a volumetric average of grout and 10% high permeability materials. Two-phase flow properties of the grout are based on a grout with similar composition (Taylor and Phifer 2012, Phifer *et al*. 2006).

3.1.4.7 Parameter Summary

Initial estimates of material properties are summarized in Table 3-1, based on the discussions outlined in Section 3.1.4.1 to Section 3.1.4.6, and Section 2.2. Hydraulic conductivities for the overburden and bedrock are calibrated, and the values provided in this table are an initial estimate. Calibration methods, results and final calibrated values are presented in Section 3.2. Concrete fill, concrete walls and grout were not calibrated in this groundwater model. Concrete walls were calibrated in the resaturation model (Sgro, 2023). van Genuchten-Mualem two-phase flow curves are defined to describe unsaturated flow, requiring a residual liquid saturation, shape parameter and alpha parameter. All grid elements located within the river are given a very high hydraulic conductivity (0.1 m/s), zero capillary pressure and linear relative permeability curves, to allow water to travel quickly through the river to the river boundary condition (described in Section 3.1.5 below).

Table 3-1 Material Properties Initial Estimate

(See Sections 3.3.1 to 3.3.6, and Section 2.2)

	Hydraulic Conductivity (m/s)	Anisotropy Ratio (Kh/Kv) (-)	Porosity (-)	Specific Storage (1/m)	Residual Water Saturation (-)	Shape Parameter (-)	Alpha (1/m)
Sand	$5x10^{-5}$	10	0.4	10^{-5}	0.05	2.0	3.5
Till	$3x10^{-8}$	1	0.3	10^{-5}	0.05	1.7	0.66
Till Near River	$7x10^{-5}$	1	0.3	10^{-5}	0.05	1.7	0.66
Boulder Till	$2x10^{-5}$	1	0.3	10^{-5}	0.05	1.7	0.66
Fill	$1x10^{-4}$	1	0.3	10^{-5}	0.05	2.0	10
Bedrock	$7x10^{-8}$	1	0.005	$1.2x10^{-6}$	0.28	2.0	0.22
Bedrock Near River	$4x10^{-7}$	1	0.005	$1.2x10^{-6}$	0.28	2.0	0.22
Concrete Fill	$1x10^{-10}$	1	0.125	10^{-6}	0.2	1.4	0.01
Concrete Wall	$3x10^{-11}$	1	0.125	10^{-6}	0.2	1.4	0.01
Grout	$6x10^{-11}$	1	0.4	10^{-6}	0.2	1.4	0.10
River	0.1	1	1	10^{-9}	-	-	-

During calibration, hydraulic conductivities of overburden and bedrock materials were adjusted within a reasonable range, based on the range of measured hydraulic conductivity for that unit. The range provided for each calibrated hydraulic conductivity parameter is provided in Table 3-2. Note that final calibrated hydraulic conductivities are provided in Table 3-3.

Table 3-2 Range in Hydraulic Conductivity used for Model Calibration

m/s	Initial Estimate	Lower Bound	Upper Bound
Fill	$1x10^{-4}$	$1x10^{-6}$	$1x10^{-3}$
Sand	$5x10^{-5}$	$3x10^{-7}$	$1x10^{-3}$
Sand Anisotropy Ratio	10	2	10
Till	$3x10^{-8}$	$5x10^{-9}$	$1x10^{-7}$
Till Near River	$7x10^{-5}$	$1x10^{-5}$	$5x10^{-4}$
Boulder Till	$2x10^{-5}$	$5x10^{-6}$	$2x10^{-3}$
Bedrock	$7x10^{-8}$	$1x10^{-9}$	$2x10^{-6}$
Bedrock Near River	$4x10^{-7}$	$1x10^{-8}$	$2x10^{-6}$

3.1.4.8 Property Assignment

Figure 3-5 shows material assignments applied to the discretization in Section 3.1.3 for a cross section profile through the building, at a model X location of -14.7 m through the building and pipe trench. The bottom cross-section highlights a portion of the full cross-section focused on the facility. Both cross-section views are exaggerated vertically by a factor of 2. Figure 3-6 shows material assignments for several plan views of different layers of the model, highlighting the heterogeneity of the overburden and bedrock materials.

Figure 3-5 Cross-section Showing Material Property Assignment

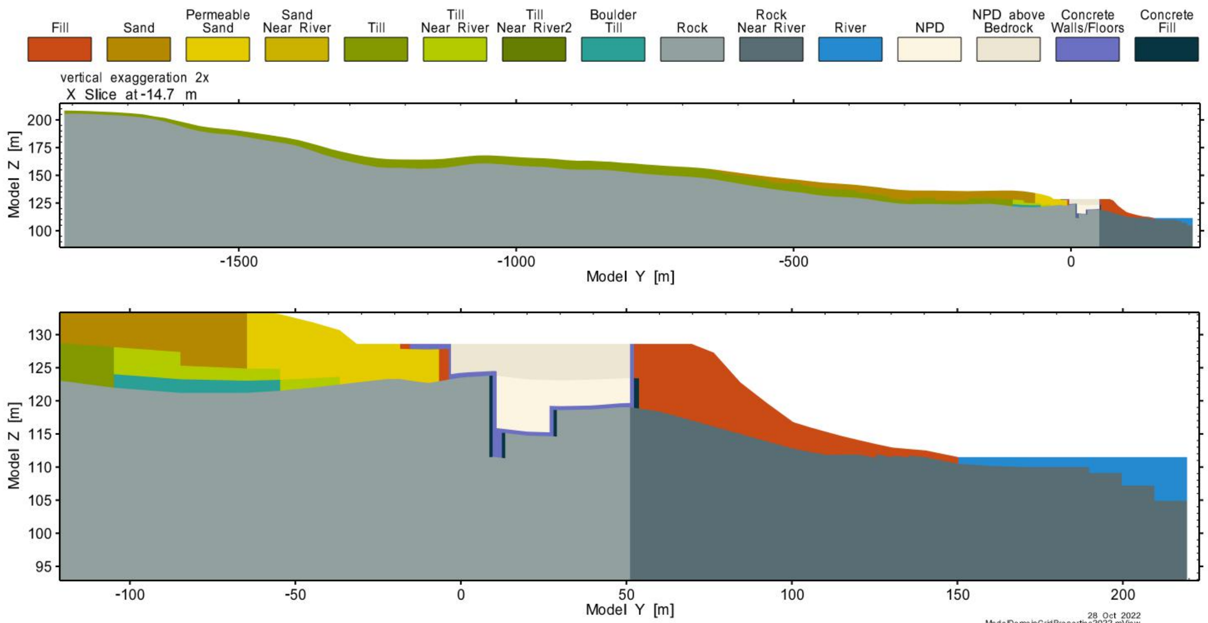

Figure 3-6 Plan Views Showing Material Property Assignment

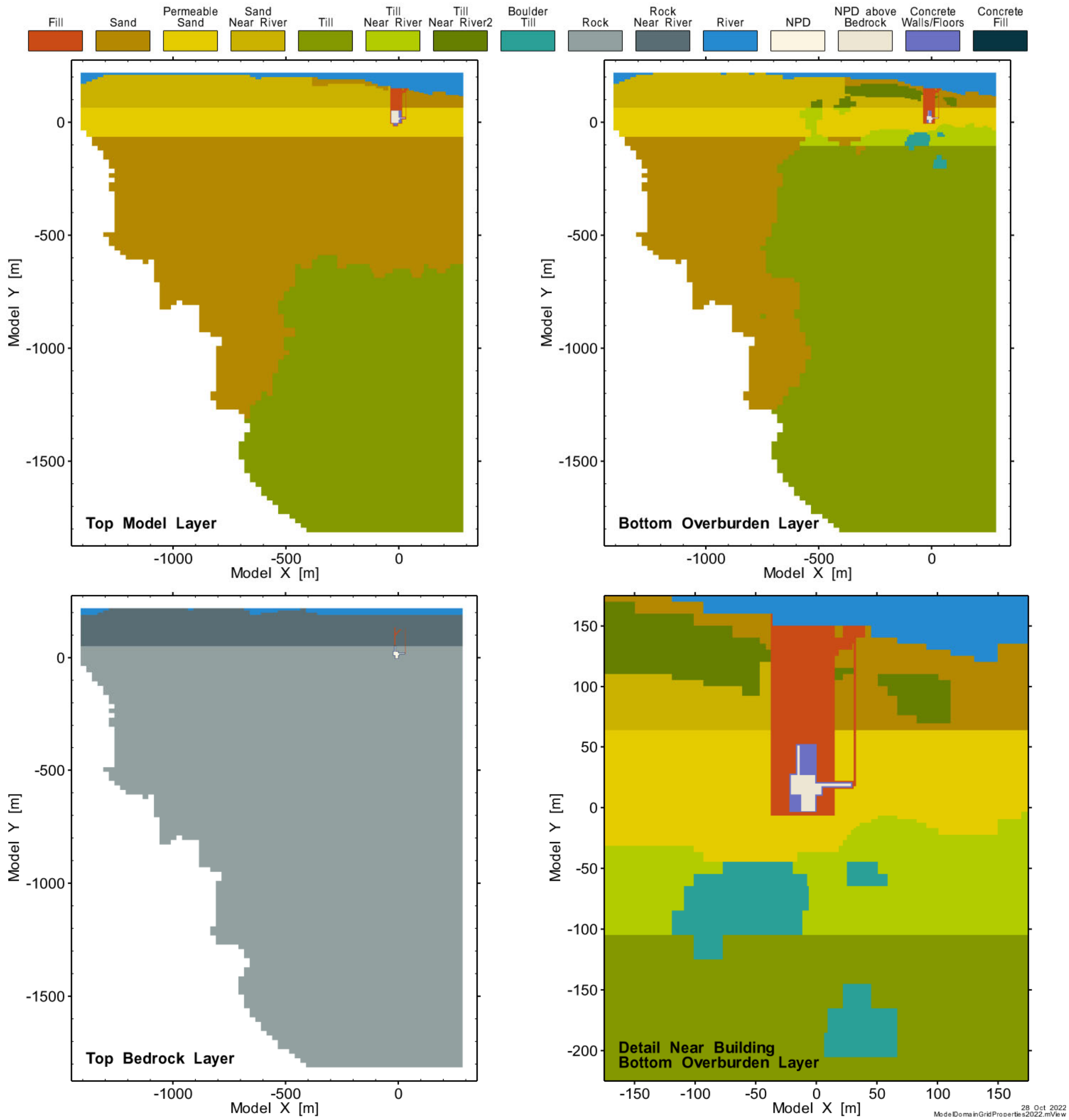

Properties were assigned based on surfaces developed for the bedrock, till and boulder till. The bedrock surface is described for grid generation in Section 3.1.3. The till surface was developed using a minimum curvature algorithm based on Geofirma and Golder boreholes, taking into consideration boreholes where no till was found. Artificial points were added to the surface development, with the till elevation depth based on the expected till depth based on borehole data and surficial geology. The boulder till surface used kriging and the Geofirma boreholes, and the till near the river surface is simply a plane through Geofirma boreholes near the river. Properties above the till were designated as sand.

Both bedrock and till were divided into two groups, one near the river, and one farther from the river. The bedrock was divided halfway between the measurement points near the facility (BH-18-05 and BH-18-06) and near the river (BH-18-07and BH-18-08). The till was divided halfway between the closest conductivity measurement points in the two different till units (BH-18-04 and BH-18-10).

The rock excavation and facility dimensions within the excavated rock were estimated based on the powerhouse excavation plan (drawing NA25-f-2201, 1958), NPD Plant Arrangement Plans (201-E-279 through 201-E-279 and 201-E-301, 2013) and NPD Building Arrangement Sections Reactor Process Area drawings (201-E-302, 1960). Grid elements on the exterior of the NPD facility are designated as concrete walls or floors, while the interior was designated grout. Fill surrounds the building above the bedrock surface, but below the top of bedrock surface, the space between the building and bedrock is a concrete fill.

The river was given an approximate triangular profile, assuming a river depth of 40 m at a distance of 200 m from the shoreline based on the western shoreline profile used in a RBEL (1994) model located near Deep River. Closer to the shoreline, the river has a depth generally consistent with the s-borings under water (drawing NA-25-EG-120-1 R0 1958).

For the purposes of calibration, the sand unit was divided into three parts (as shown in Figure 3-6):

1. a permeable sand parallel to the river with a high hydraulic conductivity. The purpose of this sand unit is to transport water towards the tile drains at the facility.
2. A less permeable sand between the permeable sand and the river, west of the facility. This unit is intended to prevent water from flowing into the river, and direct it towards the facility.
3. Sand upgradient of the facility and the permeable sand, as well as sand near the river but east of the facility.

The sand units are defined as far west as is feasible given the topography and geology. However, the entire sand units to the west will not be required to obtain expected tile drain flow rates. The calibrated hydraulic conductivities of the units will define the portion of the units to the west that will contribute to flow at the facility. Groundwater in the remainder of the units not contributing flow to the tile drains will flow into the river to the west of the facility.

While such horizontal sand units parallel to the river have not been characterized by drilling and well testing, it is consistent with the geological deposition of sediments at the site, the heterogeneity of sands observed at the site, and is currently the only mechanism in the groundwater model capable of increasing tile drain flowrates to near observed values. To ensure groundwater south-west of the site provides water to the tile drains, the kriged bedrock surface also required adjustment, as described in Section 3.1.3, to prevent dips in the bedrock surface west of the facility that are not supported by any data. Without this adjustment in the bedrock surface, groundwater south-west of the facility would be redirected towards the river before reaching the facility, and high tile drain flow rates would be unattainable. It should also be noted that the additional water near the facility results in the generation of springs along the bluff downgradient of the facility when the tile drains fail, which is consistent with historical observations of springs along this bluff prior to facility construction. These springs do not occur without the additional water directed towards the facility.

The till near the river was also divided into two parts for calibration purposes (as shown in Figure 3-5 and Figure 3-6), to allow till adjacent to the river and downgradient of the permeable sand to be reduced in permeability to prevent water from flowing into the river, rather than towards the facility. West of the facility, sand was assigned between the till near the river and the river to ensure the water table remained below ground surface.

Hydraulic conductivity values for the different sand and till units developed for calibration purposes use ranges consistent with measurements and the ranges for these units are provided in Table 3-2.

It should be noted that the cross-sections, while generally consistent with the cross-sections presented in the geosynthesis (Raven *et al* 2021), are not exactly the same. This is due in part to the difference in interpolating and interpreting borehole data onto a three-dimensional surface, rather than onto a two-dimensional cross-section as was done in the geosynthesis. Both interpretations are valid, and the differences represent some of the uncertainty in subsurface interpretation.

3.1.5 Boundary and Initial Conditions

The southern, sides, and bottom of the model domain are no flow boundary conditions. The southern boundary condition is no flow as it is located along a natural flow divide at a topographic high. The east side boundary is approximately parallel to the flow path to the river and the west side boundary coincides with the watershed boundary. Flow across these side boundaries is expected to be negligible. The northern boundary of the model is also no flow, except the top layer defined at a specified head of 111.5 m, the elevation of the Ottawa River at this location. All river elements in the top layer are defined at the specified head of 111.5 m. Elements located within the river below the top layer are defined as highly permeable, resulting in heads equivalent to the specified head boundary. The entire river is not specified as a boundary condition in order to improve the flow description entering the river.

Infiltration was applied to the overburden materials on the surface of the model. Recharge, water entering saturated groundwater, is typically an input parameter in groundwater flow models. However, as the water is applied to the surface of a model that includes the unsaturated zone above the water table, infiltration is the appropriate term for water obtained from precipitation sources for this model. Infiltration can be estimated as the amount of precipitation minus evapotranspiration and runoff. Average annual precipitation at the Chalk River AECL station is 859 mm/yr, based on precipitation normals for 1981 to 2010. Climate normals are used instead of more recent data. The use of climate normals is standard practice since climate normals include rigorous consideration of missing or suspect data and ensure consistency across projects that consider climatic data. Evapotranspiration in the Ottawa River Watershed is estimated to be approximately 50% (Telmer and Veizer 2000, Environment Canada 1978 and Ontario Water Resources Commission and Quebec Water Board 1971), and 60% has been used at CRL (Robertson and Barry 1985, McCrank 2016). The amount of runoff at the NPD site is unknown. In some CRL studies (where 60% evapotranspiration is assumed), runoff is assumed to be very small (Scheier and Killey, 2009), and a recharge of 300 mm/yr is applied. Where the overburden at the site is mainly sand, high infiltration and recharge and low runoff may be expected. Initial calculations of infiltration for previous versions of the groundwater model were calculated using the US Soil Conservation Service method for determining runoff, estimating 220 mm/yr over the sand and 130 mm/yr over a relatively permeably till. These estimates were found to be too low over the sand, making model calibration to tile drain flow rates intractable, likely due to an overestimation of runoff. Assuming no runoff, and evapotranspiration of 60% (as used at CRL) and an annual precipitation value of 859 mm/yr, infiltration will be 344 mm/yr. Assuming evapotranspiration of 50%, infiltration will be 430 mm/yr. The actual infiltration rate over the catchment area is not easily measured or estimated, but an uncertain value within bounds can be reasonably estimated.

Infiltration over the sand overburden was assumed fixed at 400 mm/yr. Infiltration over the till is limited by the low conductivity of the till. Initial flow simulations found that infiltration in excess of 10 mm/yr caused the surface of the model to flood. Consequently, infiltration over the till was fixed at 10 mm/yr. Note that previous groundwater models obtained a higher infiltration rate over the till due to the higher assumed conductivity of the till. Site characterization that has occurred after the development of previous groundwater models has reduced the estimated conductivity of the till.

Infiltration over the building was assumed to be 1 mm/yr for calibration, based on previous models of the engineered cap and cover. While the calibration model doesn’t have a cap and cover, this was considered a reasonable approximation of existing conditions taking into consideration that, as observed in previous modelling and the scenario cases presented here, the effects of changes to building flows (including infiltration) are limited to the building itself and result in negligible changes to the geosphere flows in the vicinity of the facility.

Tile drains on the west side of the facility (tile drain 1) were implemented as seepage nodes on the bottom of the overburden (one node layer above the top node layer of bedrock) following simplified tile drain pathways. Seepage nodes behave as constant head boundary conditions, set to the node elevation, only when the head at the node would exceed the node elevation. Otherwise, the node is inactive. The location of the simplified tile drain 1 pathway is shown in Figure 3-7.

The shallow section of tile drain 2 on the east side of the facility is not implemented; only the deep section of tile drain 2 below the pressure relief duct is implemented. The shallow section of tile drain 2 has been observed to be dry without any water flow (see Section 2.3).

The deep section of tile drain 2 under the pressure relief duct is below the water table and flow has been observed in the discharge pipe (CNL 2022), although there is no data available to confirm flow rates. The deep section of tile drain 2 under the pressure relief duct also follows a simplified pathway, but is implemented using high permeability materials instead of seepage nodes. Both seepage nodes and high permeability pathways have been used in previous models for tile drain 1 on the western side of the facility, with negligible difference in model results. The choice to use different methods for representing the tile drains is to ensure the flows out of tile drain 1 can be quantified independently of those in tile drain 2, since calibration is dependent on the flow rates of tile drain 1. The simplified pathway representing the deep section of tile drain 2 is shown in Figure 3-8. The deep tile drain 2 trench contains fill.

Figure 3-7 Location of Simplified Tile Drain 1 in Model

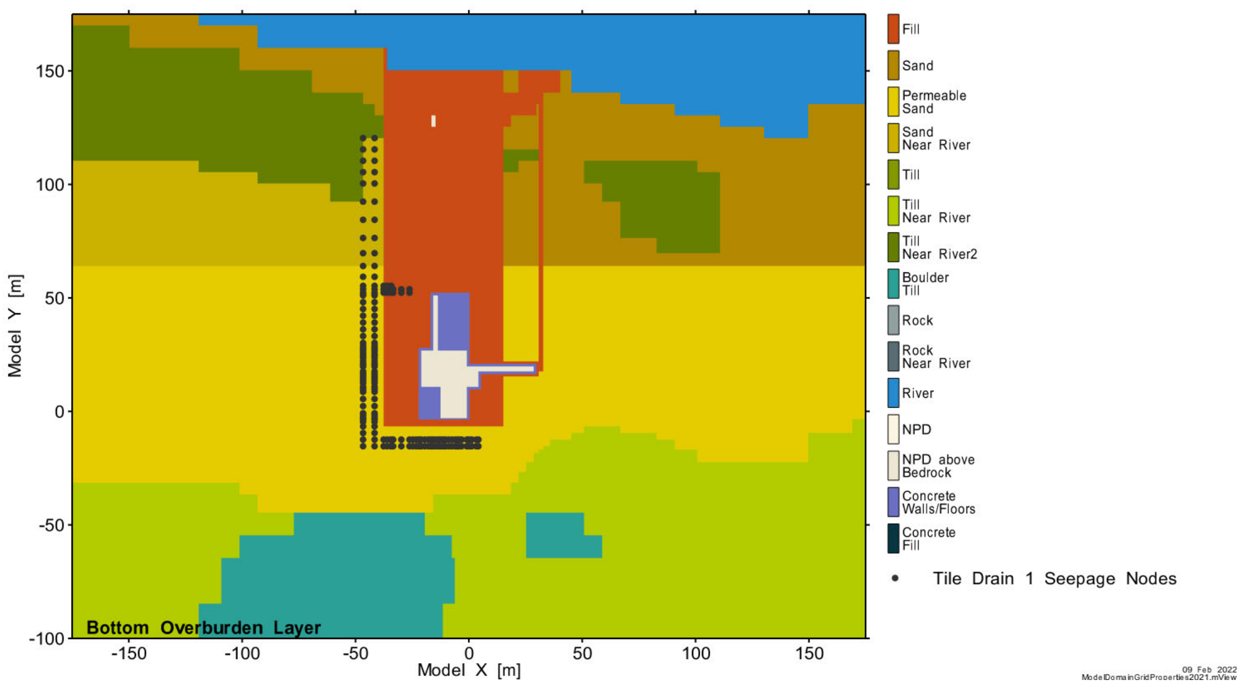

Figure 3-8 Location of Simplified Deep Section of Tile Drain 2 in Model

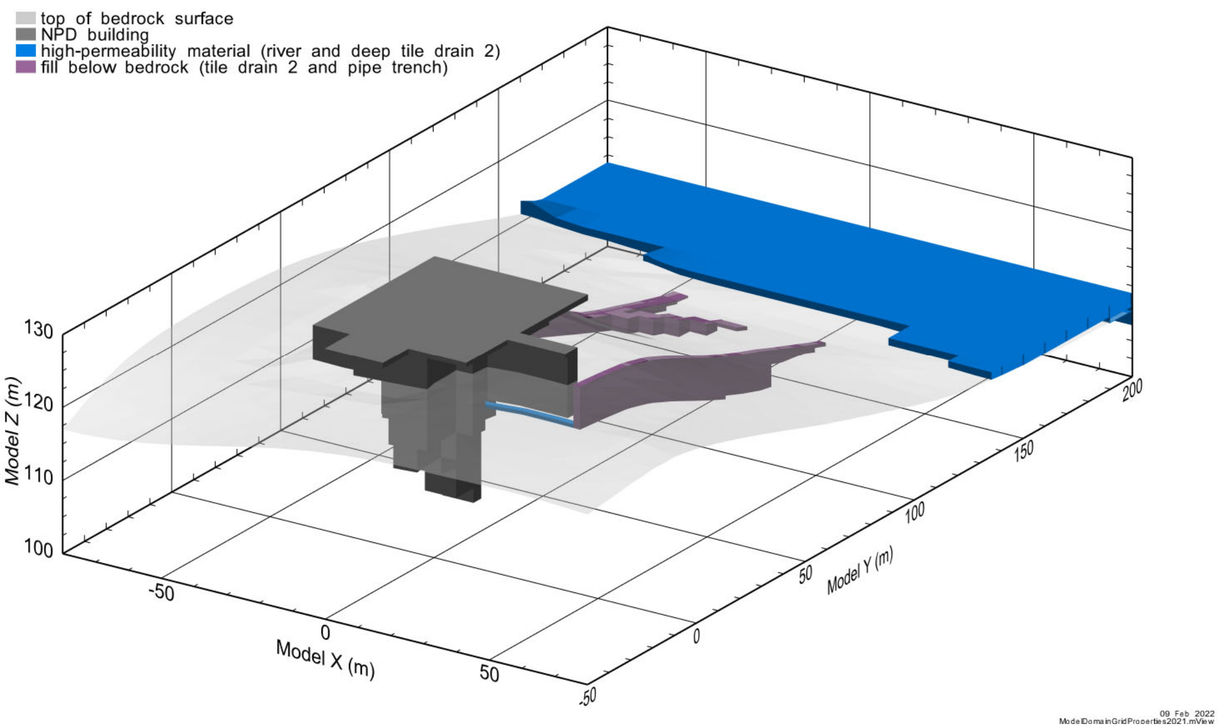

A constant head boundary condition was applied to a small wetland in the topographic low south of the highway, based on satellite photos and GIS data. Such a pond or wetland would collect runoff from the surrounding topography, which then can slowly seep into the groundwater. A similar boundary condition was applied to the wetland west of the facility. The locations of these two wetlands are shown in Figure 3-1 and Figure 3-3, with the boundary conditions defined by the inner wetland polygons.

Initial conditions assumed a constant head of 120 m where the head was not already specified by a boundary condition. Once the first initial simulation was complete, the results of this simulation were used as initial conditions.

3.1.6 Calibration Data

Two types of calibration targets were selected: measured water levels and tile drain flow measurements.

When selecting water levels for model calibration, water levels that are contemporaneous are preferred. An overview of the available water levels is provided within Section 2.2. The July 2014 water levels are the most complete data set with 22 water level measurements. The most recent water levels from Geofirma (December 2018 and January 2019) provide water levels in areas where they were previously absent, particularly in the till upgradient of the facility and within the shallow bedrock near the facility, and were also used for model calibration. Where the same wells are measured, the Geofirma water levels are between 0.4 and 0.7 m lower than July 2014 water levels, with an average difference of 0.5 m over the four wells.

While these two data sets are not contemporaneous, the differences where measurable are relatively small and together provide a greater spatial representation across the site in different hydrogeologic units. To improve their temporal representation for the steady-state model, the magnitude of water levels used as calibration targets were adjusted. July 2014 water levels were decreased by 0.25 m and December 2018/January 2019 water levels were increased by 0.25 m. Where the same well is measured, the July 2014 water levels are used, decreased by 0.25 m as the other wells in the July 2014 data set. Figure 3-9 shows the locations of water levels used for model calibration.

Figure 3-9 Location of Measured Water Levels Used in Model Calibration

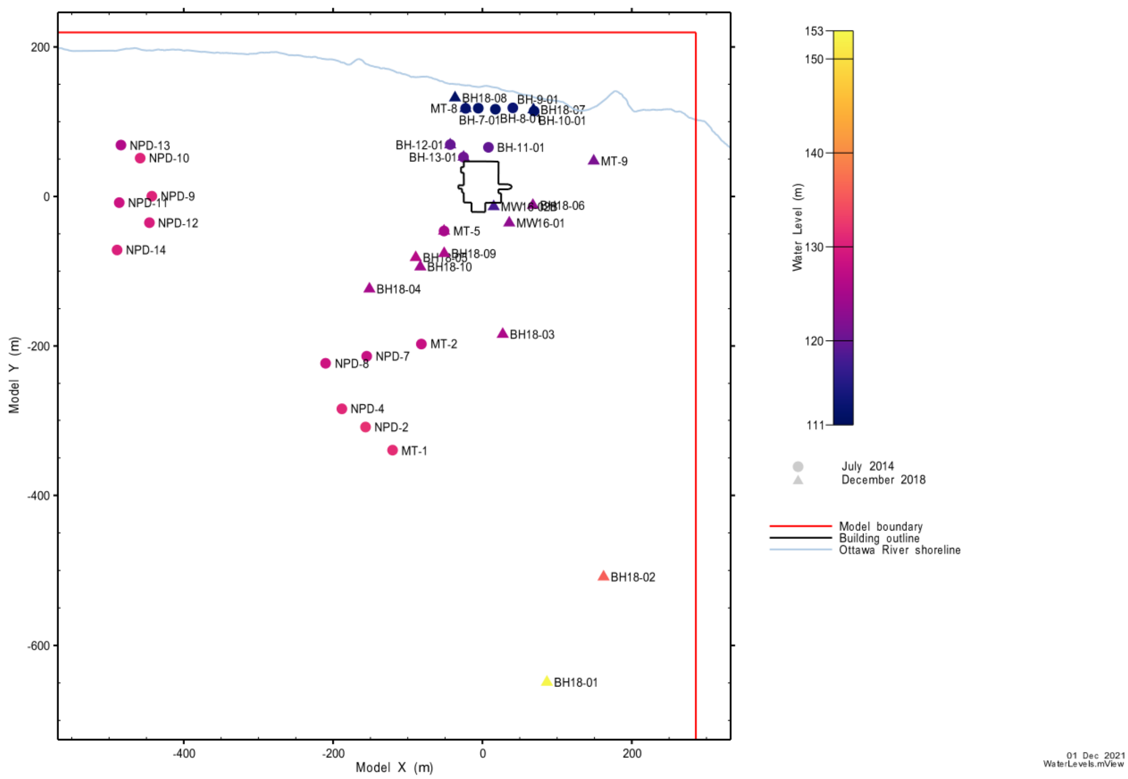

*Figure Note: two legends describe each water level symbol: the colour bar indicates the water level of the measurement, and the legend associates the shape of each water level symbol with the measurement date. The legend colours are grey, as the colour of each water level symbol can vary according to the colour bar.

The model had a second calibration objective: tile drain 1 flow at a steady-state estimate of 7.0 L/s. This is an annual steady-state estimate, and the calculation of this estimate is provided in Section 2.3 and Appendix C. This calibration objective was weighted by a factor of 1000, to place the magnitude of the residual in the tile drain flow in the same order of magnitude as water level residuals. Without such a weighting, the tile drain calibration objective would have no impact on the calibration.

Previous groundwater models were unable to calibrate to a high tile drain flow, due to the large catchment area required to obtain such a flow rate. In the early groundwater models, tile drain flow rates were approximately an order of magnitude lower than the current target of 7.0 L/s. Over the evolution of the groundwater models, the site characterization work and geosynthesis, it has been demonstrated that:

a) The magnitude of tile drain flow rate measurements are reasonable, based on alternate measurement methods and historical observations. Tile drain flows are discussed in detail within Section 2.3.

b) Water in tile drain 1 originates from the overburden. Other sources of water to the tile drains are limited. This is determined from geochemistry, as noted in Section 2.3 and the Geosynthesis Report (Raven *et al*. 2021).

c) The water balance for a groundwater model that only assumes a topographically driven overburden groundwater system has an insufficient amount of water to obtain the observed tile drain 1 flow rates. In a topographically-only driven overburden groundwater system at the NPD site, groundwater moves from topographic highs in the south-west towards the river in the north-east and the groundwater catchment area is similar to the surface water catchment. The surface water catchment containing the NPD facility is a smaller area than the total area modelled in the current groundwater model (see Figure 3-1). For this smaller catchment area, the sum of annual recharge over the catchment area (10 mm/yr over approximately 8.5E5 m^2 of till overburden and 400 mm/yr over approximately 1.6E5 m^2 of sand overburden results in 2.3 L/s, an overestimation as most of the sand area is downgradient of the tile drain) is significantly less than the annual average tile drain 1 flow rate (7.0 L/s). Based on this water balance, an alternate means of obtaining overburden groundwater must be available, in addition to topographically driven overburden groundwater.

d) The overburden is heterogeneous, particularly in the sand and gravel and till near the river, with expected layers of raised permeable washed alluvial-fluvial gravel occurring subparallel to the shoreline.

The current conceptual model extends the tile drain capture zone to the west of the facility, by assuming a permeable overburden feature parallel to the river. Further supporting the presence of this permeable unit is the documented dewatering of surface water (ponds, marshes) in this area during NPD construction and the very high hydraulic conductivity intervals (1 to 2E-03 m/s) observed at the top of bedrock and top of boulder till proximate to the tile drain (Raven *et al*. 2021). While the presence of this permeable overburden feature cannot be confirmed with existing data, it is currently the only explanation consistent with available data that can explain the high flow rates in the tile drains. Many other approaches to calibrating the model have been considered, as evidenced in previous versions of the groundwater model, without successful model calibration, and the high tile drain flowrates have been studied extensively to confirm their appropriateness as a calibration target. Consequently, the permeable overburden feature is considered the only approach currently available to successfully calibrate the model with high tile drain flow rates.

3.2 Calibration Results

Model calibration is completed with a scenario closely represented by present day conditions. Present day conditions allow the model to be calibrated to present day observations. The model is steady-state, and consequently does not consider transient processes such as resaturation or seasonal variations.

For convenience, the building is assumed to be filled with grout, while in actuality it is currently empty. Extensive modelling, both in previous versions of the model and in scenario cases for the current model, has shown that the materials in the building have negligible impact on flows exterior to the building.

The parameter estimation tool PEST++ uses the non-linear Gauss-Marquardt-Levenberg method to calibrate the model by adjusting specified parameters and running the model many times until the fit between model outputs and measured observations is minimized according to a weighted least squares method. All water level measurements are provided the same weighting; the tile drain measurement is weighted such that the magnitude of the residual is the same order of magnitude as the water level residuals.

Model parameters adjusted in the model calibration include hydraulic conductivity (k) for all overburden, overburden fill and bedrock materials. Both sand horizontal hydraulic conductivity and anisotropy ratio were calibrated. Initial hydraulic conductivity parameter values and ranges were presented in Table 3-2. Hydraulic conductivity for the NPD grout, facility concrete walls and floors, and concrete fill were fixed and not calibrated. The hydraulic conductivity of the concrete walls of the facility were calibrated with the resaturation model (Sgro, 2023). Grout properties cannot be calibrated as grout has not yet been emplaced. All other parameters, including infiltration, were fixed and not calibrated.

Calibration objectives include measured water levels, and, the average annual steady-state tile drain 1 flow rate, as described in Section 3.1.5. Modelled and observed water levels were compared by extracting the model water level at the borehole XY location of the observed water levels.

A good match to observed water levels across the site was obtained for the calibration. The tile drain 1 flowrate for the calibrated model is 7.0 L/s, equal to the calibration objective of 7.0 L/s. Figure 3-10 shows a cross plot of modelled and observed water levels for the calibrated model, along with water level calibration statistics. A similar plot, Figure 3-11, shows water level residuals compared to observed water levels. Calibration statistics include the root mean square of residuals, which is derived from the sum of least squares, the value minimized during calibration. The smaller the root mean square of residuals, the better the fit. A normalized root mean square less than 5% is indicative of a strong calibration, and for this calibrated model this statistic is 3.4%. Calibration statistics alone do not indicate a good fit. The consistent fit across the model, at water level measurements near the river (low head) and far (high head), is another indicator of good fit. Residuals are consistent across the model, as shown in both Figure 3-10 and Figure 3-11. Particular fit outliers are discussed below.

Figure 3-10 Cross-plot of Modelled and Observed Water Levels

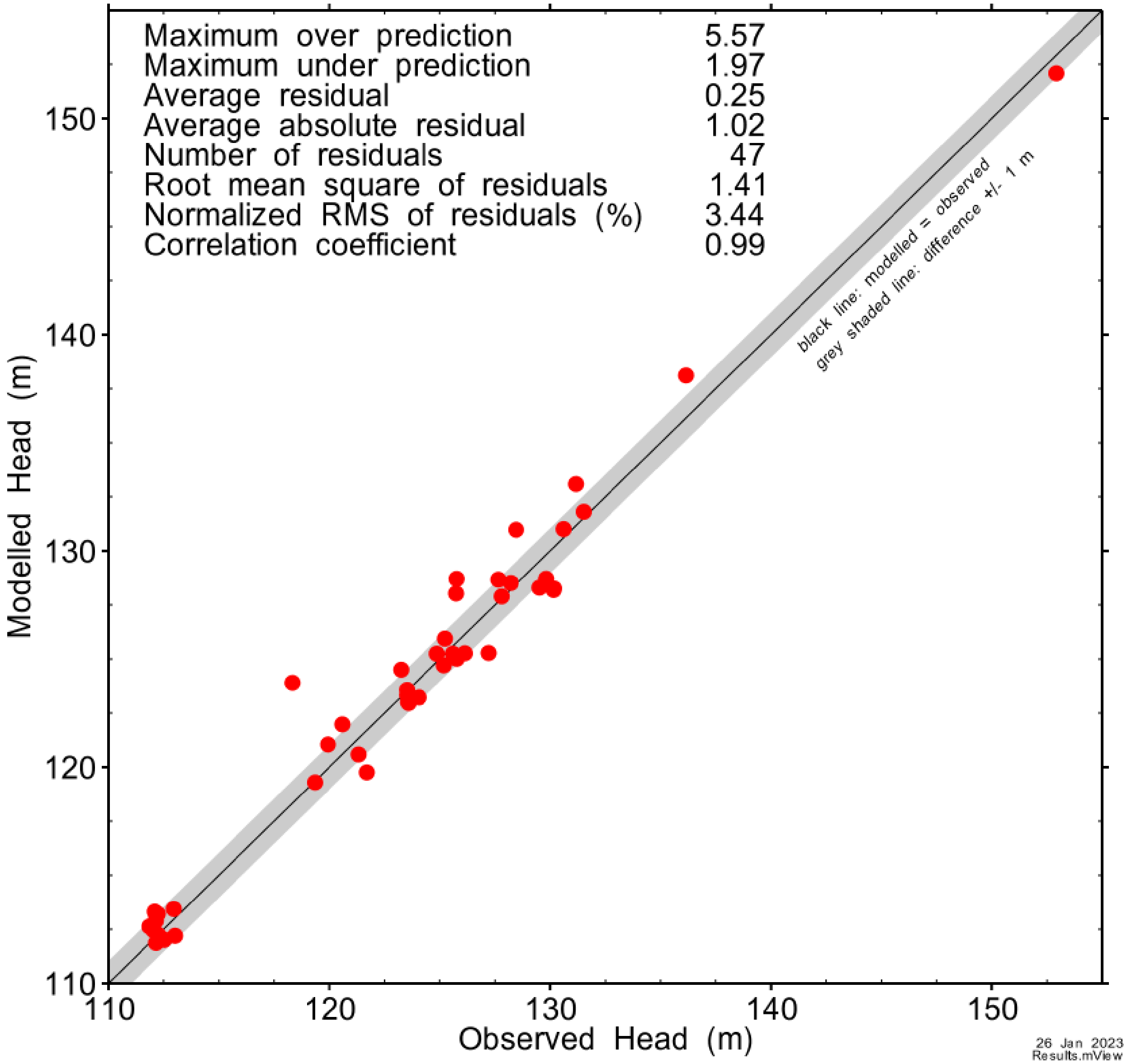

Figure 3-11 Residual Water Levels (Observed - Modelled) vs Observed Water Levels

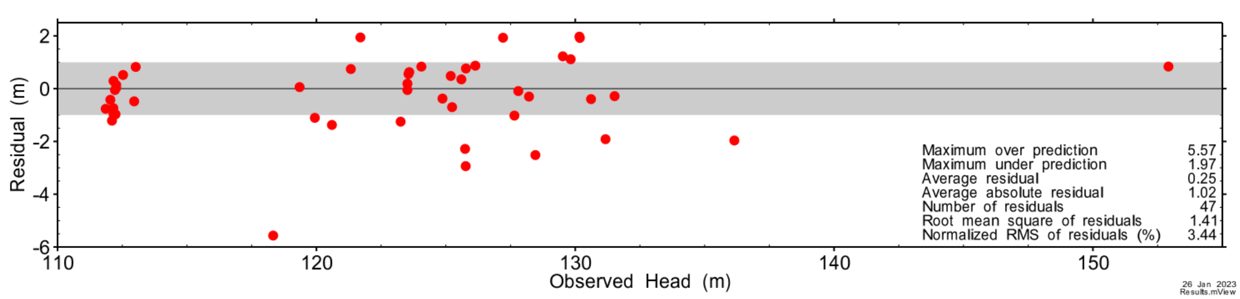

Figure 3-12 shows the modelled water table elevation, compared to point observations. Figure 3-12 also compares modelled water table contours to contours kriged from the point observations of water levels. It is not expected to get a perfect match between the two sets of contours, due to the different methods used to generate the contours. Modelled contours provide a more physically realistic set of contours than those generated from a kriging algorithm. However, it is expected that the general trend in direction and gradient of the water table contours is similar between the two sets of contours, and that there is a strong similarity in the vicinity of observation points. The calibrated model contours meet this expectation in comparison to the kriged water table contours. Near the wells south-west of the facility there is a relatively large difference in the contours; however, the water levels in this area are quite flat, with model water levels in the order of 0.5 m greater than observed.

In both Figure 3-10 and Figure 3-12, there are single observation wells that are outliers to the calibration. One well in particular (BH16-02B – see Figure 2-3 for well location) has a residual of 5.82 m. The observed water elevation is 118.3 m, compared to a modelled water elevation of 124.1 m. A previous water level elevation observed at this well in April 2017 was 122.8 m. Near-by water elevations in the bedrock (BH18-06) are between 123.5 and 124.1, and this large discrepancy suggests that the water elevation target at BH16-02B is likely in error. All other wells have residuals of 3 m or less.

The calibrated hydraulic conductivities, and their sensitivity to calibration, are outlined in Table 3-3. Values are listed from most sensitive to least sensitive parameter. Mean sensitivity is a statistical measure of the importance of specific calibrated parameters to the final model solution, calculated from a composite of the derivatives of model-generated observations (water levels and tile drain 1 flow rate), and adjusted by the weight attached to each observation. As calibration objectives include the high tile drain 1 flow rate, which is influenced by overburden, particularly sand, and many water levels are observed in the sand, the hydraulic conductivities of the three different types of sand are the most sensitive parameters.

Figure 3-12 Plan View of Modelled and Observed Water Levels

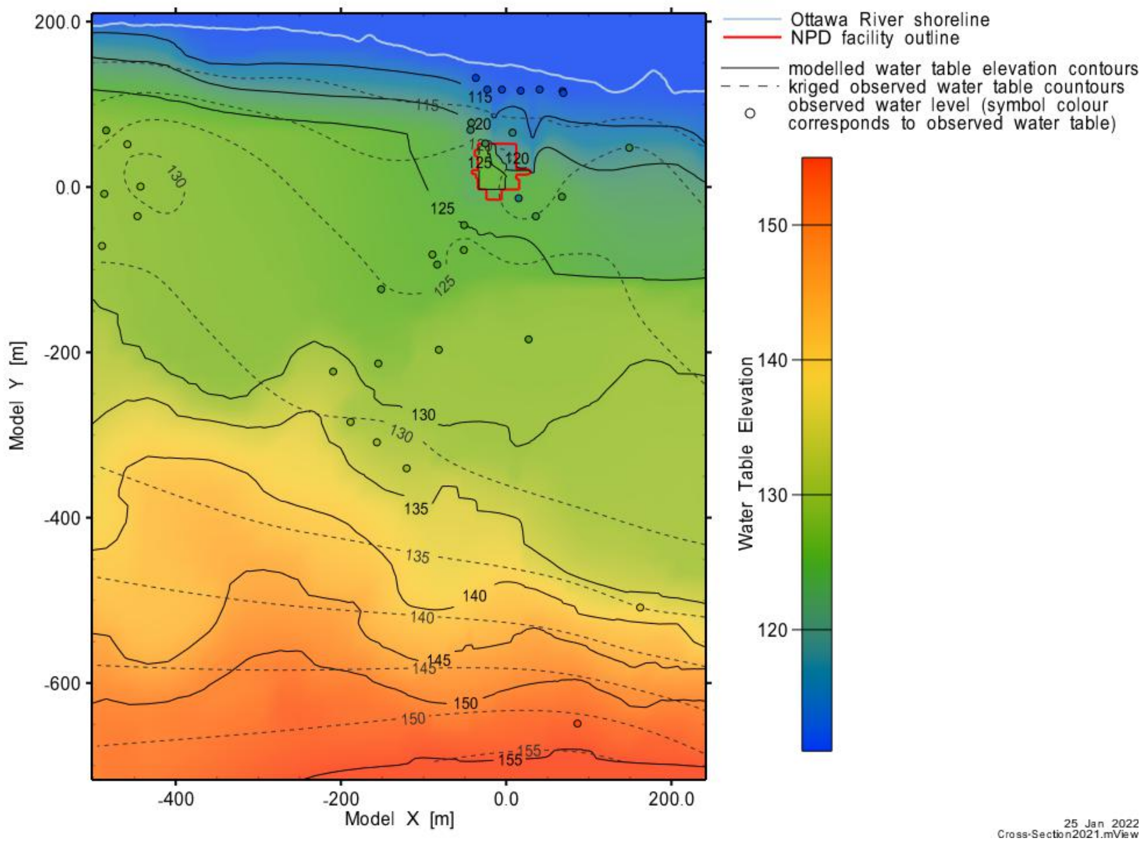

Table 3-3 Final Calibrated Material Hydraulic Conductivities and Parameter Sensitivity

Calibrated Parameter	Final Calibrated Value	Mean Sensitivity x 100
Sand Horizontal k (m/s)	1.0×10^{-3}	153
Sand Near River Horizontal k (m/s)	1.8×10^{-5}	122
Permeable Sand Horizontal k (m/s)	6.1×10^{-4}	90
Till Near River 2 k (m/s)	3.6×10^{-5}	28
Rock Near River k (m/s)	1.7×10^{-7}	17
Rock k (m/s)	5.0×10^{-8}	12
Till Near River k (m/s)	5.0×10^{-4}	9
Till k (m/s)	7.8×10^{-9}	5
Fill k (m/s)	1.0×10^{-3}	2
Sand Anisotropic Ratio	9.96	0.3
Boulder Till k (m/s)	3.9×10^{-5}	0.2

Materials with little sensitivity to the model, including the fill, till, boulder till and vertical sand anisotropy, indicate materials that may vary substantially with little impact on the calibration results. Limited impact on calibration results does not mean that a change in the parameter value would not have a more substantial impact on simulation results, such as flow and transport between the facility and the river. The fill hydraulic conductivity in particular may have an impact on simulation results, as it is the primary overburden material between the facility and the river. A sensitivity case investigating fill conductivity is provided in Section 5.2.

Figure 3-13 compares final calibrated conductivities to measured conductivities for overburden materials, and the three types of sand are in the upper range of measured sand hydraulic conductivities. Calibrated fill conductivity is greater than the single measurement, although this is not unexpected given that the single measurement is for a small interval at the bottom of the borehole, and is expected to represent the lower end of the range of potential values. The calibrated fill has the same conductivity as the native sand material, and the model calibration was relatively insensitive to the fill conductivity. Model till conductivities are within the suggested range for these parameters, with till near the river slightly higher than the suggested range of $2x10^{-5}$ to $2x10^{-4}$ m/s at $5.0x10^{-4}$ m/s. The range allowed during calibration is larger than the suggested range to allow for the fact that a value slightly greater or less than the estimated range is reasonable. The primary till material hydraulic conductivity is low, but within the measured range for till and was also relatively insensitive to model calibration.

Figure 3-13 Comparison of Calibrated Conductivities to Measured Conductivities for Overburden Materials

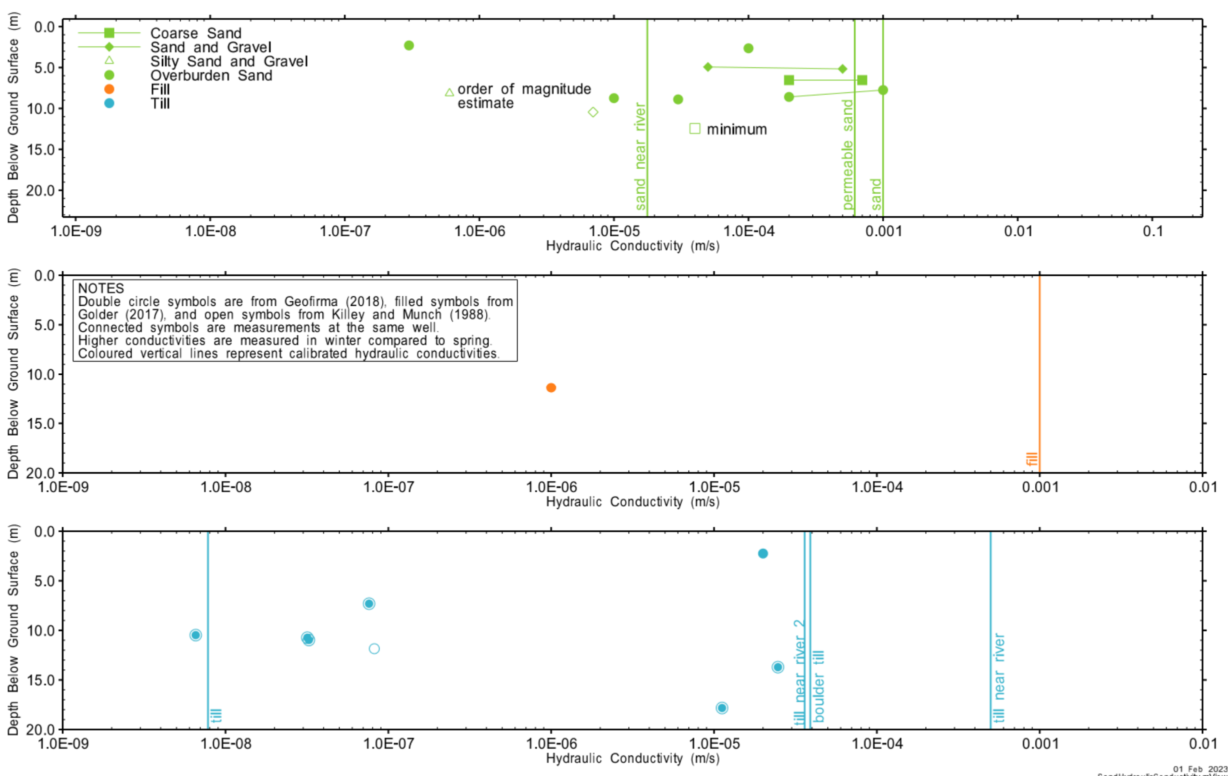

Head and velocity results for the model calibration are shown for a plan view in Figure 3-14, a plan view focused on the facility in Figure 3-15 and for cross-sections through three slices within the model in Figure 3-16, one through the middle of the pipe trench, and one either side of the NPD facility. Velocity magnitudes are shown at the same three slices within the model in Figure 3-17. Note that the slight waviness in the water table is due to grid discretization. As expected, water drains towards the overburden fill and tile drains surrounding the NPD facility. While the water table is generally near the surface of the bedrock, in some places, particularly downgradient of the facility where there is a large elevation change, the water table drops below the bedrock surface. The dry section of the tile drains (i.e., the shallow section of tile drain 2) east of the facility demonstrate that the water table does occasionally dip below bedrock surface.

Figure 3-14 Plan View Showing Calibrated Model Water Table Elevations and Velocities

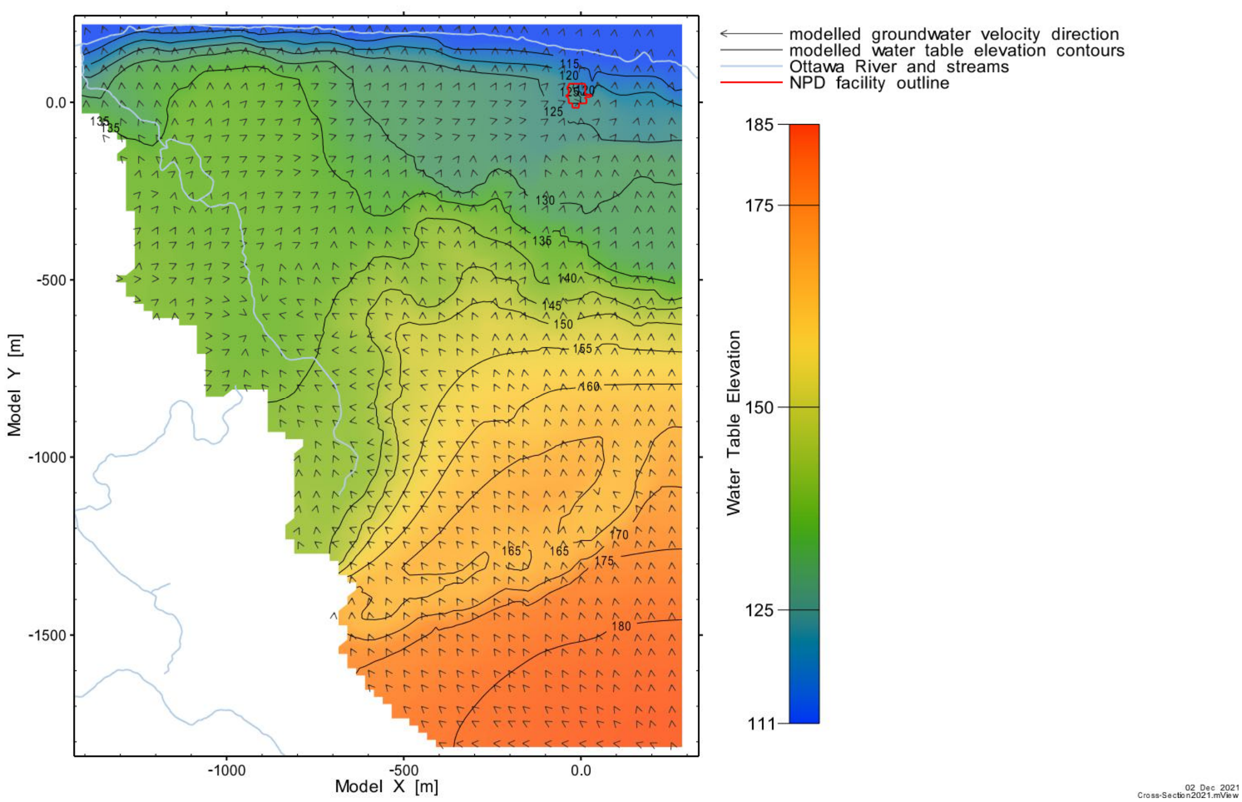

Figure 3-15 Plan View Focused on the Facility Showing Calibrated Model Water Table Elevations and Velocities

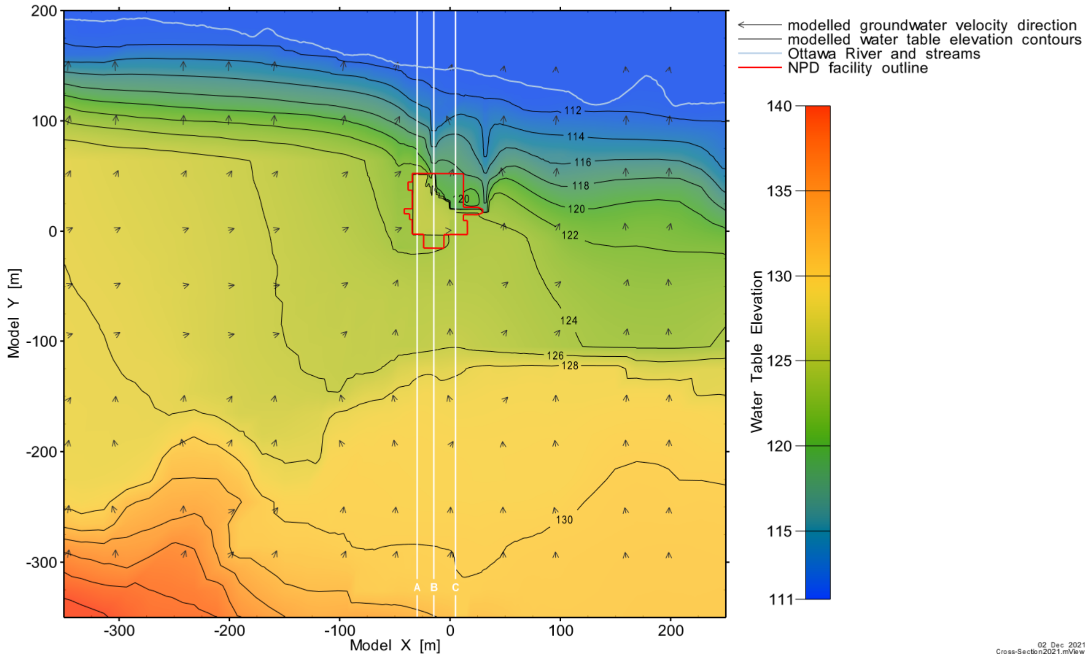

Figure 3-16 Cross-sections Showing Calibrated Model Head Contours, Velocities and Water Table

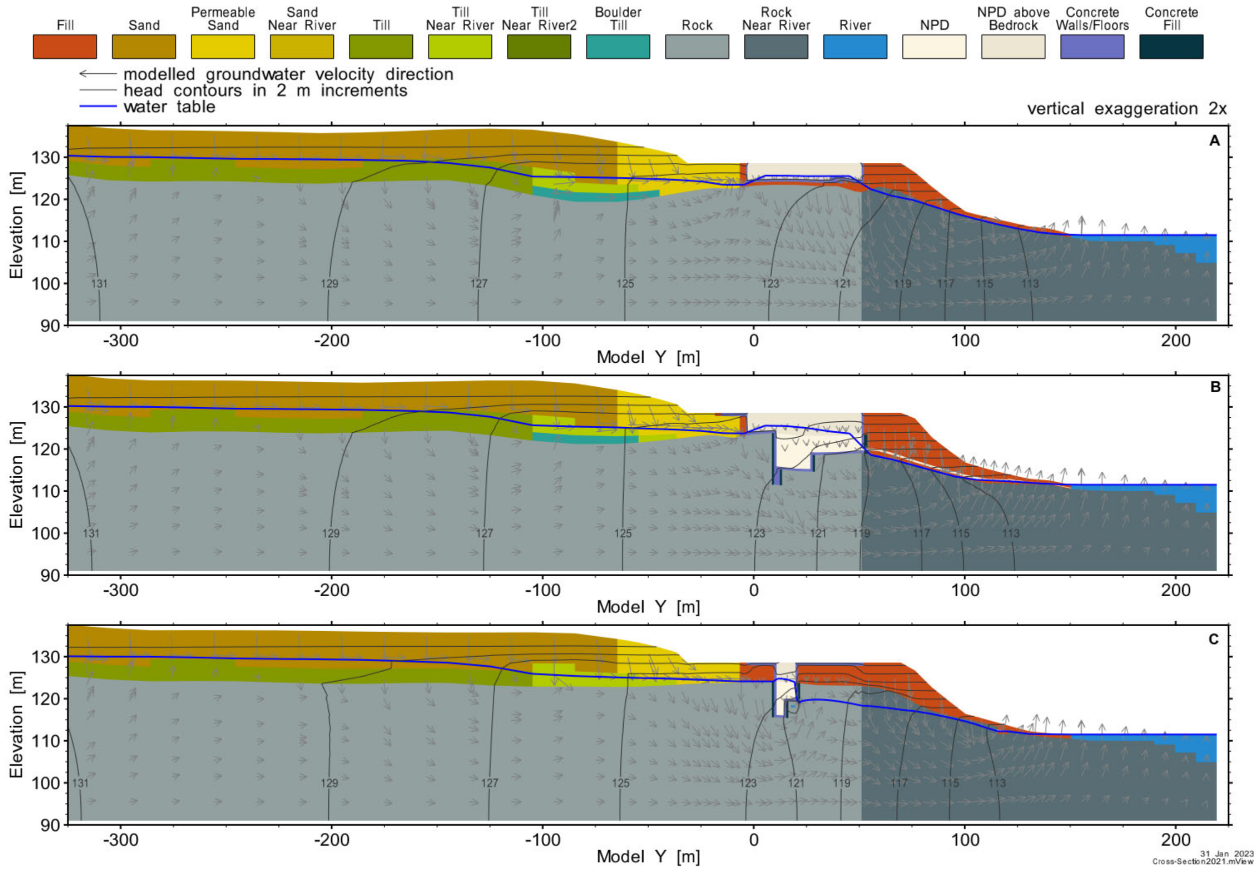

Figure 3-17 Cross-sections Showing Calibrated Model Velocity Magnitudes, Head Contours and Water Table

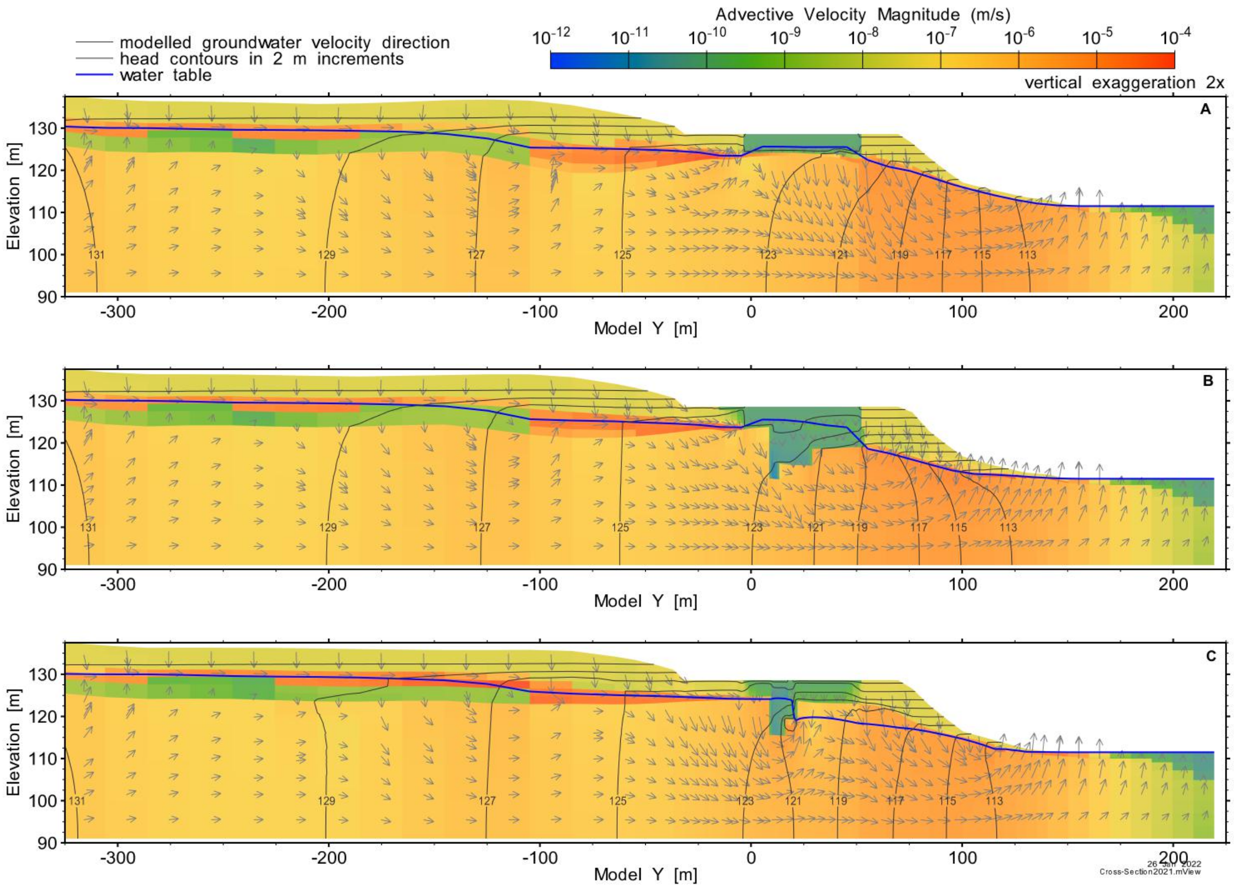

It should be emphasized that model calibrations are generally not unique, and that this model calibration represents one "best" parameter set for the conceptual model described (including parameter ranges) and the data available. It may be possible to obtain a similar calibration with an alternate conceptual model and/or additional data, or an improved calibration with different parameter ranges. The current calibrated model provides a reasonable description of the groundwater flow at the site, based on the data available, and is acceptable based on the following performance measures:

- **Model convergence:** The model convergence criteria for the calibrated model was 10^{-8}, well below an acceptable maximum change in heads.

- **Model water balance:** The water mass balance for the calibrated model is effectively zero: all water that enters the model exits the model, with a relative error $2x10^{-6}$ %, indicating a numerically stable simulation. The amount of water entering and exiting the model water balance are shown in the following table. The model represents steady-state flow, with inputs (recharge) and outputs (tile drain flowrate) representing annual average values.

Table 3-4 Calibrated Model Water Balance (m^3/s)

	Flow In	Flow Out
Fixed Head (wetlands)	0.0038230449	-
Fixed Head (Ottawa River)	-	0.0160276069
Infiltration	0.0192056435	-
Tile Drain 1	-	0.0070010820
Total	0.0230286884	0.0230286889

- **Qualitative measures:** As previously discussed in this section, estimated parameters are reasonable and within the expected range, and model results, based on head contours and flow patterns, are similar to those anticipated.
- **Quantitative measures:** As previously discussed in this section, the goodness of fit between modelled and measured water levels and the tile drain 1 flow rate is good, both spatially and based on calibration statistics.
- **Model verification:** As will be discussed in the following sub-section, verification of the model calibration was successfully undertaken to increase confidence in the groundwater model's ability to represent groundwater flow conditions at the NPD site.

3.3 Model Verification

Model verification was undertaken to test the calibrated model's ability to represent groundwater flow conditions at the NPD site. The calibrated model is a steady-state model based on present day conditions and average annual infiltration and average annual tile drain 1 flow rates. The verification case takes the calibrated model and modifies infiltration to the average annual infiltration for a specific year, 2019, and anticipates obtaining a tile drain 1 flow rate equivalent to the annual average tile drain 1 flow rate for that same year. 2019 was selected as the verification year due to the extensive tile drain 1 flow measurements in 2019; in 2019, tile drain 1 flow rates were measured continuously using an ultrasonic flow meter and monthly with the dye dilution method.

In 2019, average annual infiltration is 995 mm/yr, based on the Petawawa Hoffman Environment Canada weather station. This weather station is the closest to NPD with complete data; the Chalk River weather station has substantial missing data in 2019. The same proportion of infiltration is assumed as the calibrated case, and infiltration into the sand is assumed to be 463 mm/yr. Till infiltration is the same at 10 mm/yr, as infiltration into the till is limited by the low conductivity of this material. The average tile drain flow rate for 2019 based on the dye dilution measurements is 7.8 L/s.

With this alternate infiltration as input, the resulting tile drain 1 flow measurement obtained by the model is 7.8 L/s, the same as the measured average tile drain flow 1 rate. The verification rate improves confidence in the calibrated model, showing that a 15% increase in infiltration results in the expected tile drain 1 flow rate increase of approximately 12%.

Increasing infiltration had a small effect on the heads in the model. At the location of measured water levels (and calibration targets), water levels were on average 0.24 m higher in the verification case compared to the calibration case, with the change to head almost zero near the river, and as great as 0.72 m farther from the river.

4 SCENARIO CASES

Scenario cases are a set of conditions provided to the groundwater model to support specific scenarios developed for the Post SA. Table 4-1 outlines the scenario cases provided in this report. NES refers to the Normal Evolution Scenario in the Post SA. Note that all models are steady-state and fundamentally based on the calibrated model. A particular time frame or set of time frames is modelled for each scenario, with constant conditions in the model representative of the conditions assumed to be present during that time frame. One of three different sets of conditions are considered, each representing a specified time frame:

- Initial conditions with expected facility hydraulic conductivities and active tile drains. In the Post SA models, these conditions are representative of the first 100 years.
- Degraded cap conditions assume that the concrete cap and the geosynthetic clay liner (GCL) in the cover have degraded (hydraulic conductivity of 10^{-8} m/s), and tile drains are degraded and inactive. In the Post SA models, these conditions are representative of 100 to 1000 years. Cases with these conditions include **Degraded Cap** in the case name.
- Degraded conditions assume that the facility structure, both concrete and grout, as well as the concrete cap and the GCL in the cover, have degraded (hydraulic conductivity of 10^{-8} m/s), and tile drains are degraded and inactive. In the Post SA models, these conditions represent times after 1000 years. Cases with these conditions include **Degraded** in the case name.

Table 4-1 Scenario Cases

Case	Description
NES	Same as calibrated model, with pipe trench pipes grouted and infiltration updated based on resaturation model results. Intact cap, structure and tile drains. No well present.
NES – Degraded Cap	Same as NES case, but with degraded cap and degraded tile drains.
NES – Degraded	Same as NES Degraded Cap case, but with a degraded structure.
High Bedrock Hydraulic Conductivity	Same as NES model, but with bedrock hydraulic conductivity increased to highest measured value, 6.6 x 10^{-6} m/s (Raven et al. 2021). Both bedrock and bedrock near the river are changed to this value.
High Bedrock Hydraulic Conductivity – Degraded Cap	Same as High Bedrock Hydraulic Conductivity case, but with degraded cap and degraded tile drains.
High Bedrock Hydraulic Conductivity – Degraded	Same as High Bedrock Hydraulic Conductivity Degraded Cap case, but with a degraded structure.

Case	Description
High Overburden Hydraulic Conductivity	Same as NES case, but with fill hydraulic conductivity increased to one order of magnitude greater than the calibrated model, 1 x 10^{-2} m/s.
High Overburden Hydraulic Conductivity – Degraded Cap	Same as High Overburden Hydraulic Conductivity case, but with degraded cap and degraded tile drains.
High Overburden Hydraulic Conductivity – Degraded	Same as High Overburden Hydraulic Conductivity Degraded Cap case, but with a degraded structure.
Fault Zone Activation	Hydraulic conductivity in the bedrock is increased by one order of magnitude (5x10^{-7} m/s in bedrock, 1.7x10^{-6} m/s in bedrock near river), to simulate activation of a fault zone in the bedrock. The facility is also assumed to be extremely degraded: grout and concrete is extremely degraded (10^{-6} m/s). GCL in cover is also extremely degraded (10^{-6} m/s), so as not to provide a barrier and allow evaluation of the impact of facility degradation. Tile drains are degraded and inactive.
Overburden Well – Degraded Cap	A well completed in the overburden is added to the NES Degraded Cap case.
Overburden Well – Degraded	A well completed in the overburden is added to the NES Degraded case.
Bedrock Well – Degraded Cap	A well completed in the bedrock is added to the NES Degraded Cap case.
Bedrock Well – Degraded	A well completed in the bedrock is added to the NES Degraded case.
Extreme Concrete Degradation	Same as NES case, but concrete structure is extremely degraded (10^{-6} m/s).
Extreme Concrete Degradation – Degraded Cap	Same as Extreme Concrete Degradation case, but with degraded cap and degraded tile drains.
Extreme Concrete Degradation – Degraded	Same as Extreme Concrete Degradation Degraded Cap case, but with a degraded structure.
Extreme Grout Degradation	Same as NES case, but grout is extremely degraded (10^{-6} m/s).
Extreme Grout Degradation – Degraded Cap	Same as Extreme Grout Degradation case, but with degraded cap and degraded tile drains.
Extreme Grout Degradation – Degraded	Same as Extreme Grout Degradation Degraded Cap case, but with a degraded structure.

4.1 Modelling Approach

Scenario case models are based on the calibrated model, using the same code, discretization, properties, boundary conditions and initial conditions described in Section 3.1, with the following clarifications and exceptions:

- Geosphere hydraulic conductivities are the final calibrated values described in Section 3.2 and listed in Table 3-3.

- The pipes in the pipe trench are filled with a grout with the same properties as the grout above bedrock. In the calibrated model, these model elements have the same properties as fill. Figure 4-1 shows the location of the grouted pipes.

Figure 4-1 Cross-section Showing Material Property Assignment for Scenario Cases

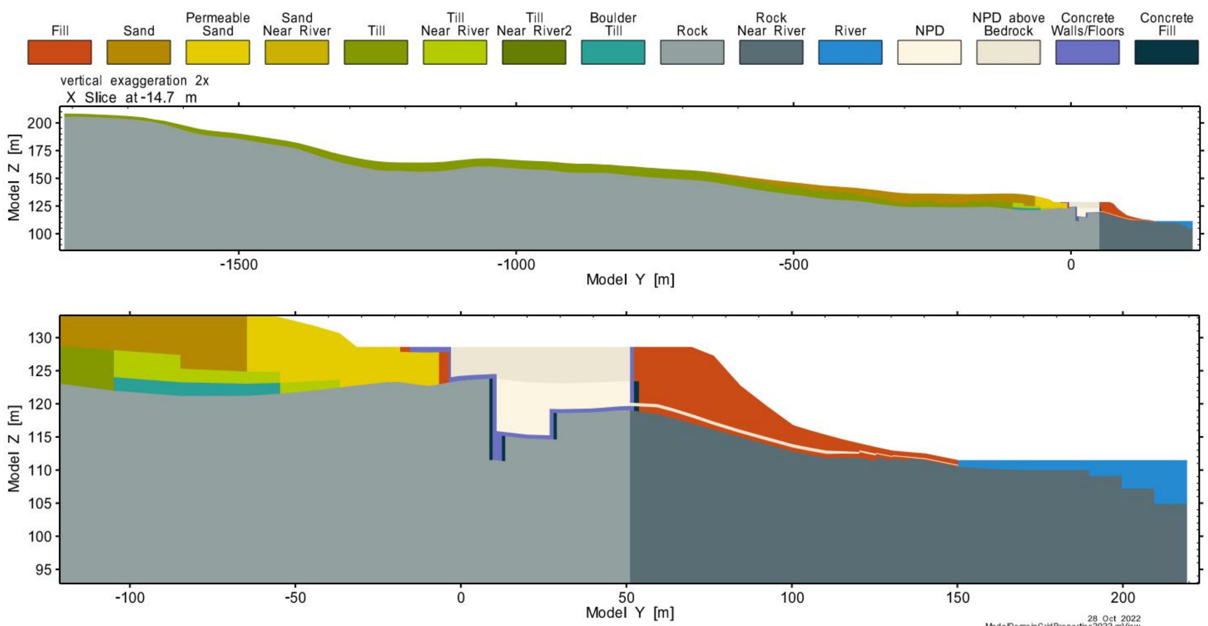

- Infiltration into the building is specified by the values obtained in the resaturation model, for comparable cases. Values of infiltration used are described for each case. The value of infiltration over the building area changes for each scenario case, estimated by the resaturation model which includes details of the engineered cap and cover. The resaturation model found infiltration over the building to be substantially reduced compared to the 1 mm/yr assumed for the calibrated model, less than 10^{-3} mm/yr for the Normal Evolution Scenario (NES). The engineered cap and cover in the scenario cases has four zones with different infiltration: infiltration through the engineered cover and concrete cap and into the building (**cap**); infiltration through the engineered cover and into the building where the concrete cap is not present (**building, not cap**); infiltration through the engineered cover and into the overburden surrounding the facility (**cover, not building**); and, infiltration through the edges of the cover. Figure 4-2 shows the location of these four infiltration zones used in the scenario modelling.

Figure 4-2 Location of Infitlration Zones beneath the Engineered Cover and Conrete Cap for Scenario Cases

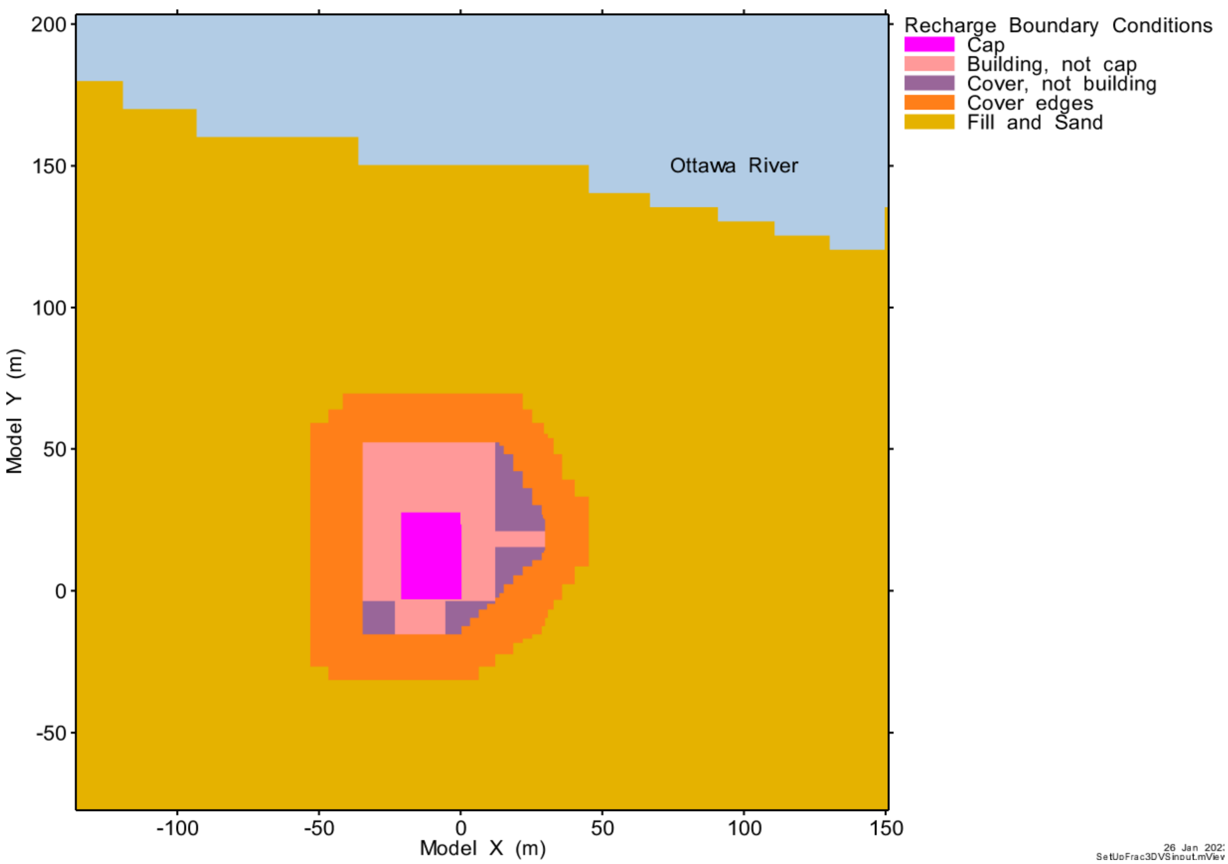

- The tracer plume simulated by the initial near-field model simulations (Calder 2023) hit the bottom of the model grid. To improve the representation of tracer transport, the elevation of the bottom of the near-field model was reduced to 80 m, adding another ten meters to the bottom of the model. As the groundwater model provides boundary conditions to the sides of the near-field model, the elevation of the bottom of the groundwater model was also reduced to 80 m. This change has a minor impact on the groundwater flow system, as shown by the water table and head contours shown in Figure 4-3. The impact on the calibration targets is also negligible, as shown in Figure 4-4. Note that this comparison is made with a post-calibration model, i.e. grouted pipe trench and infiltration rates based on resaturation model, which is slightly different from the calibrated case shown in Section 3.2. The water level at BH16-02B, previously identified to likely be in error, has been removed from the calibration statistics.

Figure 4-3 Cross-sections Showing Difference in Water Table and Head Contours with Increased Depth of Model

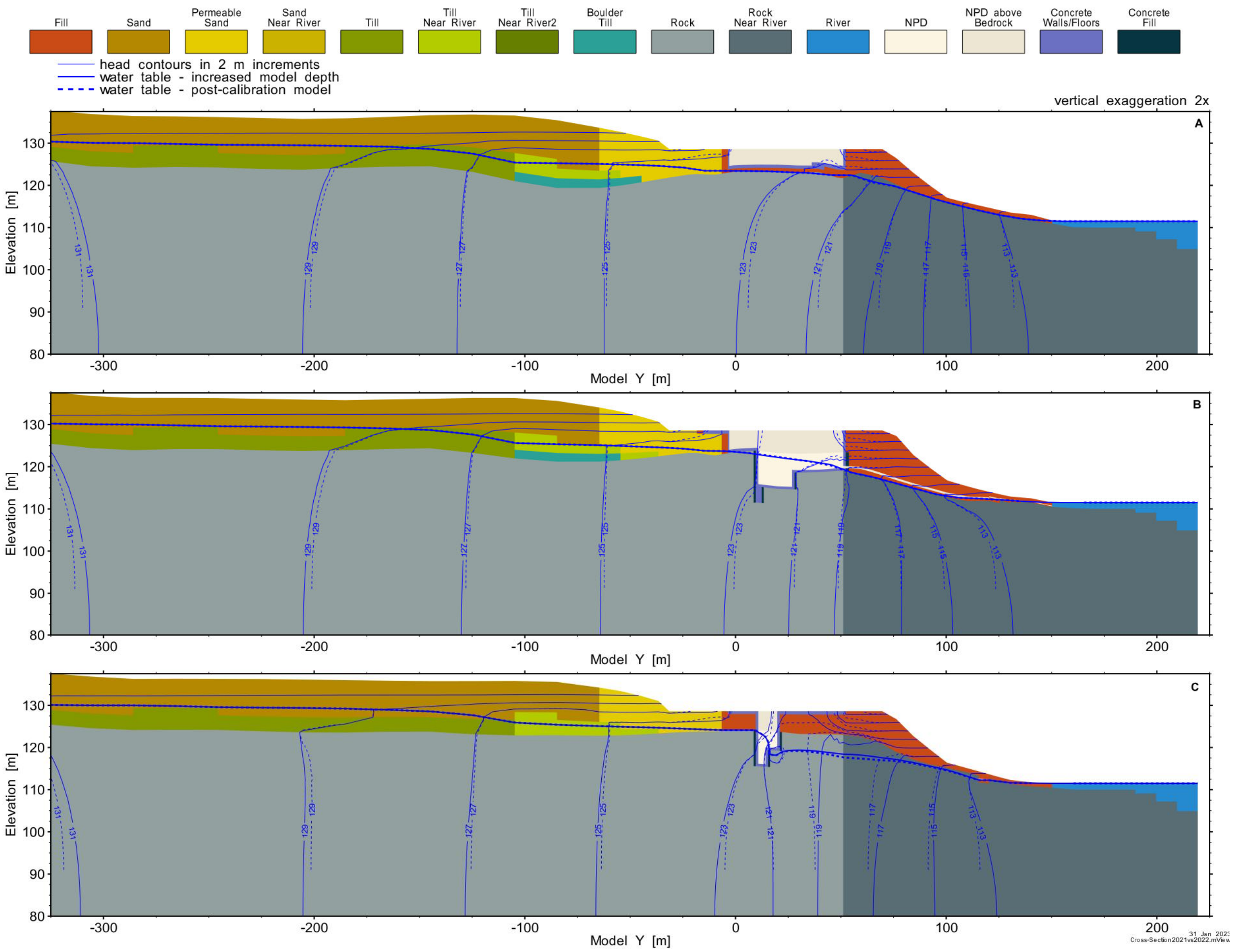

Figure 4-4 Cross-plot of Modelled and Observed Water Levels, for models with and without increased depth

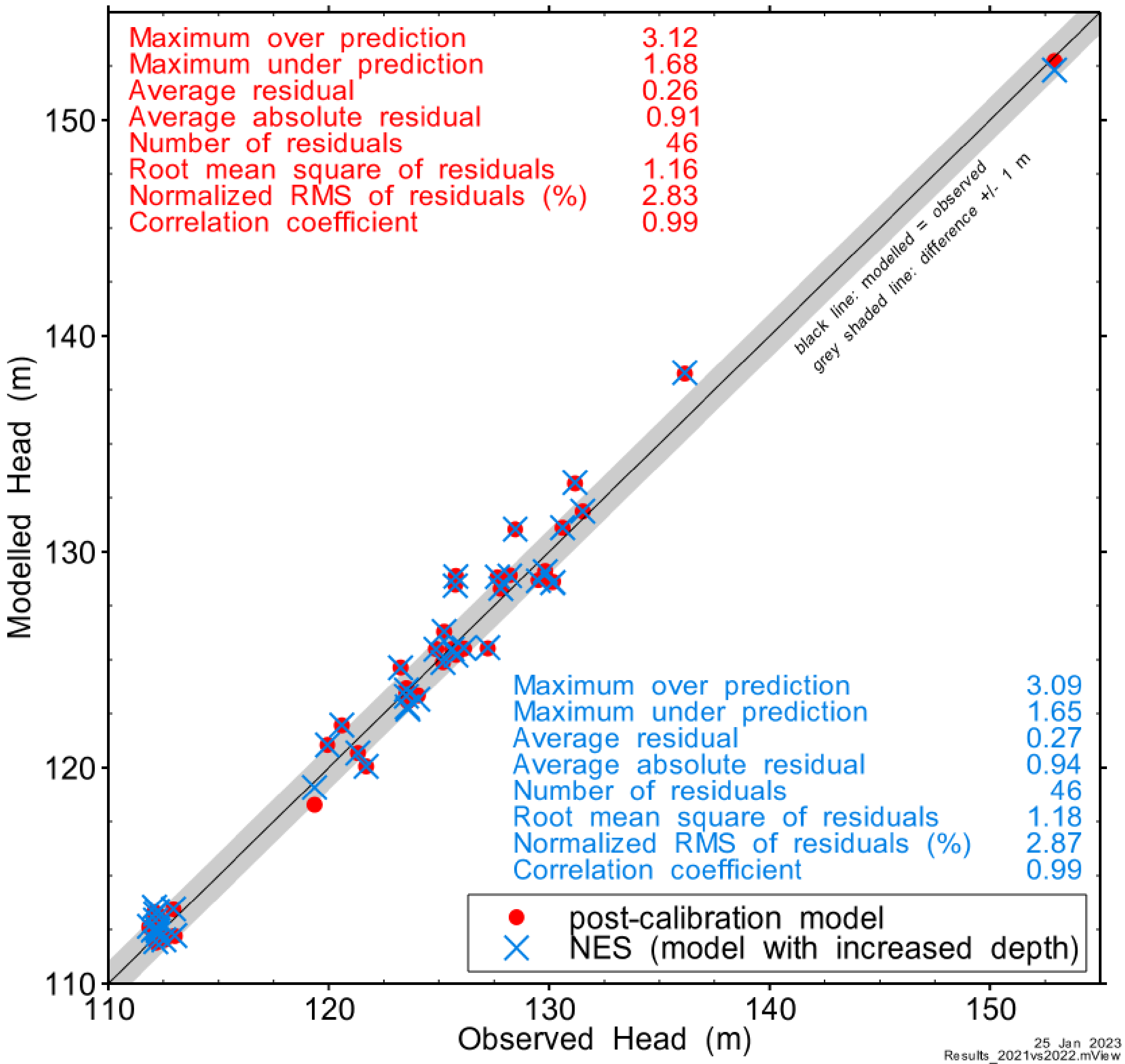

- Model attributes modified as needed to simulate each scenario, as specified for each scenario case. The NES (0 to 100 years) case has no changes to the model set-up other than the modifications specified above.

4.2 Groundwater Flow Calculations

For all scenario cases, post-simulation groundwater flows were calculated for two locations: (1) entering and leaving the area surrounding the facility, and (2) entering and leaving the building itself. The first calculation provides an indication of the flow field in the area surrounding the facility, from the top to the bottom of the model, whereas the second calculation provides values seeping into and out of the concrete walls and floors of the facility. Post-simulation flow calculations calculate flows across specified surfaces using the velocities calculated and output by the model. These post-simulation flow calculations were restricted to flows in saturated grid elements below the water table. Both groundwater flow calculations include water entering across the top of the saturated elements, referred to as recharge rather than infiltration. Infiltration refers to flow entering the top of the ground surface, whereas recharge refers to flow entering the top of the saturated groundwater system. Figure 4-5 shows the location of the boundaries used in post-simulation groundwater flow calculations.

Note that while the overall water mass balance error for the models is very low ($2x10^{-6}$ %), there is a water mass balance error in these post-simulation groundwater flow surface calculations attributed to the calculation method. FRAC3DVS velocity output is element based, calculated as the average nodal velocity of the element. Accuracy is lost when the post-simulation flow calculations consider these average elemental velocities, rather than the velocities of interest across element faces. For steady-state flow, it is expected that all flow entering the flow calculation boundary equals all flow leaving the flow calculation boundary, but the calculations for the NES case show that an excess of approximately 6.8% of groundwater flow leaves the flow calculation boundary. Smaller mass balance errors are observed for flow through the building for the NES, approximately 0.9%. In all scenario cases, the mass balance error is less than 6.8%.

Groundwater flows are provided for each scenario and sensitivity case described below. Particle tracks are also provided for NES case (Section 4.3.1.1), a simulation case similar to present day conditions but with facility decommissioning complete, to provide further insight into flow patterns at the NPD site.

Figure 4-5 Plan Slice Through Bottom of Overburden Showing the Flow Calculation Boundaries

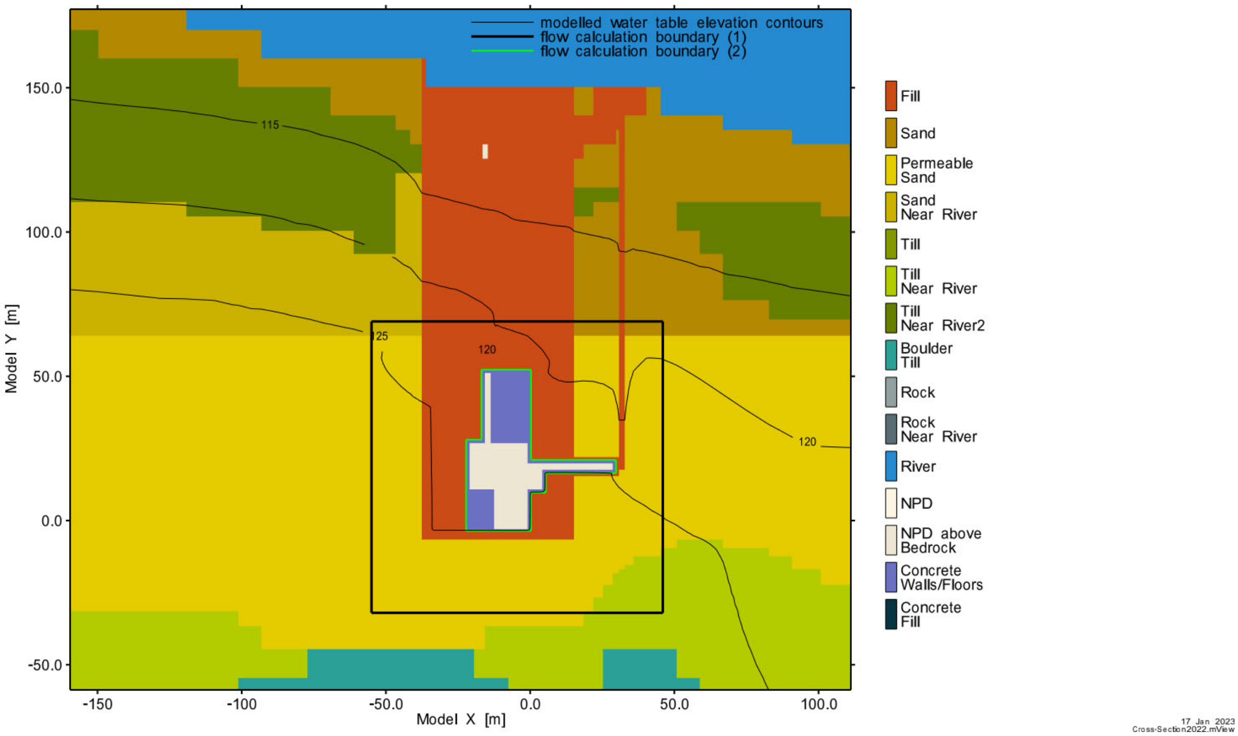

4.3 Model Results

4.3.1 NES (0 to 100 years)

This case is similar to the calibrated model, with the conceptual difference of grouted pipes in the pipe trench. Grout in the pipes has the same properties as the grout above bedrock in the facility.

As the engineered cover and cap are not represented in the groundwater model, infiltration over the areas under the cap and cover were calculated from the resaturation model (Sgro, 2023). The infiltration rates applied to the groundwater model for the NES (0 to 100 years) scenario are 10^{-3} mm/yr for areas under the cap and cover, and 571 mm/yr at the edges of the cover. Note that the resaturation model calculated lower infiltration rates under the cap and cover. Any calculated infiltration value below 10^{-3} mm/yr, a value that is effectively zero, is assumed to be 10^{-3} mm/yr in the model. This is a conservative and yet realistic approach: it limits any uncertainty associated with very small infiltration values, yet provides a value that is effectively zero. Infiltration at the cover edges exceeds the value applied to the cover of the surface as it includes water that has travelled over the top of the less permeable layers of the engineered cover, but under the ground surface, and infiltrated into the ground at the edges where the cover ends.

Table 4-2 provides the groundwater flows, categorized by hydrogeologic material, for flows through the area surrounding the facility (calculation 1, as described in Section 4.2) for the NES case. Flow into the area occurs primarily through the overburden materials, and the bulk of the flow is captured by tile drain 1.

Table 4-3 provides a summary of the groundwater flows through the building itself (calculation 2, as described in Section 4.2), categorized by elevation, for the NES case. Note that the flows are divided by elevation, and the description of overburden and bedrock is approximate. There is very little flow into the building, due to the low conductivity of the building materials.

Table 4-2 NES: Groundwater Flows in m^3/s Through NPD Region (Calculation1)

m^3/s	Flow In	Flow Out	Difference
Fill	6.29E-05	3.17E-04	-2.54E-04
Sand	6.91E-03	7.23E-04	6.19E-03
Till	5.00E-05	2.30E-05	2.70E-05
Bedrock	3.05E-05	6.58E-05	-3.53E-05
Recharge	4.55E-04	-	-
Tile Drain 1	-	6.92E-03	-
Total	7.51E-03	8.05E-03	-5.45E-04

Table 4-3 NES: Groundwater Flows in m^3/s Through NPD facility (Calculation2)

m^3/s	Flow In	Flow Out	Difference
Lower Bedrock (102-111 m)	8.43E-10	7.62E-10	8.16E-11
Middle Bedrock (111-120 m)	2.38E-09	4.65E-09	-2.27E-09
Upper Bedrock (120-122 m)	2.77E-09	1.37E-09	1.41E-09
Saturated Overburden (above 122 m)	8.15E-11	5.68E-10	-4.86E-10
Recharge	1.34E-09	-	1.34E-09
Total	7.41E-09	7.34E-09	6.79E-11

4.3.1.1 Particle Tracks

Particle tracks help delineate the flow fields around the NPD facility. While they delineate pathways for transport, particle tracks do not consider the effects of dispersion typically observed in contaminant transport and considered in contaminant transport modelling. Transport modelling is conducted with the near-field model only.

Three sets of particle tracks were simulated: particles starting at a vertical curtain extending from the bottom of the model to ground surface upgradient of the NPD facility (model Y = -50 m), particles within the building itself, and particles in a grid at the surface of the water table over the entire domain. All particle tracks shown in this section are simulated with the NES flow field using forward particle tracks.

Figure 4-6 shows the vertical curtain and water table particle tracks passing through the flow calculation boundary (calculation 1 as described in Section 4.2), in the vicinity of the facility infrastructure, including the trench and tile drain discharges. These particle tracks delineate the area influenced by the presence of the NPD facility. The particles of short duration are collected by the tile drains, or bypass the facility all together. Particles of longer duration reach the facility and are pushed down into the bedrock (south of facility and due to the low permeability facility), resulting in long travel times. Most of the particles between the facility and the river are primarily within the bedrock and discharge at the river, both particles originating in the bedrock as well as particles that have moved into the bedrock south of the facility.

Figure 4-6 Particle Tracks Delineating the Flow Area Impacted by the NPD Facility and Associated Infrastructure

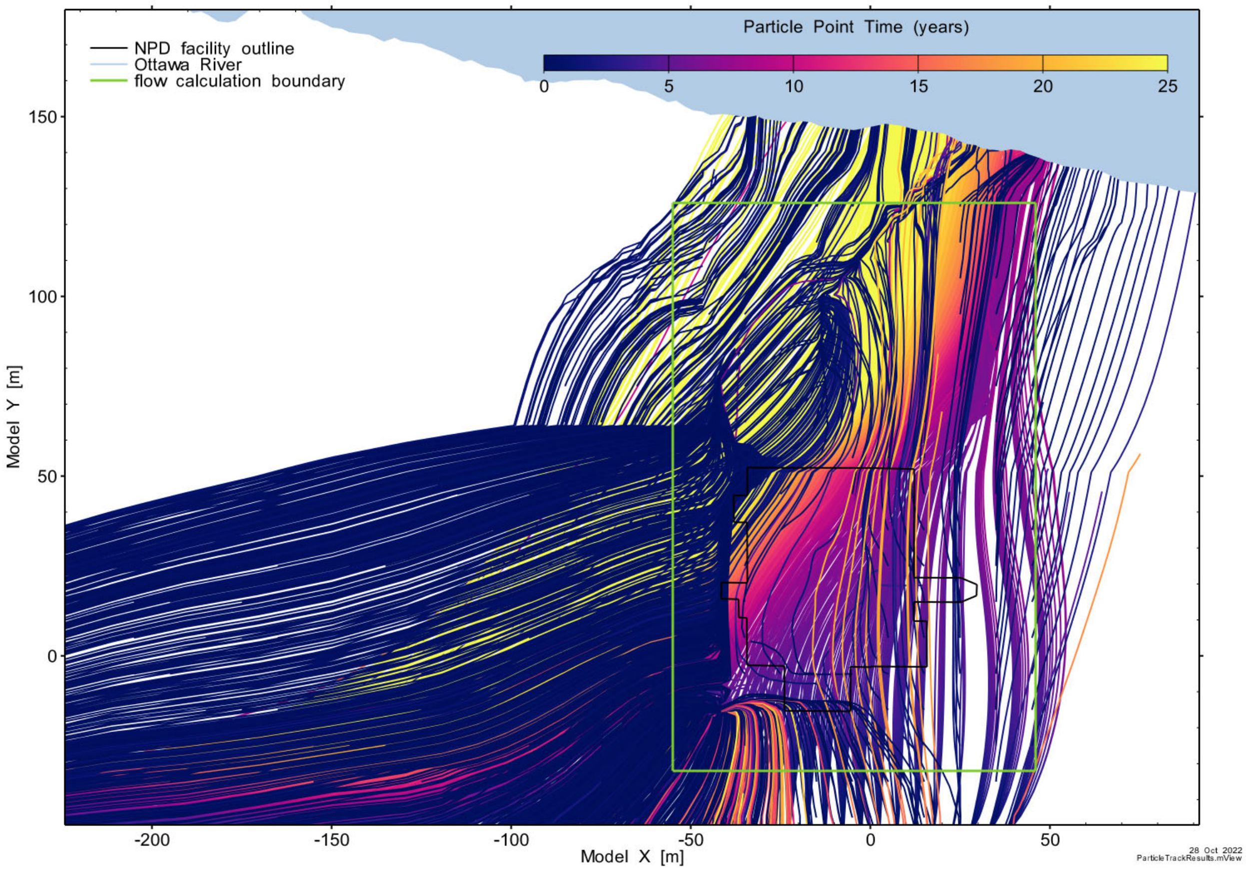

Figure 4-7 shows a plan view of particle track density for vertical curtain particles. The particle density counts the number of particles passing through each model grid block, and sums the density for each plan grid block. The model construction needs to be considered when interpreting these results; there is a greater expanse of bedrock than saturated overburden, and consequently there are more bedrock particles than overburden particles in a vertical curtain of particles. Features such as tile drains that mainly collect overburden water will therefore have a lower particle density due to the distribution of particles. Particle track density indicates the extents of the impact of the facility infrastructure on the surrounding flow field, in particular the dominance of the tile drains, pipe trench and tile drain 2 trench in collecting particles in the vicinity of the NPD facility. The deep section of tile drain 2 trench is clearly a significant feature between the facility and the river. The high density on the shoreline to the east of the facility (area in white) is an artifact of the particles ending at the edge of the river, the topography and the relatively coarse model discretization in that area.

Figure 4-7 Particle Density View for Vertical Curtain of Particles starting at Y= -50 m

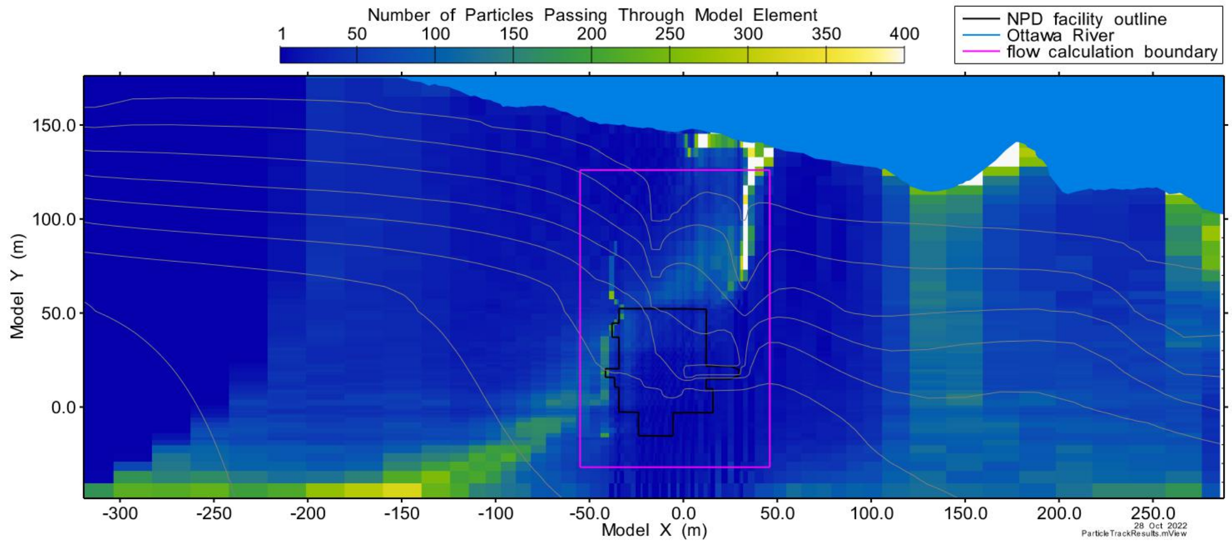

Figure 4-8 shows a plan view of particle tracks starting within the saturated facility. The figure on the left shows only those particles starting on the northern edge of the facility, which have travel times of 15 years or less, while the figure on the right shows all building particles with a travel time less than 1000 years. Particles starting on the northern edge of the facility indicate the travel time from the facility to the river, a maximum of 15 years.

Figure 4-8 Particle Tracks Starting in the Saturated Building

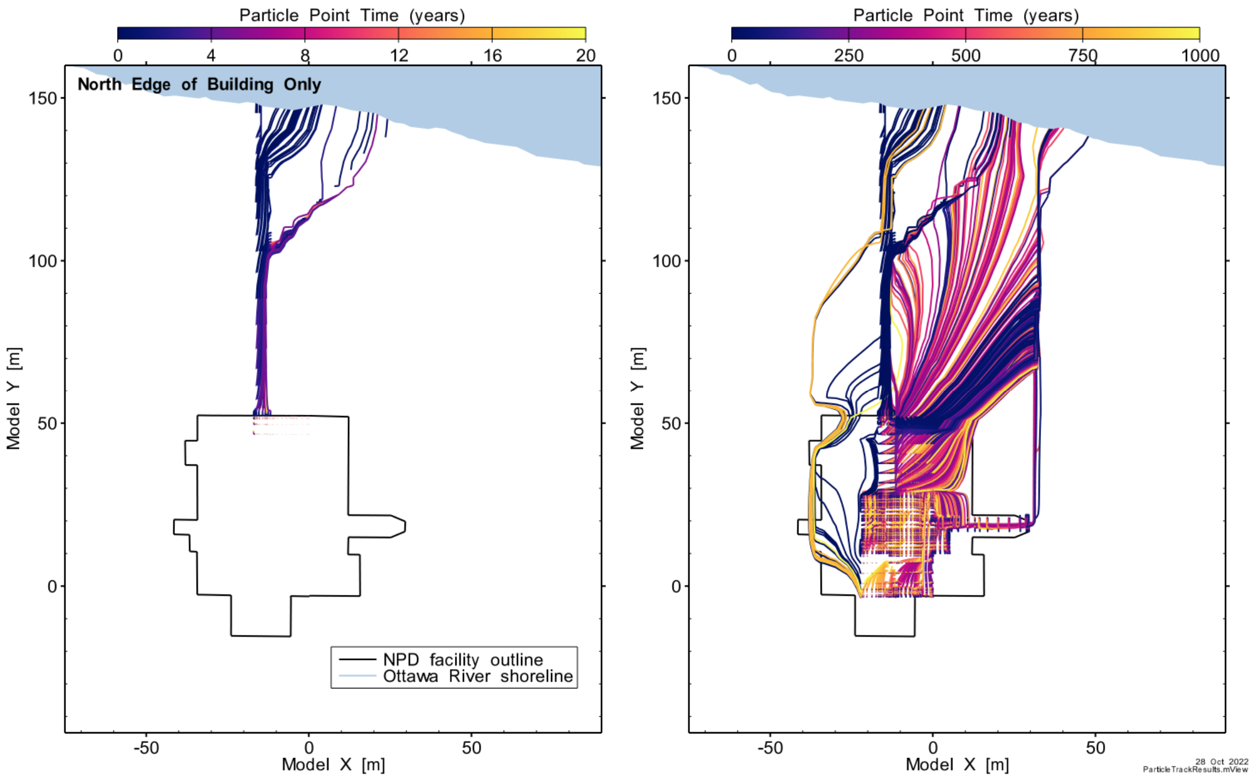

Figure 4-9 shows particles starting at the water table surface, across the domain, filtered to only show those particles that end within tile drain 1 to the west of the facility. Particles that end at the tile drain 1 delineate the capture zone for tile drain 1. The capture zone defines the amount of water available for the measured tile drain 1 flow rates. The increase in this area to the south-west of the facility allowed the model calibration to achieve the high tile drain 1 flow rate unattainable by previous groundwater flow models. The heterogeneity of the sand, particularly lower permeability sand near the river, allowed the tile drain 1 capture zone to be increased to the south-west.

Figure 4-9 Particle Tracks Ending at Tile Drain 1

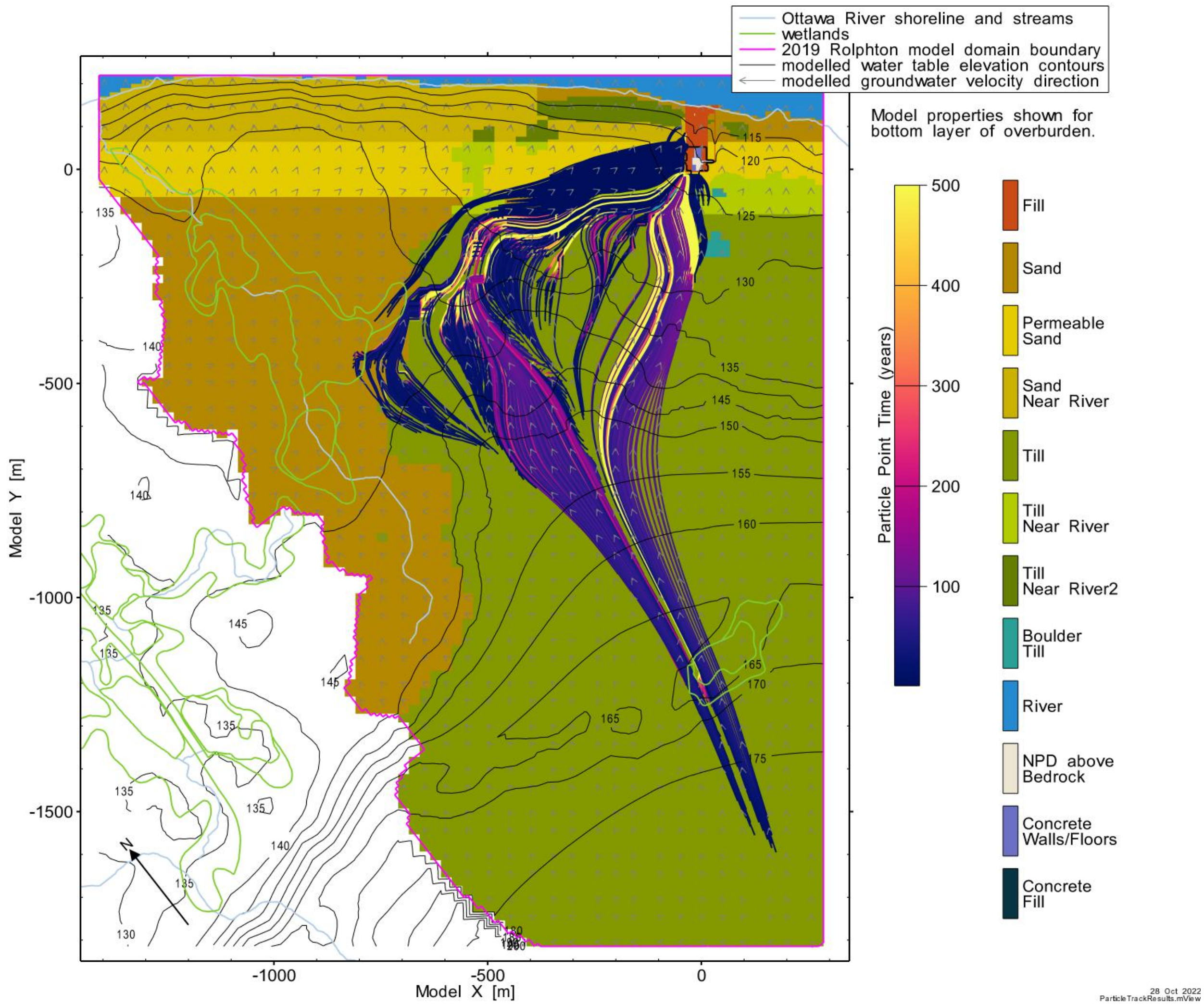

4.3.2 NES Degraded Cap (100 to 1000 years)

This case is based on the NES 0 to 100 years case, but assumes that the cap and engineered cover has degraded and the tile drains have failed.

As the engineered cover and cap are not represented in the groundwater model, degradation of the cap and cover is simulated by the resaturation model (Sgro, 2023) and new infiltration values into the building under the cover calculated. As in the NES model, a minimum recharge of 10^{-3} mm/yr is applied when very low recharge values are calculated by the resaturation model. Consequently, recharge is the same as the NES model, except for a minor increase in the recharge at the edges of the cover to 573 mm/yr (from 571 mm/yr in the NES model). In the resaturation model, degraded concrete cap and cover are represented by reduced hydraulic conductivities for the concrete cap (10^{-8} m/s) and the geosynthetic clay layer (GCL) in the cover (10^{-8} m/s). A degraded concrete conductivity of 10^{-8} m/s is consistent with degraded structural concrete (a similar concrete material) in Quintessa and Geofirma (2011) and with a “pessimistic” structural concrete or porous concrete backfill in Savage and Stenhouse (2002). The GCL is degraded to a similar value to prevent the material from limiting infiltration, relative to the concrete cap.

Tile drain failure is modelled by removal of the seepage nodes representing tile drain 1, and by replacing the high permeability nodes representing the deep section of tile drain 2 with fill. Failure of the tile drains results in springs developing along the steep face of the bluff downgradient of the facility. The existence of springs with tile drain failure is consistent with observations along this bluff prior to construction of the facility. These springs are identified in initial simulations as nodes where the groundwater table exceeds the ground surface, and in final simulations, seepages nodes are defined at these locations. Seepage nodes are only activated when the water table exceeds the elevation of the node.

Figure 4-10 shows three cross-sections through the building that highlight the effects of the degraded cap case on the water table, which is to increase the water table in the vicinity of the facility due to the failure of the tile drains. The three-cross sections are the same as Figure 3-16, and the location of the cross-sections is shown in Figure 3-15.

Figure 4-10 Head Contours and Water Table at Three Cross-Sections through the Facility: Comparison of NES and NES Degraded Cap Cases

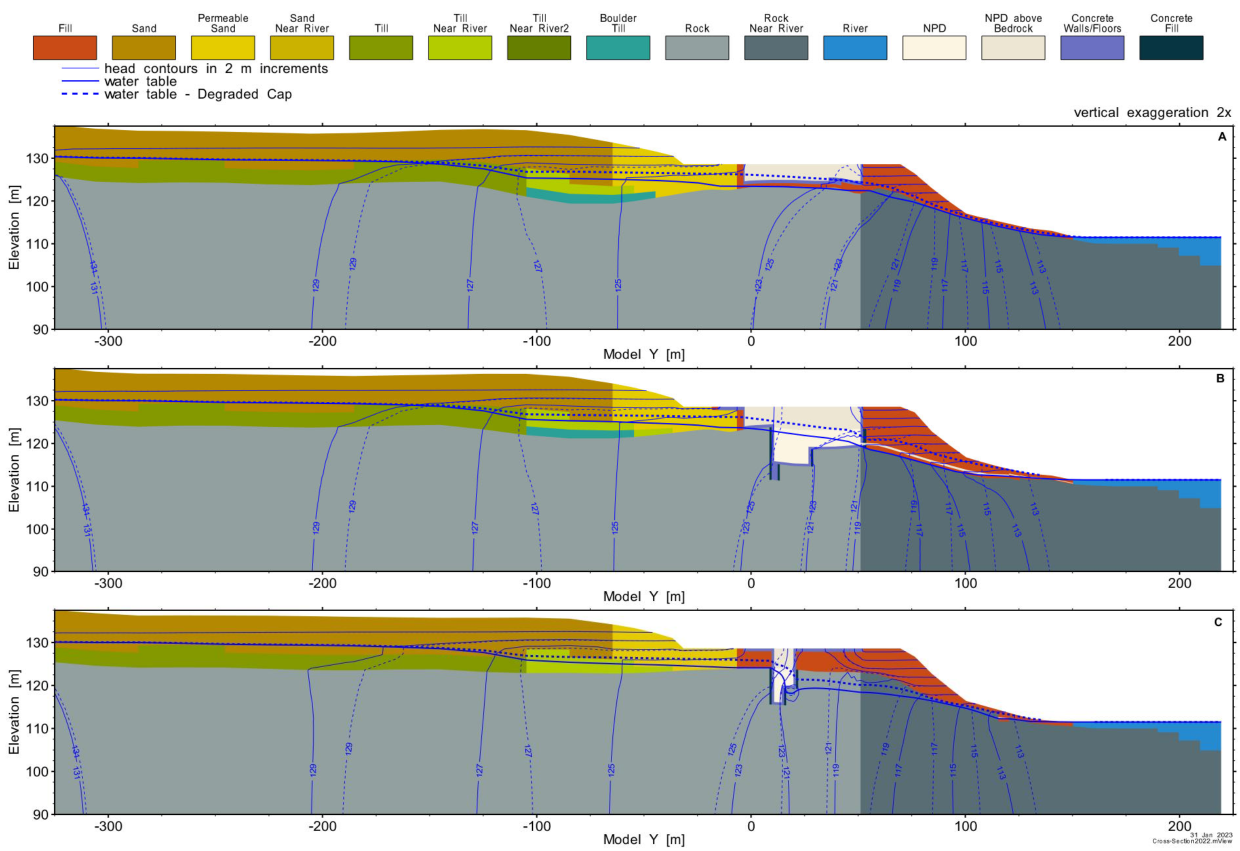

Table 4-4 provides the groundwater flows, categorized by hydrogeologic material, for flows through the area surrounding the facility (calculation 1, as described in Section 4.2) for the NES Degraded Cap case. Flow into the area occurs primarily through the overburden materials. Compared to the NES case, recharge is slightly increased, but the overall flows through the area are slightly decreased, likely due to the failure of the tile drains.

Figure 4-11 illustrates these changes in flow between the NES and NES Degraded Cap cases.

Springs, located downgradient of the facility and the calculation 1 boundary, result in flows of 2.0 L/s.

Table 4-5 provides a summary of the groundwater flows through the building itself (calculation 2, as described in Section 4.2), categorized by elevation, for the NES Degraded Cap case. Note that the flows are divided by elevation, and the description of overburden and bedrock is approximate. While there continues to be very little flow into the building, flows are approximately 2.5 times greater than the NES case. Half of this increase can be directly attributed to increased recharge over the building. The remaining increase can therefore be inferred to be a result of both increased recharge immediately adjacent to the building and tile drain failure.

Figure 4-12 illustrates the groundwater flows through the building itself, comparing flows for the NES and NES Degraded Cap cases. From this illustration, it is evident that the biggest changes in flow occur in recharge, the overburden and upper bedrock.

Table 4-4 NES Degraded Cap: Groundwater Flows in m^3/s Through NPD Region (Calculation1)

m^3/s	Flow In	Flow Out	Difference
Fill	4.65E-05	4.94E-03	-4.89E-03
Sand	4.36E-03	1.19E-03	3.17E-03
Till	1.35E-04	2.19E-04	-8.40E-05
Bedrock	1.71E-05	6.46E-05	-4.75E-05
Recharge	1.45E-03	-	-
Tile Drain 1	-	-	-
Total	6.01E-03	6.41E-03	-4.05E-04

Figure 4-11 Histogram of Groundwater Flows Through NPD Region (Calculation1): Comparison of NES and NES Degraded Cap Cases

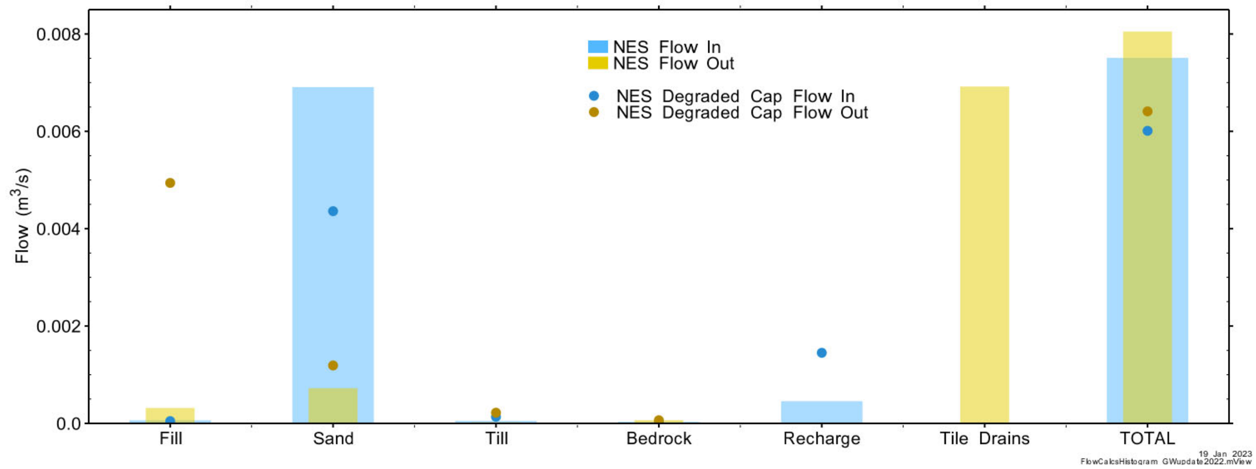

Table 4-5 NES Degraded Cap: Groundwater Flows in m^3/s Through NPD facility (Calculation2)

m^3/s	Flow In	Flow Out	Difference
Lower Bedrock (102-111 m)	7.87E-10	8.77E-10	-8.99E-11
Middle Bedrock (111-120 m)	2.29E-09	6.82E-09	-4.54E-09
Upper Bedrock (120-122 m)	4.63E-09	5.29E-09	-6.59E-10
Saturated Overburden (above 122 m)	4.44E-09	5.74E-09	-1.30E-09
Recharge	6.10E-09	-	6.10E-09
Total	1.83E-08	1.87E-08	-4.85E-10

Figure 4-12 Flow Through the Building (Flow Calculation 2): Comparison of NES and NES Degraded Cap Cases

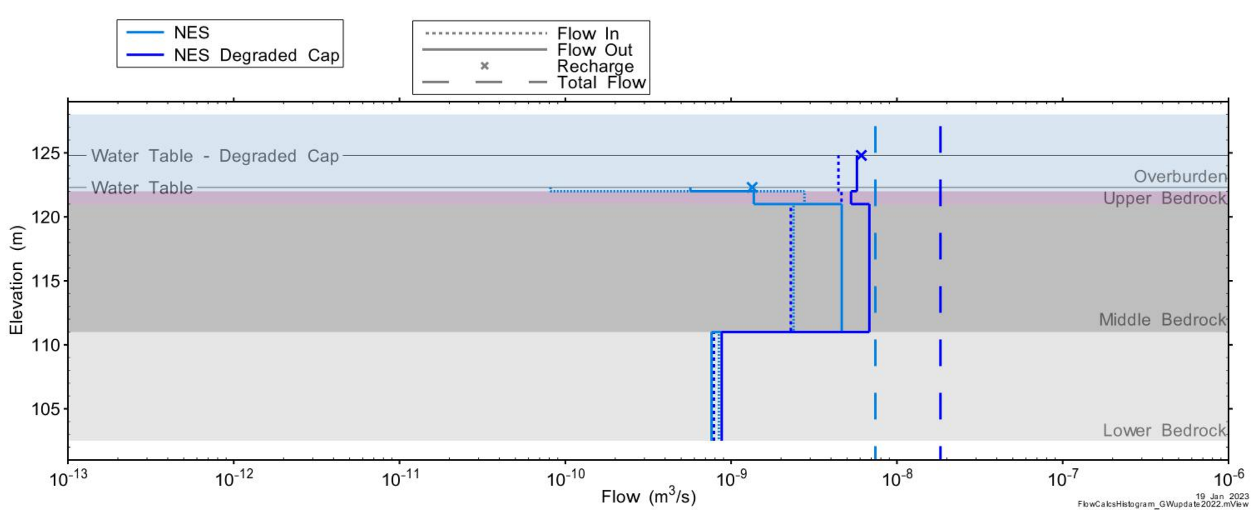

4.3.3 NES Degraded (1000+ years)

This case is similar to the NES Degraded Cap case, but assumes that the structure has also degraded. Structure degradation is modelled by increasing the hydraulic conductivity of the facility structure's concrete and grout, including the grout in the pipes within the pipe trench, to 10^{-8} m/s. The value for degraded concrete is based on the degraded structural concrete (a similar concrete material) in Quintessa and Geofirma (2011) and a "pessimistic" structural concrete or porous concrete backfill in Savage and Stenhouse (2002). It was assumed that the grout and concrete fill around the walls have the same degraded hydraulic conductivity. This last assumption is not expected to occur in reality, but provides a conservative and straightforward assessment of the effects of material degradation.

Infiltration values were calculated from the resaturation model with a degraded cap, cover and facility (Sgro, 2023). Infiltration for areas under the cover and at the edges of the cover are unchanged from the NES Degraded Cap case.

The water table and head contours are very similar to the Degraded Cap case, as shown in Figure 4-13. As will be discussed below, changes to the conductivity in the structure had limited, almost indistinguishable impact on the flow field within the geosphere. Differences primarily occur within the facility.

Figure 4-13 Head Contours and Water Table at Three Cross-Sections through the Facility: Comparison of NES, NES Degraded Cap and NES Degraded Cases

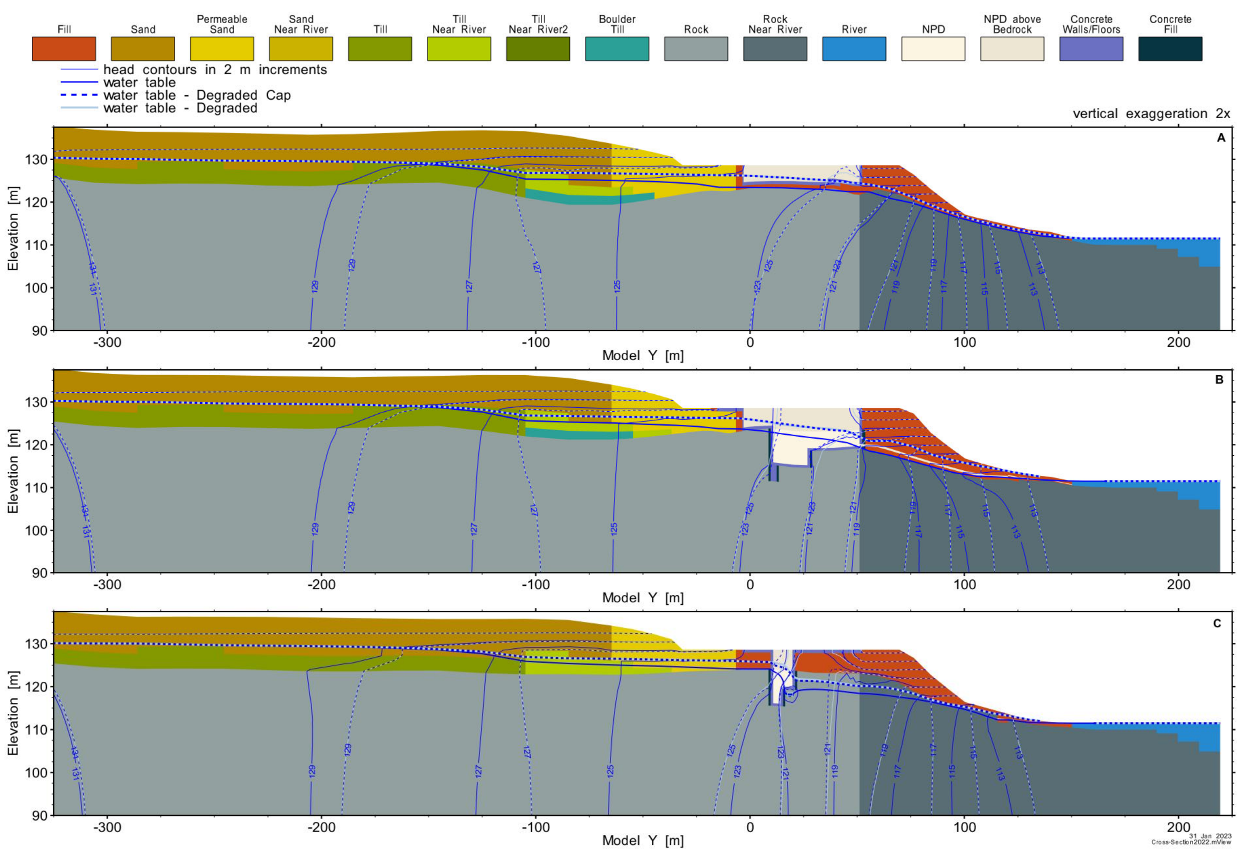

Table 4-6 provides the groundwater flows, categorized by hydrogeologic material, for flows through the area surrounding the facility (calculation 1, as described in Section 4.2) for the NES Degraded case. Flow into the area and spring flows are indistinguishable from the NES Degraded Cap case. This indicates that the hydraulic conductivity of the facility has negligible impact on the flow system in the adjacent geosphere.

Table 4-7 provides a summary of the groundwater flows through the building itself (calculation 2, as described in Section 4.2), categorized by elevation, for the NES Degraded case. Note that the flows are divided by elevation, and the description of overburden and bedrock is approximate. While there continues to be very little flow into the building, flows are significantly increased by approximately 2 orders of magnitude compared to the NES Degraded Cap case. The amount entering as recharge in this case is greater than the total amount of flow entering the building in the NES Degraded Cap case, by an order of magnitude, despite similar recharge inputs. Recharge into the building is calculated at the saturated surface, so additional recharge will occur due to both the increased conductivity of the building and additional inputs from the unsaturated overburden into the upper unsaturated zone of the building. This additional recharge only represents 11% of the additional flow in the building. The remaining additional flow enters the building through both the saturated overburden and bedrock, with the greatest flow entering from the upper bedrock, and exiting through the middle bedrock. The increase in flow in the NES Degraded case, in comparison to the NES and Degraded Cap cases, is illustrated in Figure 4-14.

Table 4-6 NES Degraded: Groundwater Flows in m^3/s Through NPD Region (Calculation1)

m^3/s	Flow In	Flow Out	Difference
Fill	4.24E-05	4.94E-03	-4.90E-03
Sand	4.36E-03	1.19E-03	3.17E-03
Till	1.35E-04	2.19E-04	-8.40E-05
Bedrock	1.72E-05	6.50E-05	-4.78E-05
Recharge	1.45E-03	-	1.45E-03
Tile Drain 1	-	-	-
Total	6.00E-03	6.41E-03	-4.09E-04

Table 4-7 NES Degraded: Groundwater Flows in m^3/s Through NPD facility (Calculation2)

m^3/s	Flow In	Flow Out	Difference
Lower Bedrock (102-111 m)	1.30E-07	1.44E-07	-1.37E-08
Middle Bedrock (111-120 m)	3.97E-07	1.05E-06	-6.57E-07
Upper Bedrock (120-122 m)	1.20E-06	8.78E-07	3.18E-07
Saturated Overburden (above 122 m)	5.38E-07	4.70E-07	6.84E-08
Recharge	2.70E-07	0.00E+00	2.70E-07
Total	2.53E-06	2.54E-06	-1.43E-08

Figure 4-14 Flow Through the Building (Flow Calculation 2): Comparison of NES, NES Degraded Cap and NES Degraded Cases

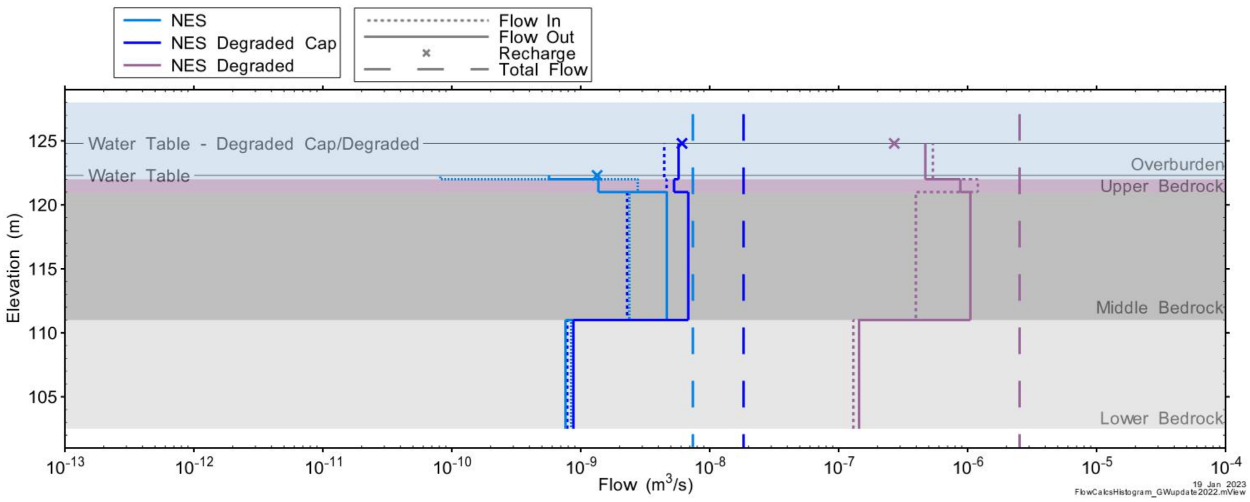

4.3.4 High Overburden Hydraulic Conductivity

The high overburden hydraulic conductivity cases increase the fill conductivity by one order of magnitude greater than the calibrated value. The calibrated hydraulic conductivity of the fill is at the maximum of the expected fill conductivity range, 10^{-3} m/s. The calibration was relatively insensitive to the fill conductivity, as is explored in Section 5.2. The conductivity of the fill in the high overburden hydraulic conductivity cases is 10^{-2} m/s, which is an extremely permeable value for the fill, but provides an illustration of the impacts of an increase in conductivity of this material.

Infiltration values were calculated from the resaturation model (Sgro, 2023). Infiltration for building areas, both with and without the concrete cap, are unchanged from the NES cases at 10^{-3} mm/yr. Infiltration for areas under the cover, but not into the building are increased to 1.6×10^{-2} mm/yr. Infiltration into the cover edges is unchanged from the NES cases.

From the point of view of head contours and water table in the geosphere, the effect of a permeable overburden is almost indistinguishable from the NES case. Figure 4-15 shows three cross-sections through the facility for the three high overburden hydraulic conductivity bedrock cases, with the water table for the NES case (0 to 100 years) shown for comparison.

Figure 4-15 Head Contours and Water Table at Three Cross-Sections through the Facility: Comparison of High Overburden Hydraulic Conductivity Cases

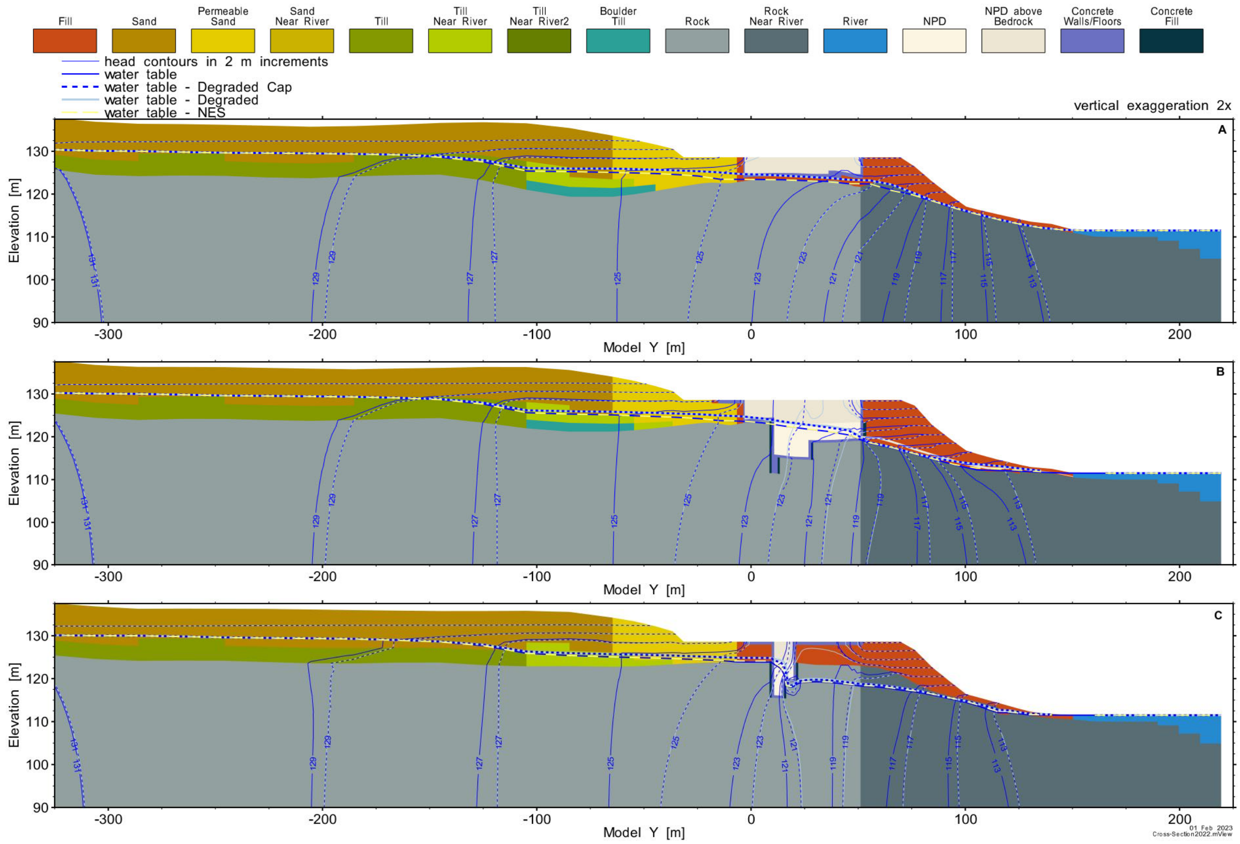

Table 4-8 provides the groundwater flows, categorized by hydrogeologic material, for flows through the area surrounding the facility (calculation 1, as described in Section 4.2) for the three high overburden hydraulic conductivity cases. Figure 4-16 illustrates the changes in flow between the NES and high overburden hydraulic conductivity cases. The high overburden hydraulic conductivity case is very similar to the NES case. As with the NES cases, groundwater flow in the geosphere is nearly indistinguishable for the Degraded Cap and Degraded cases. In both the Degraded Cap and Degraded cases, flow out of the faciility and into the fill is substantially increased, likely due to the raising of the water table due to tile drain failure in these cases.

Spring flow in the Degraded Cap and Degraded cases are reduced to 0.7 L/s, from 2 L/s in the NES cases.

Table 4-9 provides a summary of the groundwater flows through the building itself (calculation 2, as described in Section 4.2), categorized by elevation, for all three high overburden hydraulic conductivity cases. The building flows are illustrated in Figure 4-17. Note that the flows are divided by elevation, and the description of overburden and bedrock is approximate. Building flows for the high overburden hydraulic conductivity cases are very similar to the NES cases, with increased flows in the overburden and upper bedrock.

Table 4-8 High Overburden Hydraulic Conductivity Cases: Groundwater Flows in m^3/s Through NPD Region (Calculation1)

m^3/s	High Overburden Hydraulic Conductivity			High Overburden Hydraulic Conductivity – Degraded Cap			High Overburden Hydraulic Conductivity – Degraded		
	Flow In	Flow Out	Difference	Flow In	Flow Out	Difference	Flow In	Flow Out	Difference
Fill	2.33E-04	4.80E-04	-2.47E-04	7.10E-04	7.06E-03	-6.35E-03	7.11E-04	7.07E-03	-6.36E-03
Sand	6.90E-03	7.79E-04	6.12E-03	5.61E-03	7.97E-04	4.81E-03	5.61E-03	7.97E-04	4.81E-03
Till	5.26E-05	2.52E-05	2.74E-05	1.03E-04	6.68E-05	3.62E-05	1.03E-04	6.68E-05	3.62E-05
Bedrock	3.54E-05	7.18E-05	-3.64E-05	8.45E-05	4.31E-04	-3.47E-04	8.47E-05	4.32E-04	-3.47E-04
Recharge	5.10E-04	-	-	2.41E-03	-	-	2.41E-03	-	-
Tile Drain 1	-	6.79E-03	-	-	-	-	-	-	-
Total	7.73E-03	8.14E-03	-4.14E-04	8.89E-03	8.36E-03	5.30E-04	8.89E-03	8.36E-03	5.30E-04

Figure 4-16 Histogram of Groundwater Flows Through NPD Region (Calculation1): Comparison of High Overburden Hydraulic Conductivity (OBK) Cases to NES Case

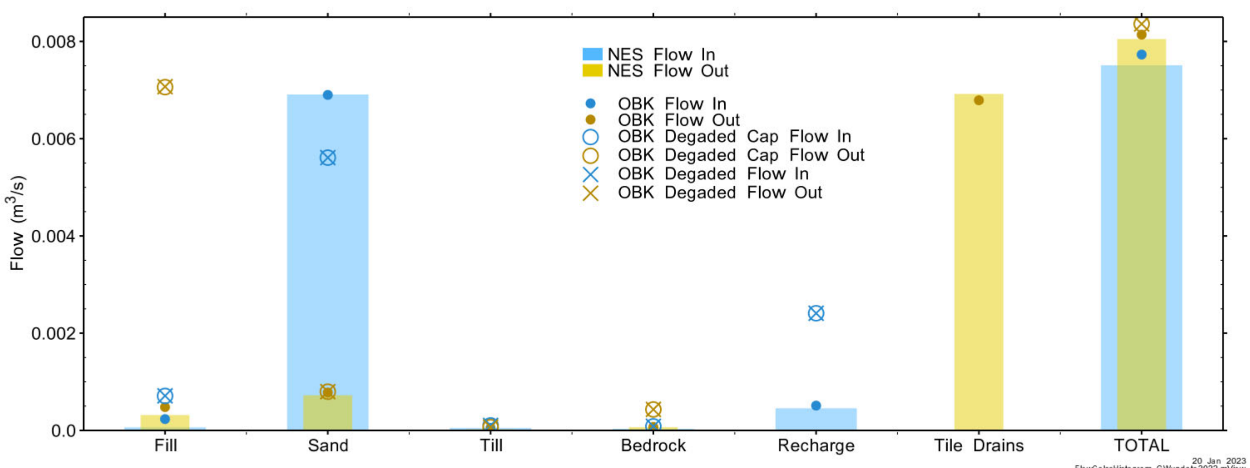

Table 4-9 High Overburden Hydraulic Conductivity Cases: Groundwater Flows in m³/s Through NPD facility (Calculation2)

m³/s	High Overburden Hydraulic Conductivity			High Overburden Hydraulic Conductivity – Degraded Cap			High Overburden Hydraulic Conductivity – Degraded		
	Flow In	Flow Out	Diff	Flow In	Flow Out	Diff	Flow In	Flow Out	Diff
Lower Bedrock (102-111 m)	8.64E-10	7.81E-10	8.25E-11	9.37E-10	8.93E-10	4.38E-11	1.43E-07	1.41E-07	1.55E-09
Middle Bedrock (111-120 m)	2.46E-09	4.60E-09	-2.14E-09	2.63E-09	5.79E-09	-3.16E-09	4.39E-07	8.99E-07	-4.59E-07
Upper Bedrock (120-122 m)	2.77E-09	1.35E-09	1.42E-09	2.90E-09	1.99E-09	9.09E-10	6.05E-07	3.20E-07	2.85E-07
Saturated Overburden (above 122 m)	3.92E-11	5.96E-10	-5.57E-10	9.38E-10	1.22E-09	-2.86E-10	1.03E-07	6.03E-08	4.27E-08
Recharge	1.27E-09	0.00E+00	1.27E-09	2.24E-09	0.00E+00	2.24E-09	1.48E-07	0.00E+00	1.48E-07
Total	7.40E-09	7.33E-09	7.19E-11	9.64E-09	9.90E-09	-2.58E-10	1.44E-06	1.42E-06	1.79E-08

Figure 4-17 Flow Through the Building (Flow Calculation 2): Comparison of High Overburden Hydraulic Conductivity Cases

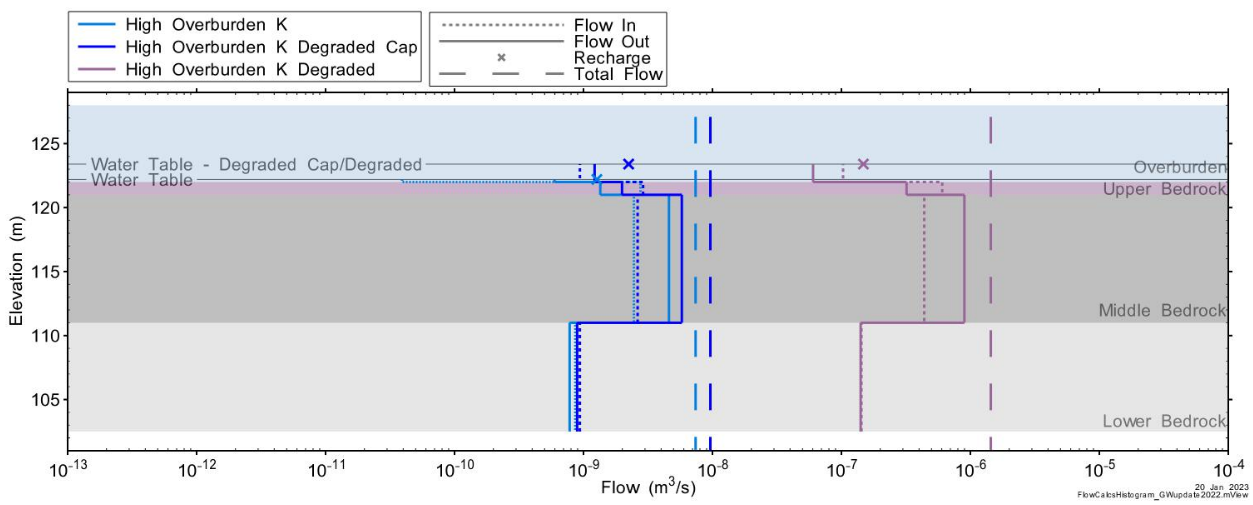

4.3.5 High Bedrock Hydraulic Conductivity Cases

The high bedrock hydraulic conductivity cases increase the bedrock conductivity to the maximum measured value of 6.6 x 10^{-6} m/s (Raven *et al*. 2021). Both bedrock and bedrock near the river are changed to this value. This high bedrock hydraulic conductivity is applied to the three conditions considered in the scenarios: initial conditions with tile drains active, degraded cap with tile drains inactive and degraded with tile drains inactive.

Infiltration values were calculated from the resaturation model (Sgro, 2023). Infiltration for areas under the cover and at the edges of the cover are unchanged from the NES cases.

The effect of a permeable bedrock results in a lower water table in the vicinity of the facility and downstream of the facility in all cases. Figure 4-18 shows three cross-sections through the facility for the three high bedrock hydraulic conductivity bedrock cases, with the water table for the NES (0 to 100 years) case shown for comparison. As the water table is below the elevation of the tile drains in all three high bedrock hydraulic conductivity bedrock cases, the tile drains are effectively inactive. With no active tile drains in any of the cases, the water table and head contours within the geosphere are nearly identical in all three cases. Differences occur within the building, where recharge and conductivities change between the cases.

With such a low water table, the high bedrock hydraulic conductivity is not a realistic representation of the site. It is possible that a narrow zone has a higher conductivity, but it should be noted that even a narrow zone would likely result in a significant drop in the water table within the zone.

Figure 4-18 Head Contours and Water Table at Three Cross-Sections through the Facility: Comparison of High Bedrock Hydraulic Conductivity Cases

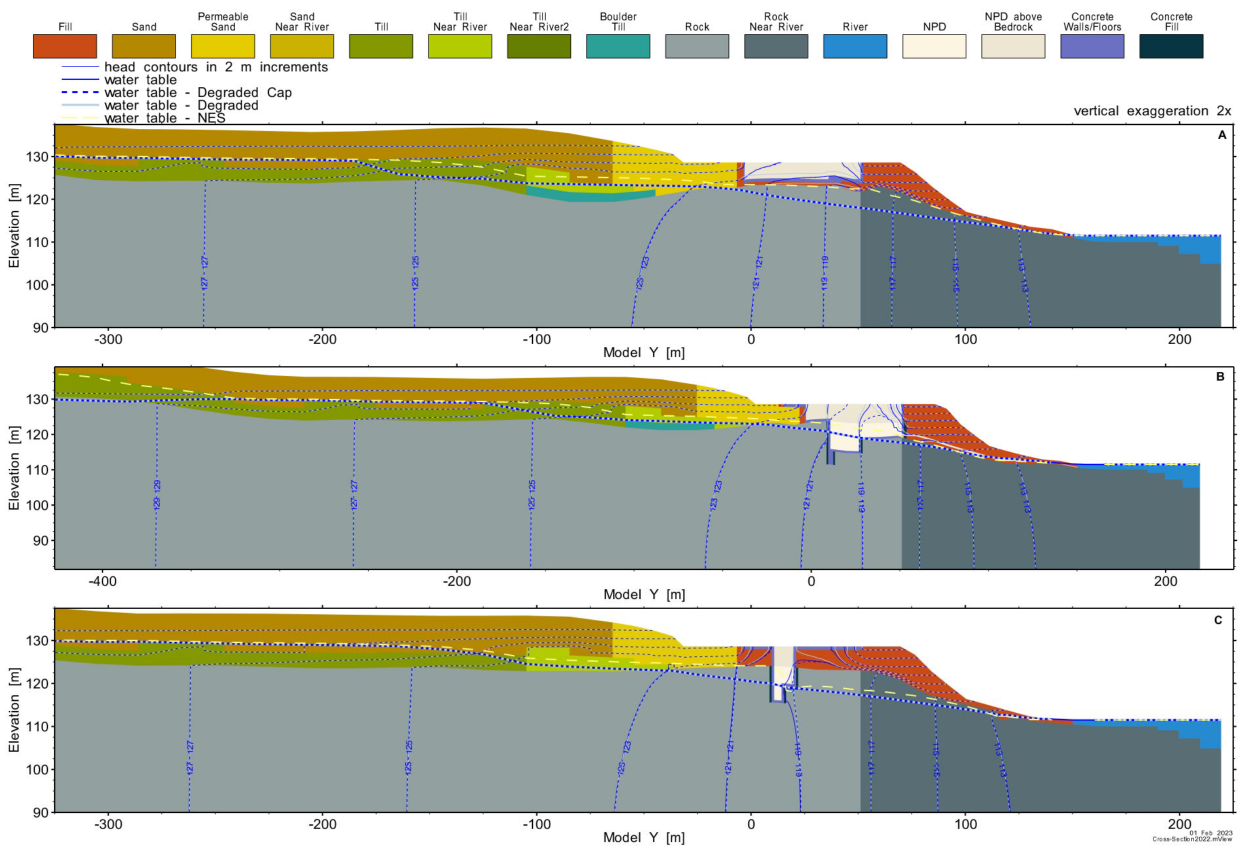

Table 4-10 provides the groundwater flows, categorized by hydrogeologic material, for flows through the area surrounding the facility (calculation 1, as described in Section 4.2) for the three high bedrock hydraulic conductivity cases. As expected from the water table and head contours, the flow into the area is near indistinguishable for the three cases. Note that the water table is also too low to generate spring flows for these cases.

Figure 4-11 illustrates the changes in flow between the NES and high bedrock hydraulic conductivity cases.

Table 4-11 provides a summary of the groundwater flows through the building itself (calculation 2, as described in Section 4.2), categorized by elevation, for all three high bedrock hydraulic conductivity cases. Note that the flows are divided by elevation, and the description of overburden and bedrock is approximate. Building flow for the high bedrock hydraulic conductivity and high bedrock hydraulic conductivity degraded cap cases are very similar. While there continues to be very little flow into the building for the high bedrock hydraulic conductivity degraded case, flows are significantly increased from the current conditions and degraded cap case by approximately 2 orders of magnitude, as in the NES cases. The building flows are illustrated in Figure 4-20. Within this illustration, the water table shown is the average water table over the building footprint, with some flow occurring above the water table in some portions of the building.

Table 4-10 High Bedrock Hydraulic Conductivity Cases: Groundwater Flows in m^3/s Through NPD Region (Calculation1)

m^3/s	High Bedrock Hydraulic Conductivity			High Bedrock Hydraulic Conductivity – Degraded Cap			High Bedrock Hydraulic Conductivity – Degraded		
	Flow In	Flow Out	Difference	Flow In	Flow Out	Difference	Flow In	Flow Out	Difference
Fill	1.87E-05	2.52E-04	-2.33E-04	3.37E-05	2.42E-04	-2.08E-04	3.38E-05	2.43E-04	-2.09E-04
Sand	4.38E-04	2.37E-04	2.01E-04	4.39E-04	2.33E-04	2.06E-04	4.39E-04	2.33E-04	2.06E-04
Till	0.00E+00	0.00E+00	0.00E+00	0.00E+00	0.00E+00	0.00E+00	0.00E+00	0.00E+00	0.00E+00
Bedrock	1.46E-03	1.95E-03	-4.90E-04	1.46E-03	1.96E-03	-5.00E-04	1.46E-03	1.96E-03	-5.00E-04
Recharge	3.63E-04	-	-	3.60E-04	-	-	3.60E-04	-	-
Tile Drain 1	-	0.00E+00	-	-	-	-	-	-	-
Total	2.28E-03	2.41E-03	-1.30E-04	2.29E-03	2.40E-03	-1.10E-04	2.29E-03	2.40E-03	-1.10E-04

Figure 4-19 Histogram of Groundwater Flows Through NPD Region (Calculation1): Comparison of High Bedrock Hydraulic Conductivity (BRK) Cases to NES Case

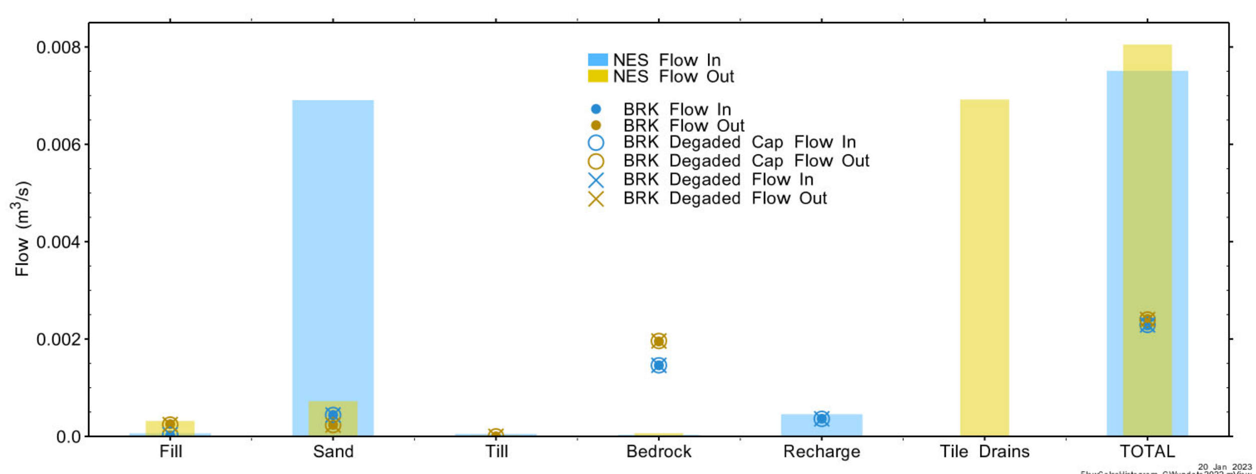

Table 4-11 High Bedrock Hydraulic Conductivity Cases: Groundwater Flows in m³/s Through NPD facility (Calculation2)

m³/s	High Bedrock Hydraulic Conductivity			High Bedrock Hydraulic Conductivity – Degraded Cap			High Bedrock Hydraulic Conductivity – Degraded		
	Flow In	Flow Out	Diff	Flow In	Flow Out	Diff	Flow In	Flow Out	Diff
Lower Bedrock (102-111 m)	5.52E-10	4.67E-10	8.53E-11	5.20E-10	4.69E-10	5.08E-11	1.17E-07	9.59E-08	2.11E-08
Middle Bedrock (111-120 m)	1.47E-09	1.95E-09	-4.76E-10	1.43E-09	2.13E-09	-6.94E-10	3.02E-07	3.56E-07	-5.44E-08
Upper Bedrock (120-122 m)	2.92E-10	1.33E-10	1.58E-10	5.26E-10	3.55E-10	1.71E-10	7.69E-08	1.49E-08	6.20E-08
Saturated Overburden (above 122 m)	0.00E+00	3.10E-10	-3.10E-10	0.00E+00	0.00E+00	0.00E+00	0.00E+00	5.04E-08	-5.04E-08
Recharge	4.97E-10	0.00E+00	4.97E-10	4.11E-10	0.00E+00	4.11E-10	2.88E-08	0.00E+00	2.88E-08
Total	2.81E-09	2.86E-09	-4.53E-11	2.89E-09	2.95E-09	-6.10E-11	5.25E-07	5.18E-07	7.06E-09

Figure 4-20 Flow Through the Building (Flow Calculation 2): Comparison of High Bedrock Hydraulic Conductivity Cases

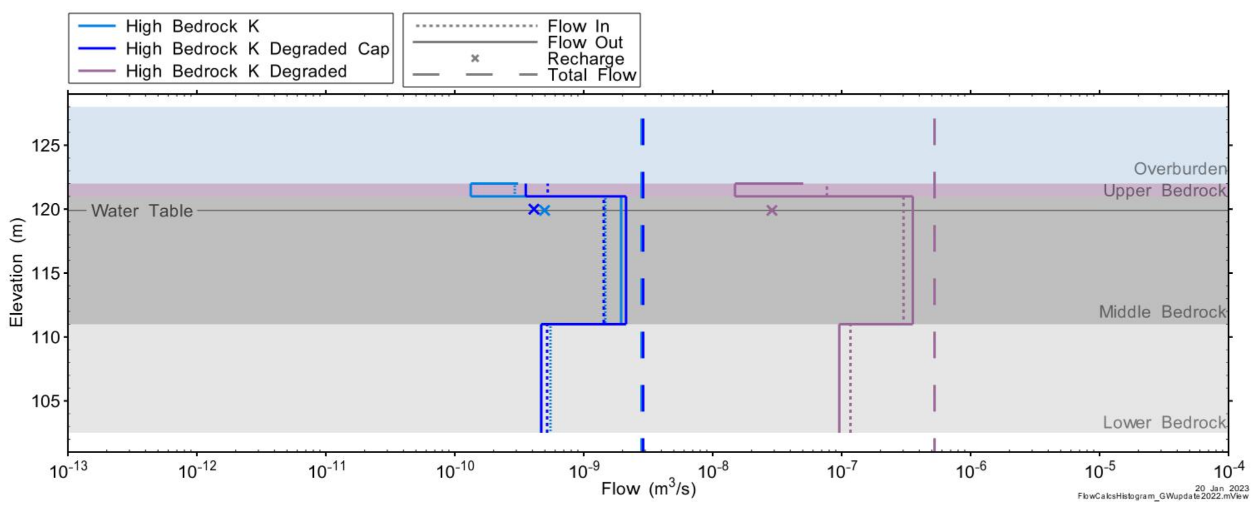

4.3.6 Fault Zone Activation

Fault zone activation is approximated by increasing the bedrock hydraulic conductivity by one order of magnitude ($5x10^{-7}$ m/s in bedrock, $1.7x10^{-6}$ m/s in bedrock near river). It is assumed that the facility also becomes degraded when the fault is reactivated, such as might occur during a seismic event. Facility degradation in this case assumes:

- grout above and below bedrock is extremely degraded (10^{-6} m/s),
- concrete, both facility concrete and the concrete cap, are extremely degraded (10^{-6} m/s), and
- cover GCL is also extremely degraded (10^{-6} m/s) so as not to provide a barrier to flow.

It is assumed that an event that would cause fault zone activation and facility degradation occurs after one hundred years, and the tile drains are consequently degraded and inactive.

Infiltration values were calculated from the resaturation model with extremely degraded facility conditions as described above (Sgro, 2023). Infiltration for areas under the cover remain below the threshold of 10^{-3} mm/yr and are therefore unchanged from the NES cases, and infiltration in the area at the edges of the cover are increased slightly to 574 mm/yr.

As expected from the high bedrock conductivity cases above, increasing the conductivity of the bedrock results in a lowering of the water table. The increase in bedrock conductivity is not as large as for the high bedrock conductivity cases in Section 4.3.5, and consequently, the drop in the water table is smaller. Figure 4-21 shows three cross-sections through the facility for the fault zone activation case, with the water table for the NES degraded case (1000+ years) shown for comparison. The NES degradation case is shown for comparison, as the facility is also degraded and tile drains removed in this case. Note that degradation of the facility is more severe in the fault zone activation case, although this is not likely to be significant for geosphere flows.

Figure 4-21 Head Contours and Water Table at Three Cross-Sections through the Facility: Fault Zone Activation Case

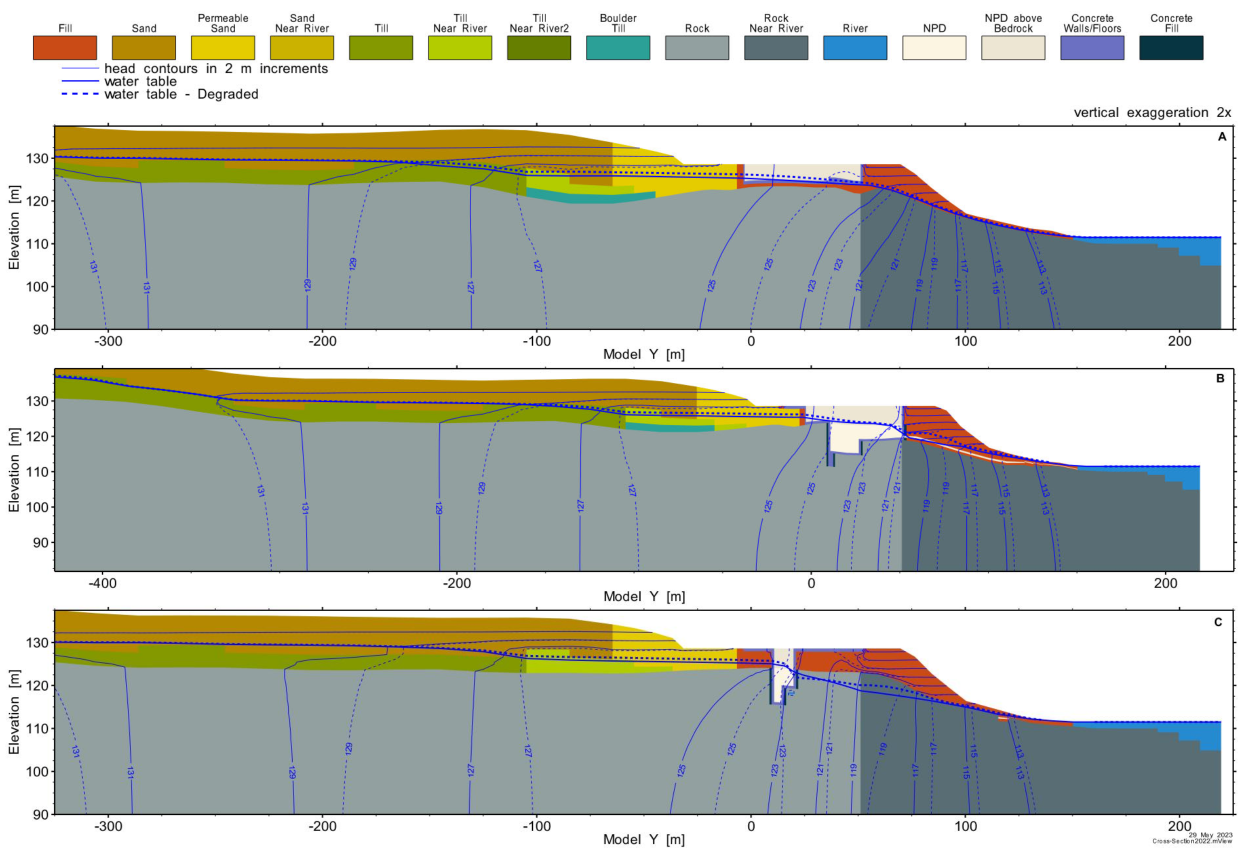

Table 4-12 provides the groundwater flows, categorized by hydrogeologic material, for flows through the area surrounding the facility (calculation 1, as described in Section 4.2) for the fault zone activation case. Figure 4-22 illustrates the changes in flow between the NES degraded case and the fault zone activation case. Geosphere flows are reduced in the fault zone activation case, attributed to the lower water table.

Spring flows, not within the calculation area, are approximately 0.8 L/s, less than the 2 L/s in the NES Degraded case. The reduced spring flows are attributed to the lower water table.

Table 4-13 provides a summary of the groundwater flows through the building itself (calculation 2, as described in Section 4.2), categorized by elevation, for the fault zone activation case. The building flows are illustrated in Figure 4-23. Note that the flows are divided by elevation, and the description of overburden and bedrock is approximate. Building flows are increased compared to the NES degraded case, as expected given the extreme degradation of concrete and grout above bedrock.

Table 4-12 Fault Zone Activation Case: Groundwater Flows in m^3/s Through NPD Region (Calculation1)

m^3/s	Flow In	Flow Out	Difference
Fill	4.65E-05	2.57E-03	-2.52E-03
Sand	2.46E-03	5.72E-04	1.89E-03
Till	7.09E-05	9.76E-05	-2.67E-05
Bedrock	1.43E-04	6.45E-04	-5.02E-04
Recharge	1.04E-03	-	-
Tile Drain 1	-	-	-
Total	3.75E-03	3.87E-03	-1.20E-04

Figure 4-22 Histogram of Groundwater Flows Through NPD Region (Calculation1): Comparison of Fault Zone Activation Case to NES Degraded Case

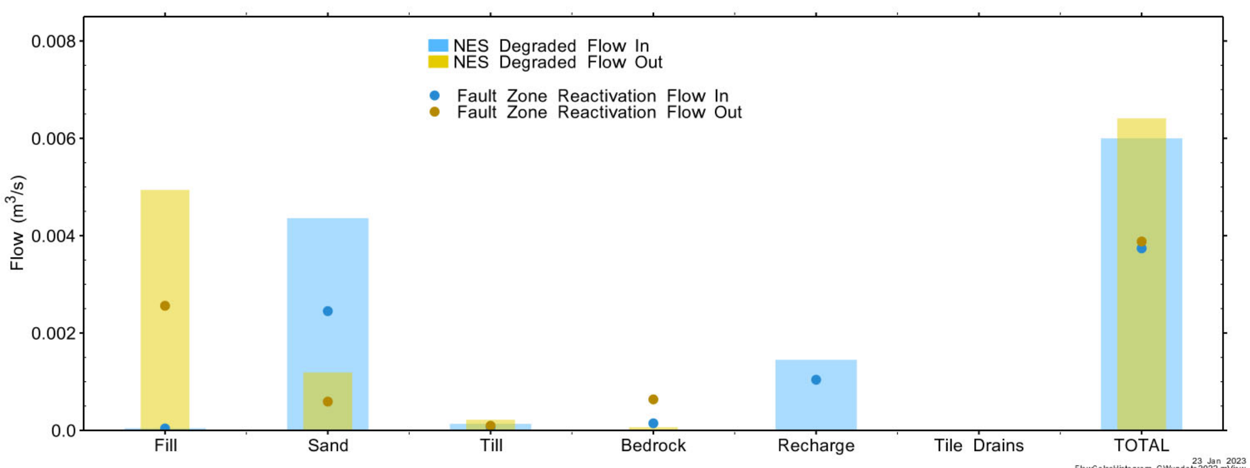

Table 4-13 Fault Zone Activation Case: Groundwater Flows in m³/s Through NPD facility (Calculation2)

m³/s	Flow In	Flow Out	Difference
Lower Bedrock (102-111 m)	5.39E-06	9.35E-06	-3.96E-06
Middle Bedrock (111-120 m)	1.73E-05	5.22E-05	-3.50E-05
Upper Bedrock (120-122 m)	7.28E-05	5.09E-05	2.20E-05
Saturated Overburden (above 122 m)	2.26E-05	1.19E-05	1.07E-05
Recharge	1.17E-05	0.00E+00	2.87E-06
Total	1.30E-04	1.24E-04	5.47E-06

Figure 4-23 Flow Through the Building (Flow Calculation 2): Comparison of Fault Zone Activation Case to NES Degraded Case

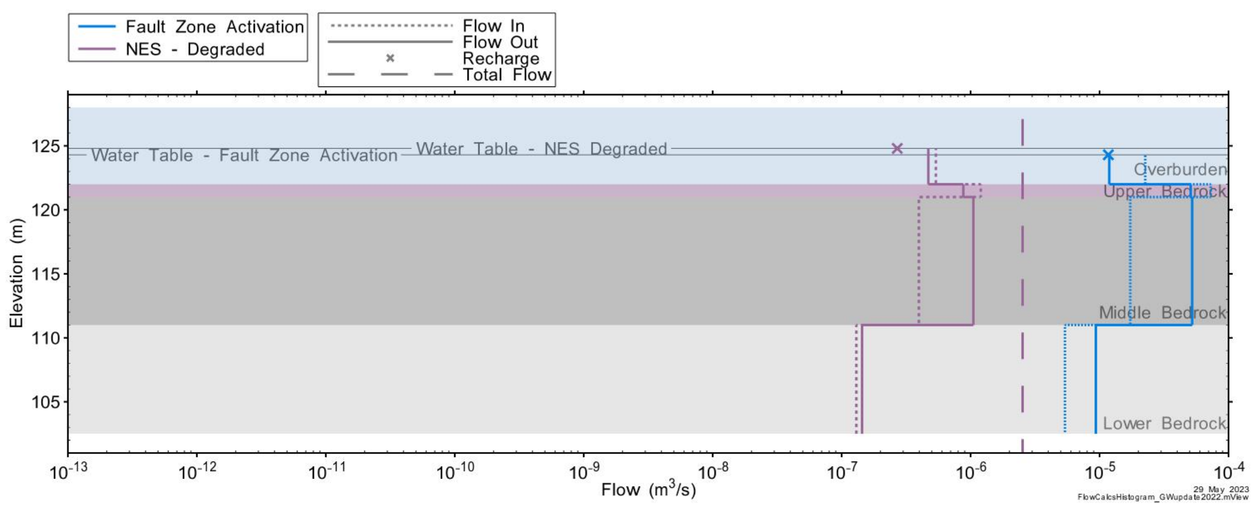

4.3.7 Overburden Well

The overburden well cases place a well in the overburden at a pumping rate of 5000 m³/a, at a location that intersects with the expected transport plume in the near-field model (Calder, 2023). The water table is very close to the top of bedrock, and consequently, a well cannot be supported in most locations. However, a well can be supported within the fill of the tile drain 2 trench, and the overburden well was placed within this trench, near but downgradient from the facility as illustrated in Figure 4-24. The overburden well was applied to the conditions of the NES Degraded Cap and NES Degraded cases.

Figure 4-24 Location of Overburden Well

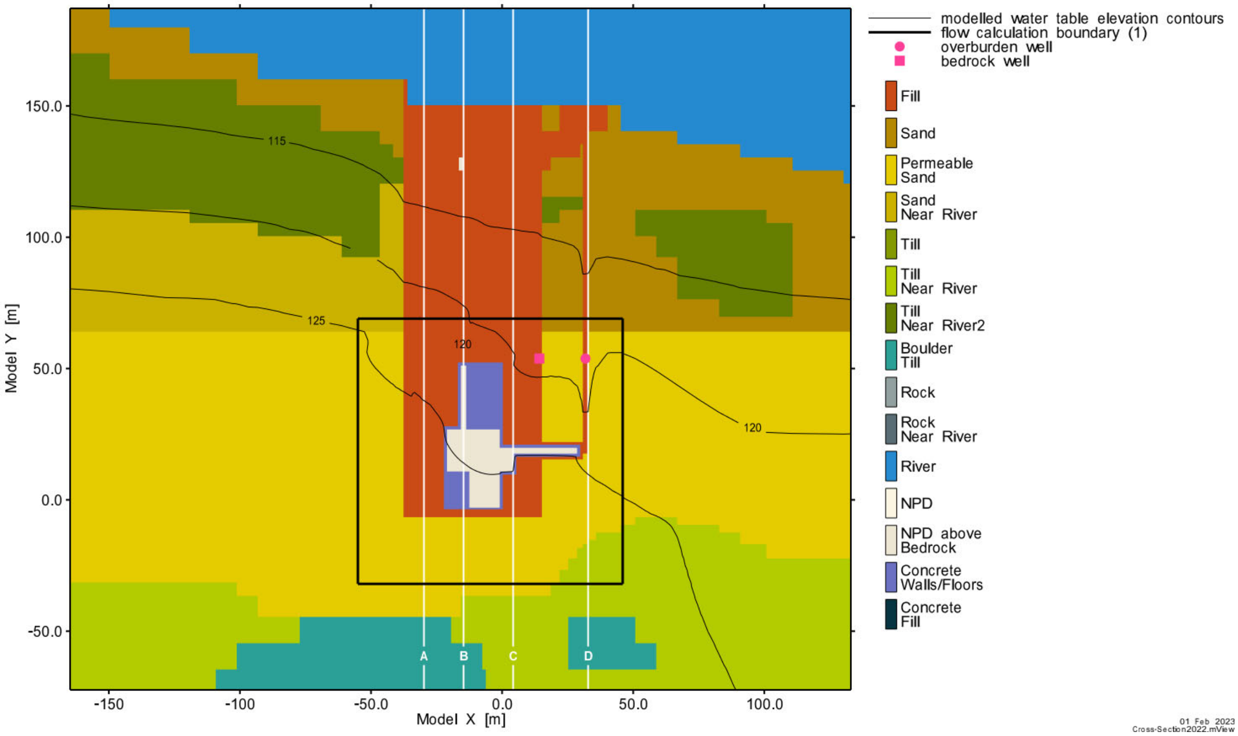

The addition of the well had a very marginal impact on the water table and geosphere flow system, as shown in Figure 4-25. This figure shows three cross-sections through the facility as in previous cross-section figures, with an additional D cross-section through the well (location shown in Figure 4-24).

Figure 4-25 Head Contours and Water Table at Four Cross-Sections through the Facility: Comparison of Overburden Well Cases

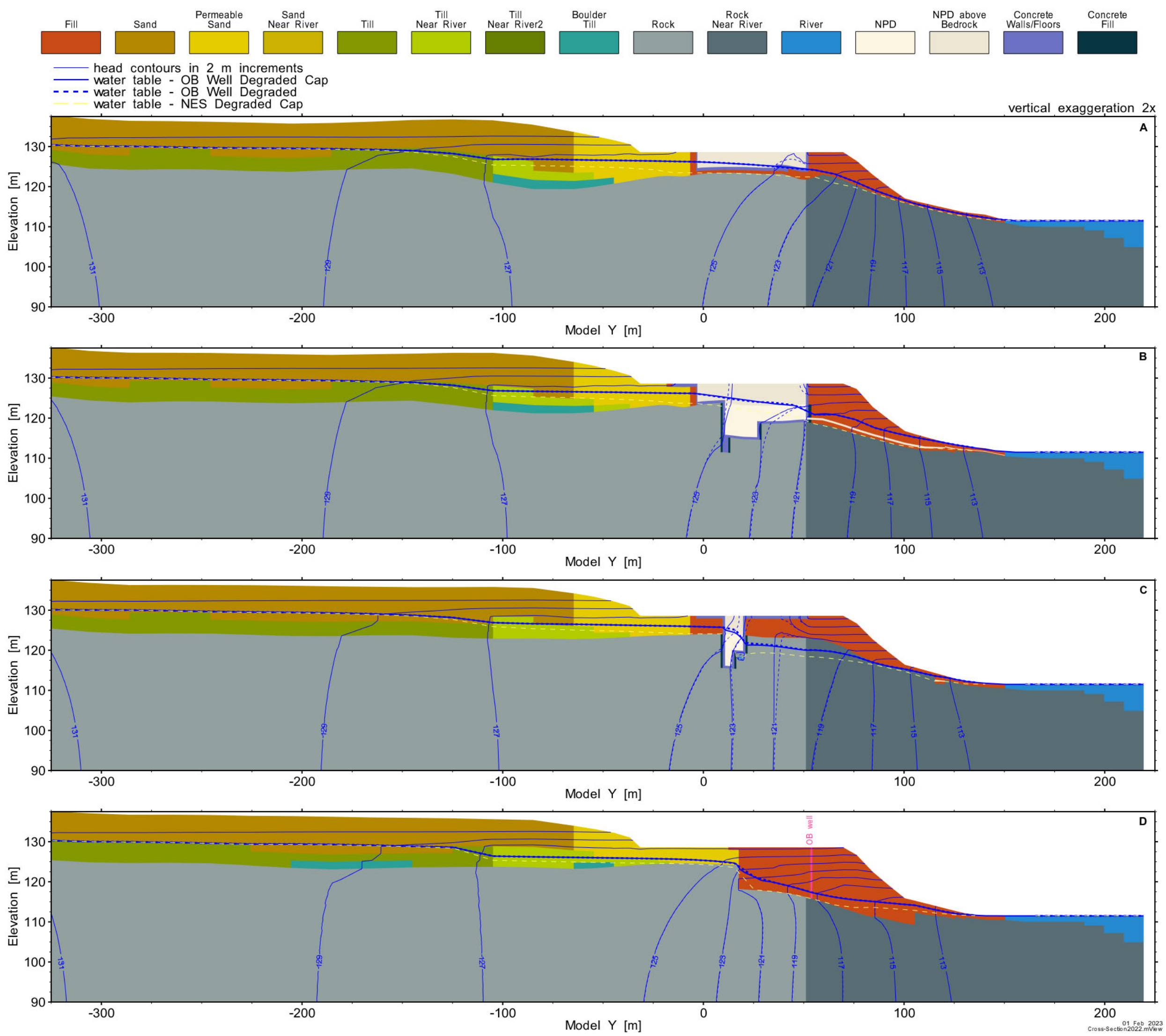

Table 4-14 provides the groundwater flows, categorized by hydrogeologic material, for flows through the area surrounding the facility (calculation 1, as described in Section 4.2) for the two overburden well cases. Figure 4-26 illustrates the changes in flow between the NES degraded cap case and the overburden well cases. The table and illustration confirm the limited impact of the overburden well on the geosphere flow system.

Table 4-15 provides a summary of the groundwater flows through the building itself (calculation 2, as described in Section 4.2), categorized by elevation, for the two overburden well cases. Building flows are very similar to the associated NES cases, with a slight increase in building flow of 3-4% for the Degraded Cap case and 1% for the Degraded case.

Table 4-14 Overburden Well Cases: Groundwater Flows in m^3/s Through NPD Region (Calculation1)

m^3/s	Overburden Well – Degraded Cap			Overburden Well – Degraded		
	Flow In	Flow Out	Difference	Flow In	Flow Out	Difference
Fill	1.90E-05	4.81E-03	-4.79E-03	6.13E-06	4.81E-03	-4.80E-03
Sand	4.48E-03	1.30E-03	3.18E-03	4.36E-03	1.19E-03	3.17E-03
Till	1.35E-04	2.19E-04	-8.40E-05	1.35E-04	2.19E-04	-8.40E-05
Bedrock	2.76E-05	6.68E-05	-3.92E-05	1.92E-05	6.68E-05	-4.76E-05
Recharge	1.51E-03	-	-	1.51E-03	-	-
Tile Drain 1	-	-	-	-	-	-
Total	6.14E-03	6.37E-03	-2.30E-04	6.01E-03	6.27E-03	-2.60E-04

Figure 4-26 Histogram of Groundwater Flows Through NPD Region (Calculation1): Comparison of Overburden Well Cases to NES Case

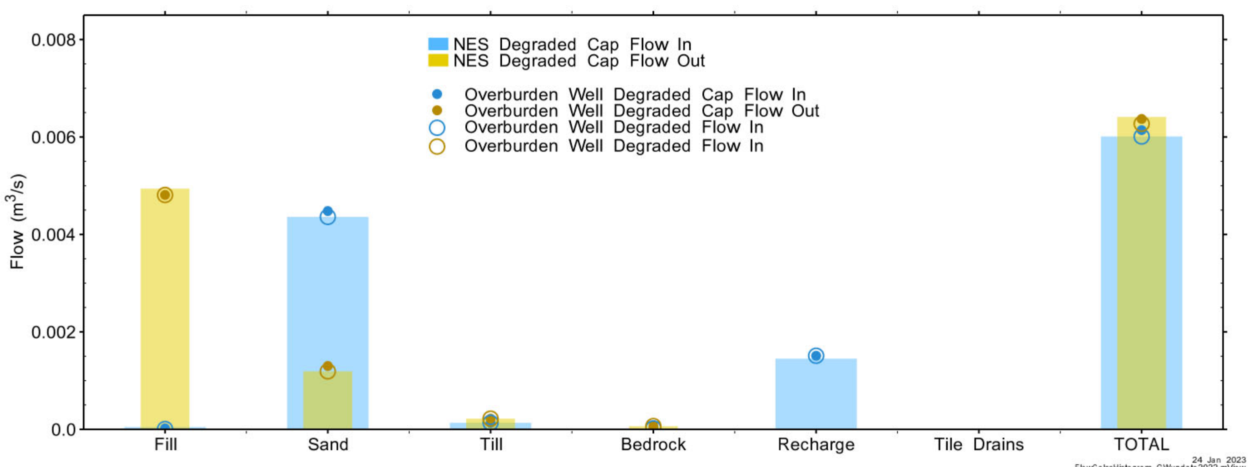

Table 4-15 Overburden Well Cases: Groundwater Flows in m^3/s Through NPD facility (Calculation2)

m^3/s	Overburden Well – Degraded Cap			Overburden Well – Degraded		
	Flow In	Flow Out	Diff	Flow In	Flow Out	Diff
Lower Bedrock (102-111 m)	7.92E-10	8.74E-10	-8.26E-11	1.32E-07	1.46E-07	-1.39E-08
Middle Bedrock (111-120 m)	2.28E-09	6.99E-09	-4.71E-09	4.01E-07	1.06E-06	-6.62E-07
Upper Bedrock (120-122 m)	6.10E-09	5.83E-09	2.72E-10	1.21E-06	8.86E-07	3.21E-07
Saturated Overburden (above 122 m)	3.56E-09	5.79E-09	-2.23E-09	5.42E-07	4.72E-07	7.01E-08
Recharge	6.12E-09	0.00E+00	6.12E-09	2.71E-07	0.00E+00	2.71E-07
Total	1.88E-08	1.95E-08	-6.31E-10	2.55E-06	2.57E-06	-1.38E-08

4.3.8 Bedrock Well

The bedrock well cases place a well in the bedrock at a pumping rate of 3500 m^3/a, at a location that intersects with the expected transport plume in the near-field model (Calder, 2023). The pumping rate is reduced by 70% compared to the overburden well, as the bedrock groundwater system was unable to support a pumping well at a rate of 5000 m^3/a. The location of the bedrock well is shown in Figure 4-24, and extends the full length of the bedrock in the model, from bedrock surface down to 80 m. The bedrock well was applied to the conditions of the NES Degraded Cap and NES Degraded cases.

The bedrock well causes local drawdown of the water table in the vicinity of the well, as shown in Figure 4-27. The water table is also shown in cross-section in Figure 4-28. Three cross-sections through the facility are shown as in previous cross-section figures, however, the C cross-section was shifted to align with the bedrock well.

Figure 4-27 Head Contours and Water Table In Plan View near the Facility: Comparison of Bedrock (BR) Well Cases

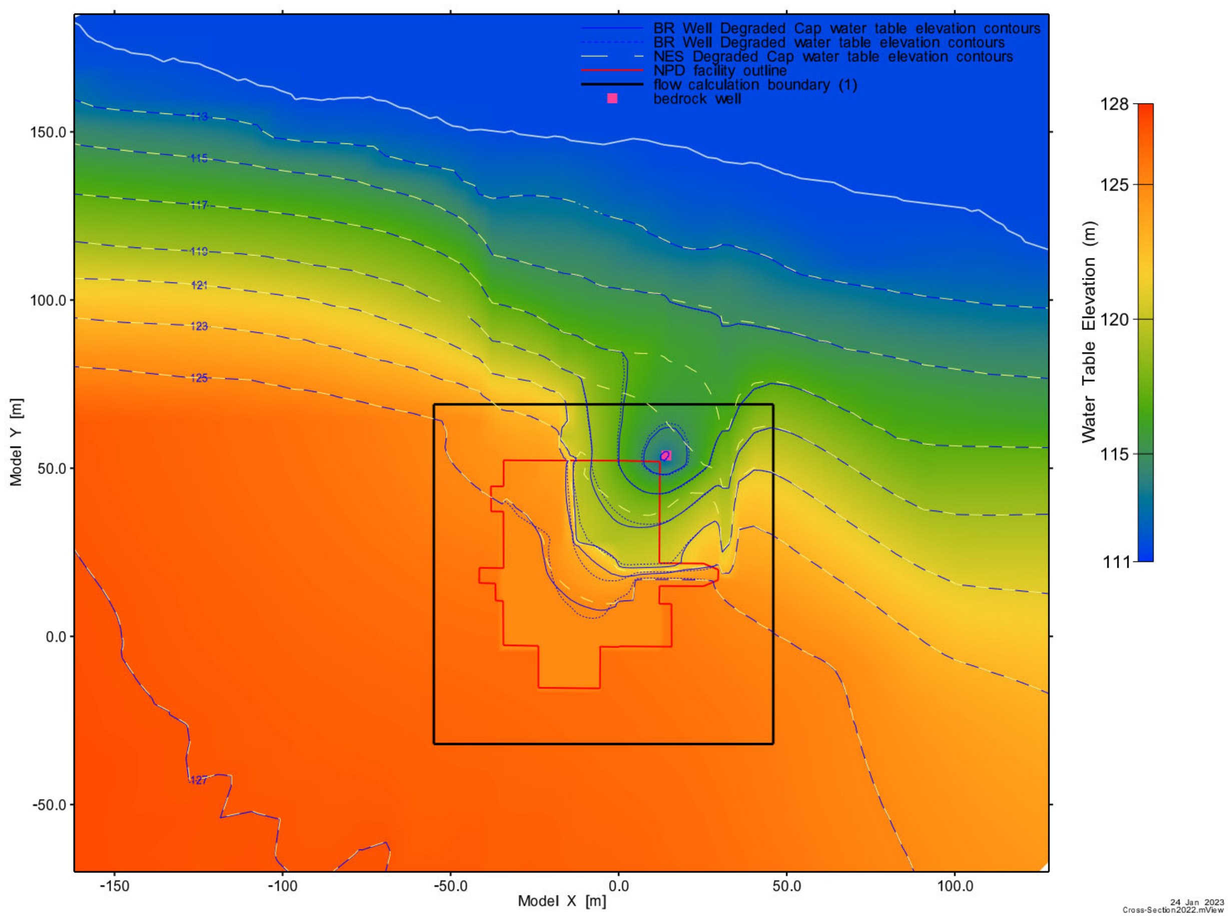

Figure 4-28 Head Contours and Water Table at Three Cross-Sections through the Facility: Comparison of Bedrock (BR) Well Cases

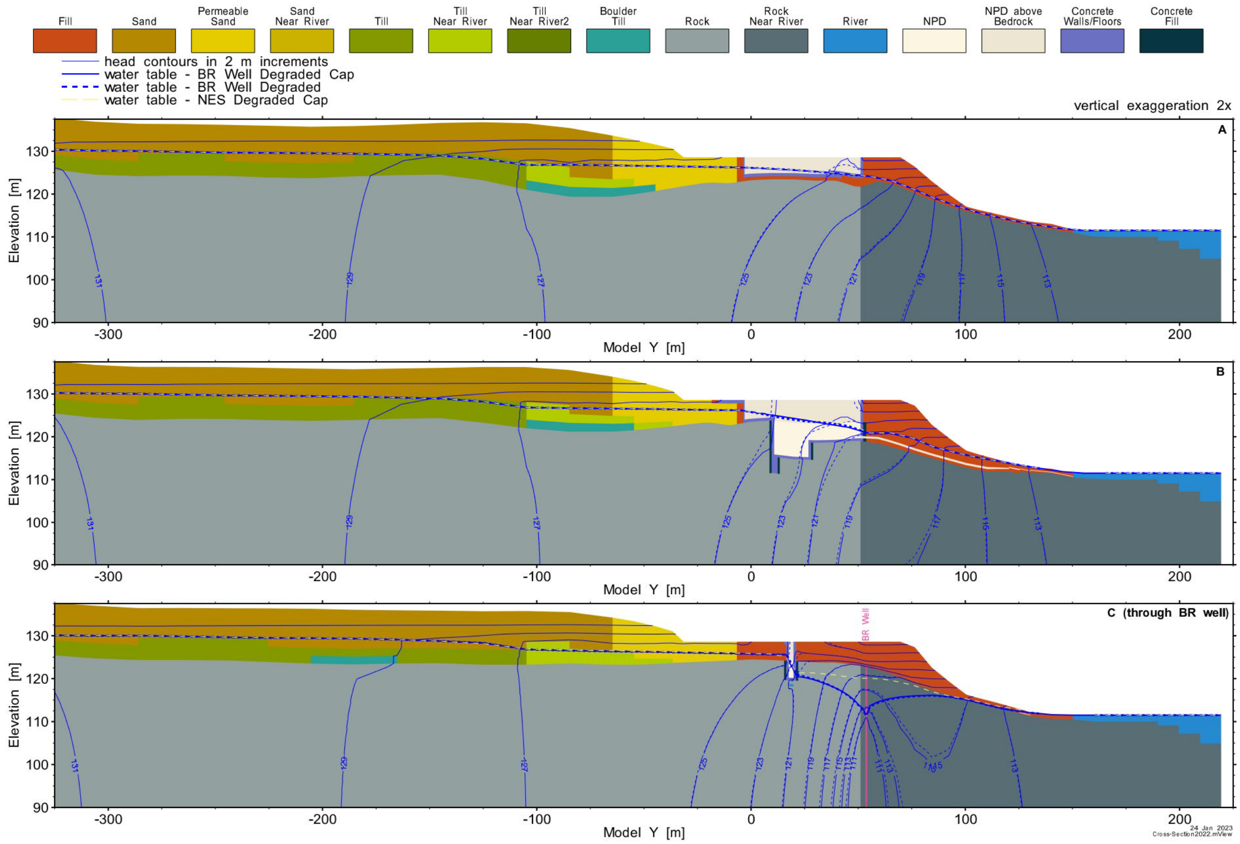

Table 4-16 provides the groundwater flows, categorized by hydrogeologic material, for flows through the area surrounding the facility (calculation 1, as described in Section 4.2) for the two bedrock well cases. Figure 4-29 illustrates the changes in flow between the NES degraded cap case and the bedrock well cases. The table and illustration show that the bedrock well has a limited impact on the geosphere flow system, despite some local impact on the water table near the facility.

Table 4-17 provides a summary of the groundwater flows through the building itself (calculation 2, as described in Section 4.2), categorized by elevation, for the two overburden well cases. Building flows are increased compared to the associated NES cases, with approximately 25% more flow through the building for both bedrock well cases.

Table 4-16 Bedrock Well Cases: Groundwater Flows in m³/s Through NPD Region (Calculation1)

m³/s	Bedrock Well – Degraded Cap			Bedrock Well – Degraded		
	Flow In	Flow Out	Difference	Flow In	Flow Out	Difference
Fill	3.29E-05	5.02E-03	-4.99E-03	3.85E-05	4.90E-03	-4.86E-03
Sand	4.36E-03	1.19E-03	3.17E-03	4.36E-03	1.19E-03	3.17E-03
Till	1.35E-04	2.18E-04	-8.30E-05	1.35E-04	2.18E-04	-8.30E-05
Bedrock	7.94E-05	3.09E-05	4.85E-05	5.53E-05	3.49E-05	2.04E-05
Recharge	1.45E-03	-	-	1.45E-03	-	-
Tile Drain 1	-	-	-	-	-	-
Total	6.14E-03	6.37E-03	-2.30E-04	6.01E-03	6.32E-03	-3.10E-04

Figure 4-29 Histogram of Groundwater Flows Through NPD Region (Calculation1): Comparison of Bedrock Well Cases to NES Case

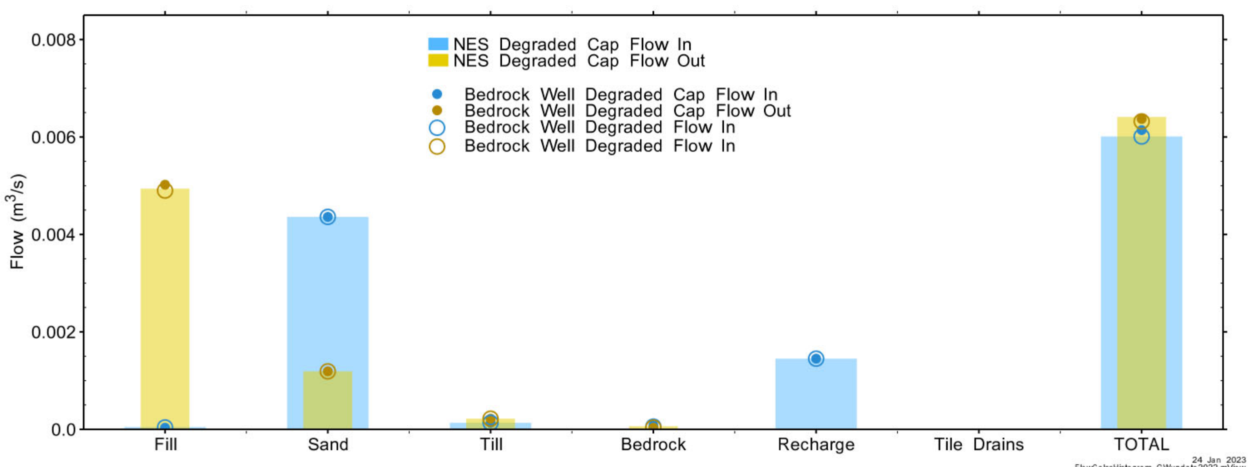

Table 4-17 Bedrock Well Cases: Groundwater Flows in m³/s Through NPD facility (Calculation2)

m³/s	Bedrock Well – Degraded Cap			Bedrock Well – Degraded		
	Flow In	Flow Out	Diff	Flow In	Flow Out	Diff
Lower Bedrock (102-111 m)	1.19E-09	1.59E-09	-4.01E-10	1.93E-07	2.43E-07	-5.04E-08
Middle Bedrock (111-120 m)	3.24E-09	9.44E-09	-6.20E-09	5.48E-07	1.34E-06	-7.89E-07
Upper Bedrock (120-122 m)	7.71E-09	7.11E-09	5.98E-10	1.48E-06	1.06E-06	4.16E-07
Saturated Overburden (above 122 m)	3.98E-09	5.33E-09	-1.35E-09	6.58E-07	4.35E-07	2.24E-07
Recharge	6.65E-09	0.00E+00	6.65E-09	2.90E-07	0.00E+00	2.90E-07
Total	2.28E-08	2.35E-08	-6.97E-10	3.17E-06	3.08E-06	9.13E-08

4.3.9 Extreme Concrete Degradation

The extreme concrete degradation cases investigate the impact of the concrete walls and floors of the facility by increasing the hydraulic conductivity of structural concrete to 10^{-6} m/s. Concrete fill hydraulic conductivity is also increased to 10^{-6} m/s.

Infiltration values were calculated from the resaturation model (Sgro, 2023). Infiltration for areas under the cover and at the edges of the cover are unchanged from the NES cases.

Changing the conductivity of facility materials (i.e. concrete and grout) has a very limited impact on the geosphere flow field, and the extreme concrete degradation cases are almost indistinguishable from the NES cases. Figure 4-30 shows three cross-sections through the facility for the three extreme concrete degradation cases, with the water table for the NES case (0 to 100 years) shown for comparison. Note that the water tables for the degraded cap and degraded extreme concrete degradation cases are nearly identical and overlap in the figure.

Figure 4-30 Head Contours and Water Table at Three Cross-Sections through the Facility: Comparison of Extreme Concrete Degradation Cases

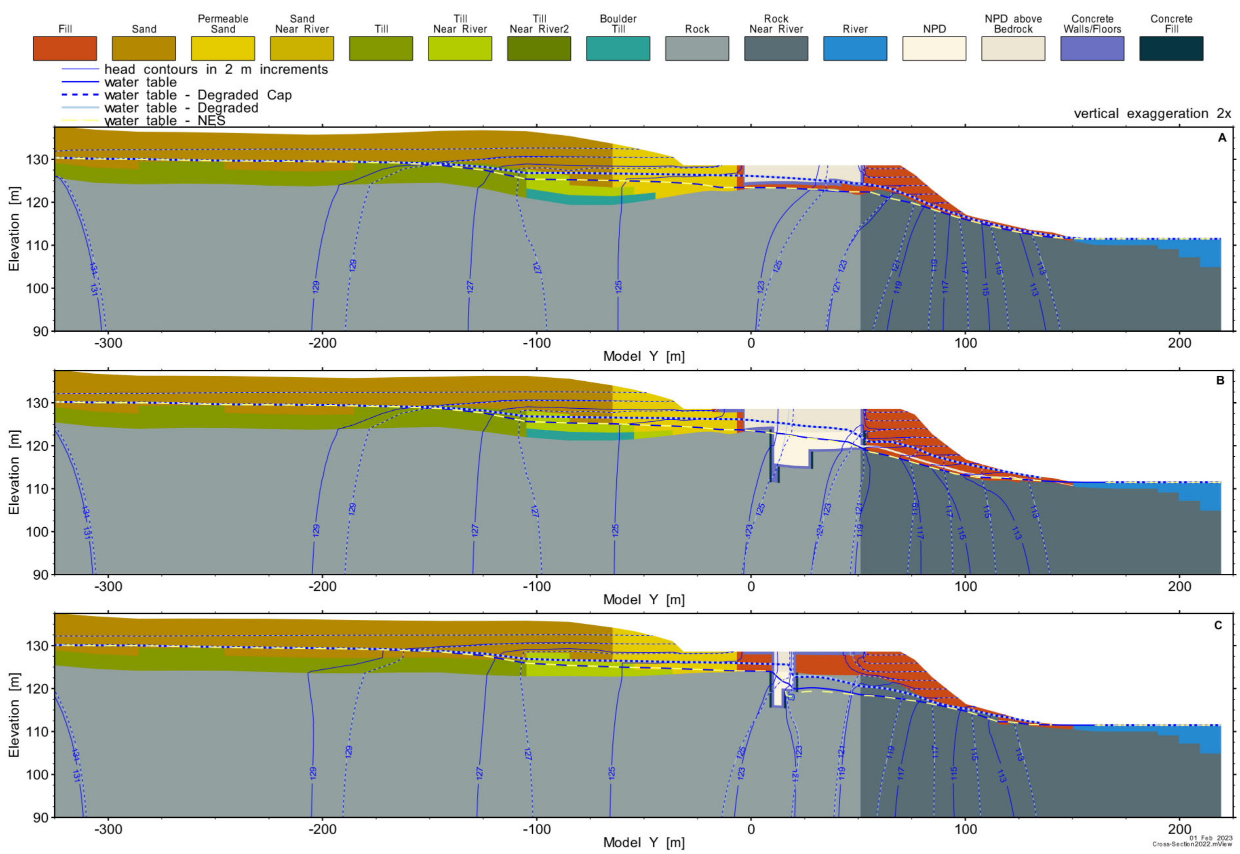

Table 4-18 provides the groundwater flows, categorized by hydrogeologic material, for flows through the area surrounding the facility (calculation 1, as described in Section 4.2) for the three extreme concrete degradation cases. Figure 4-31 illustrates the changes in flow between the NES and extreme concrete degradation cases. The table and illustration confirm the limited impact of facility conductivities on the geosphere flow system.

Table 4-19 provides a summary of the groundwater flows through the building itself (calculation 2, as described in Section 4.2), categorized by elevation, for all three extreme concrete degradation cases. The building flows are illustrated in Figure 4-32. Note that the flows are divided by elevation, and the description of overburden and bedrock is approximate. Building flows for all three cases are very similar, with the greatest differences occurring due to a lower water table (initial conditions case). The concrete conductivity plays a significant role, with high building flows in all cases compared to the NES cases. For the degraded case, flows are approximately 6 times greater with extreme concrete degradation than the NES degraded case.

Building flow calculations are conducted at the concrete wall, and do not consider flow through the middle of the facility. The building flow calculations may be influenced by flows through the permeable concrete wall that never enter the middle of the facility filled with low permeability grout. As well, the groundwater flow model only has concrete on the exterior of the building; interior walls and floors are not modelled. Transport simulations conducted with the near-field model (Calder, 2023) consider both interior walls and floors, and calculate groundwater flows within individual rooms, providing a measure of the flow through the middle of the facility.

Table 4-18 Extreme Concrete Degradation Cases: Groundwater Flows in m^3/s Through NPD Region (Calculation1)

m^3/s	Extreme Concrete Degradation			Extreme Concrete Degradation – Degraded Cap			Extreme Concrete Degradation – Degraded		
	Flow In	Flow Out	Difference	Flow In	Flow Out	Difference	Flow In	Flow Out	Difference
Fill	3.50E-05	3.29E-04	-2.94E-04	6.26E-05	4.99E-03	-4.93E-03	6.32E-05	4.99E-03	-4.93E-03
Sand	6.91E-03	7.23E-04	6.19E-03	4.36E-03	1.17E-03	3.19E-03	4.36E-03	1.17E-03	3.19E-03
Till	5.02E-05	2.29E-05	2.73E-05	1.35E-04	2.17E-04	-8.20E-05	1.35E-04	2.17E-04	-8.20E-05
Bedrock	2.70E-05	6.26E-05	-3.56E-05	1.92E-05	7.00E-05	-5.08E-05	1.93E-05	7.02E-05	-5.09E-05
Recharge	4.78E-04	-	-	1.45E-03	-	-	1.45E-03	-	-
Tile Drain 1	-	6.91E-03	-	-	-	-	-	-	-
Total	7.50E-03	8.04E-03	-5.43E-04	6.03E-03	6.45E-03	-4.20E-04	6.03E-03	6.45E-03	-4.20E-04

Figure 4-31 Histogram of Groundwater Flows Through NPD Region (Calculation1): Comparison of Extreme Concrete Degradation Cases to NES Case

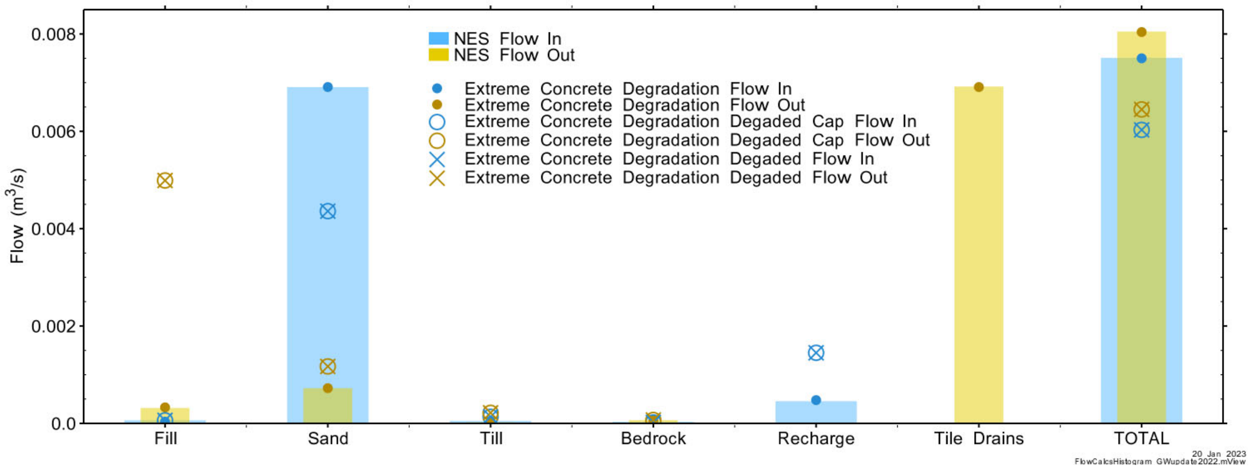

Table 4-19 Extreme Concrete Degradation Cases: Groundwater Flows in m^3/s Through NPD facility (Calculation2)

m^3/s	Extreme Concrete Degradation			Extreme Concrete Degradation – Degraded Cap			Extreme Concrete Degradation – Degraded		
	Flow In	Flow Out	Diff	Flow In	Flow Out	Diff	Flow In	Flow Out	Diff
Lower Bedrock (102-111 m)	7.69E-07	8.20E-07	-5.11E-08	7.75E-07	8.65E-07	-9.00E-08	8.22E-07	9.12E-07	-8.94E-08
Middle Bedrock (111-120 m)	4.96E-06	6.40E-06	-1.44E-06	4.79E-06	6.83E-06	-2.04E-06	4.97E-06	7.57E-06	-2.60E-06
Upper Bedrock (120-122 m)	3.90E-06	3.11E-06	7.93E-07	5.76E-06	4.55E-06	1.21E-06	7.08E-06	5.74E-06	1.34E-06
Saturated Overburden (above 122 m)	4.28E-08	1.22E-08	3.06E-08	1.72E-06	1.72E-06	1.81E-09	2.46E-06	2.33E-06	1.34E-07
Recharge	1.06E-09	0.00E+00	1.06E-09	1.56E-07	0.00E+00	1.56E-07	2.46E-07	0.00E+00	2.46E-07
Total	9.68E-06	1.03E-05	-6.62E-07	1.32E-05	1.40E-05	-7.65E-07	1.56E-05	1.66E-05	-9.65E-07

Figure 4-32 Flow Through the Building (Flow Calculation 2): Comparison of Extreme Concrete Degradation Cases

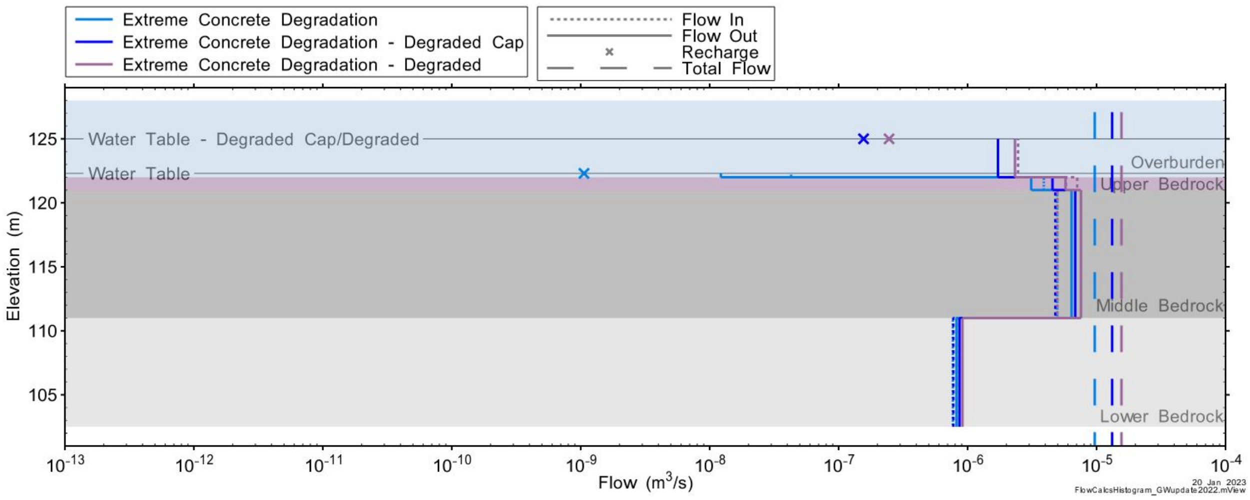

4.3.10 Extreme Grout Degradation

The extreme grout degradation cases investigate the impact of grout permeability by increasing the hydraulic conductivity of grout to 10^{-6} m/s.

Infiltration values were calculated from the resaturation model (Sgro, 2023). Infiltration for areas under the cover and at the edges of the cover are unchanged from the NES cases.

Changing the conductivity of facility materials has a very limited impact on the geosphere flow field, and the extreme grout degradation cases are almost indistinguishable from the NES cases. Figure 4-33 shows three cross-sections through the facility for the three extreme grout degradation cases, with the water table for the NES case (0 to 100 years) shown for comparison.

Figure 4-33 Head Contours and Water Table at Three Cross-Sections through the Facility: Comparison of Extreme Grout Degradation Cases

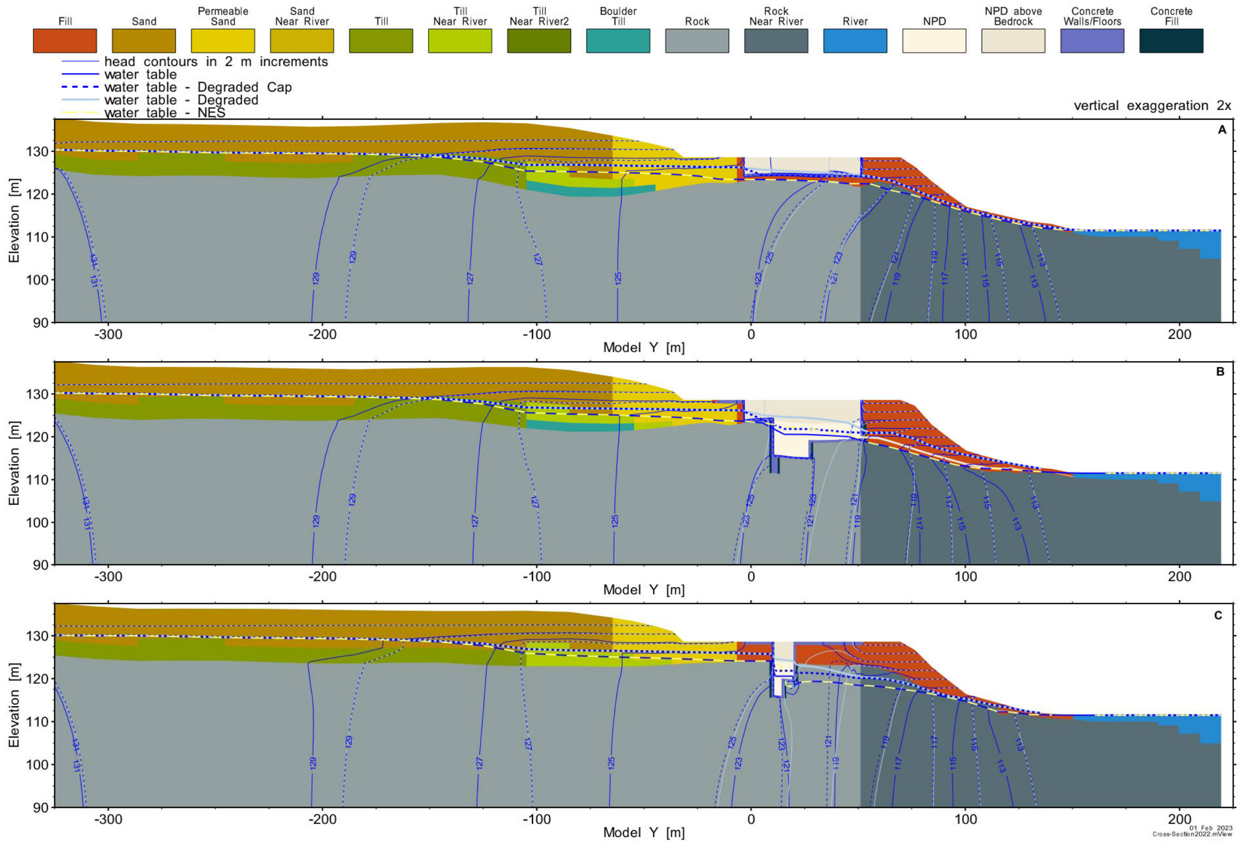

Table 4-20 provides the groundwater flows, categorized by hydrogeologic material, for flows through the area surrounding the facility (calculation 1, as described in Section 4.2) for the three extreme grout degradation cases. Figure 4-34 illustrates the changes in flow between the NES and extreme grout degradation cases. The table and illustration confirm the limited impact of facility conductivities on the geosphere flow system.

Table 4-21 provides a summary of the groundwater flows through the building itself (calculation 2, as described in Section 4.2), categorized by elevation, for all three extreme grout degradation cases. The building flows are illustrated in Figure 4-35. Within this illustration, the water table shown is the average water table over the building footprint, with some flow occurring above the water table in some portions of the building. Building flows increase with degradation, as in the NES cases, indicating the importance of the relatively tight concrete walls for limiting flow into the facility. Total flows into the building are approximately 30 times greater than the NES case for initial conditions, 150 times greater for degraded cap conditions and 6 times greater for degraded conditions.

Table 4-20 Extreme Grout Degradation Cases: Groundwater Flows in m³/s Through NPD Region (Calculation1)

m³/s	Extreme Grout Degradation			Extreme Grout Degradation – Degraded Cap			Extreme Grout Degradation – Degraded		
	Flow In	Flow Out	Difference	Flow In	Flow Out	Difference	Flow In	Flow Out	Difference
Fill	6.28E-05	3.17E-04	-2.54E-04	4.12E-05	4.94E-03	-4.90E-03	4.54E-05	4.95E-03	-4.90E-03
Sand	6.91E-03	7.23E-04	6.19E-03	4.36E-03	1.19E-03	3.17E-03	4.36E-03	1.20E-03	3.16E-03
Till	5.00E-05	2.30E-05	2.70E-05	1.35E-04	2.19E-04	-8.40E-05	1.35E-04	2.18E-04	-8.30E-05
Bedrock	3.10E-05	6.55E-05	-3.45E-05	1.72E-05	6.46E-05	-4.74E-05	1.71E-05	6.64E-05	-4.93E-05
Recharge	4.54E-04	-	-	1.45E-03	-	-	1.46E-03	-	-
Tile Drain 1	-	6.92E-03	-	-	-	-	-	-	-
Total	7.51E-03	8.05E-03	-5.45E-04	5.98E-03	6.39E-03	-4.10E-04	6.02E-03	6.43E-03	-4.17E-04

Figure 4-34 Histogram of Groundwater Flows Through NPD Region (Calculation1): Comparison of Extreme Grout Degradation Cases to NES Case

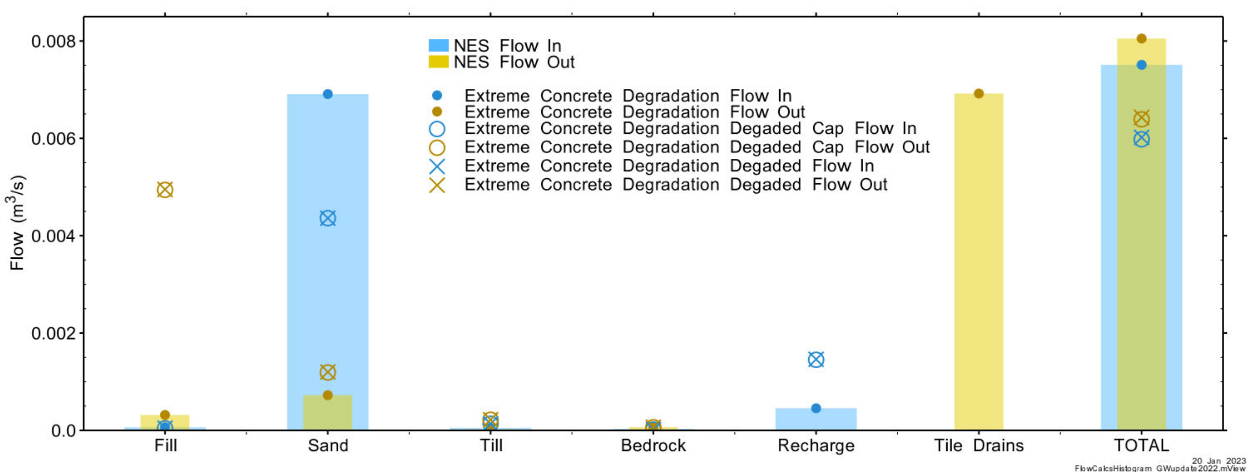

Table 4-21 Extreme Grout Degradation Cases: Groundwater Flows in m³/s Through NPD facility (Calculation2)

m³/s	Extreme Grout Degradation			Extreme Grout Degradation – Degraded Cap			Extreme Grout Degradation – Degraded		
	Flow In	Flow Out	Diff	Flow In	Flow Out	Diff	Flow In	Flow Out	Diff
Lower Bedrock (102-111 m)	9.52E-09	1.30E-09	8.22E-09	1.56E-08	7.85E-10	1.48E-08	1.76E-07	1.59E-06	-1.41E-06
Middle Bedrock (111-120 m)	7.08E-08	9.08E-08	-2.00E-08	1.05E-07	2.60E-07	-1.55E-07	1.37E-06	5.14E-06	-3.77E-06
Upper Bedrock (120-122 m)	5.30E-08	1.69E-07	-1.16E-07	6.42E-08	2.00E-07	-1.36E-07	3.05E-06	3.81E-06	-7.55E-07
Saturated Overburden (above 122 m)	0.00E+00	0.00E+00	0.00E+00	0.00E+00	0.00E+00	0.00E+00	3.24E-06	4.13E-06	-8.97E-07
Recharge	1.02E-07	0.00E+00	1.02E-07	2.29E-07	0.00E+00	2.29E-07	6.65E-06	0.00E+00	6.65E-06
Total	2.36E-07	2.61E-07	-2.51E-08	4.14E-07	4.61E-07	-4.71E-08	1.45E-05	1.47E-05	-1.84E-07

Figure 4-35 Flow Through the Building (Flow Calculation 2): Comparison of Extreme Grout Degradation Cases

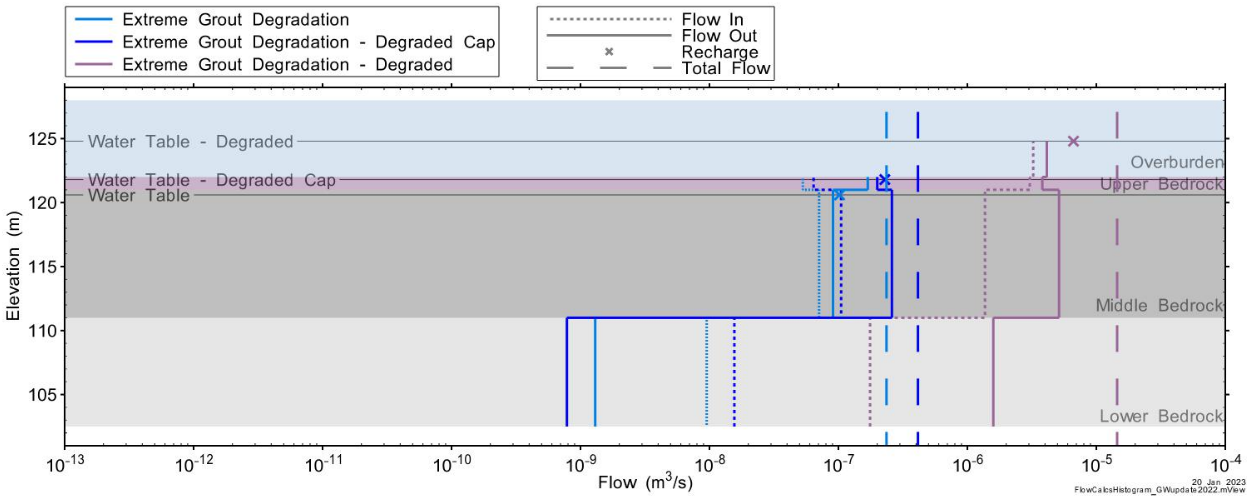

5 SENSITIVITY CASES

Sensitivity cases investigate the impact of model inputs, both site-specific data-based inputs and numeric inputs, that are not considered in the scenario cases. These cases provide additional confidence in the groundwater model, addressing uncertainties associated with the model. The sensitivity cases considered in this section include:

- **Side Boundary Location** – Initial models found the location of the eastern side boundary to have a negligible impact on model results. This case confirms these conclusions with the existing calibrated model.

- **Fill Conductivity** – The calibrated model is relatively insensitive to the fill hydraulic conductivity and the final calibrated value is at the upper range of expected values for this material (10^{-3} m/s). This suggests that the fill conductivity could be reduced with limited impact on model calibration. Several cases with lower fill hydraulic conductivity are considered to explore the extent to which fill conductivity can be lowered with minimal impact on the model calibration.

- **Tile Drain Flowrate** – The model is currently calibrated to an average tile drain flow rate and an average annual recharge. In these sensitivity cases, the model is recalibrated for a tile drain flow rate one standard deviation below the average (low tile drain rate case) and one standard deviation above the average (high tile drain rate case). These cases illustrate the impact of the tile drain flow rate on model calibration.

5.1 Side Boundary Location

The eastern boundary of the model appears close to the facility, relative to the other model boundaries. Previous versions of the groundwater model adjusted this boundary and found that flow generally flowed from topographic highs towards the river. Consequently, placing the eastern boundary near the surface-water watershed boundary was a logical, efficient and numerically sound location for the eastern boundary.

The intention of this sensitivity case is to repeat some of the previous work with the current version of the groundwater model to demonstrate the suitability of the eastern boundary. In this case, the eastern boundary of the calibrated groundwater model is extended by 300 m, as shown in Figure 5-1.

Figure 5-1 Plan View Showing Extended Side Boundary Model Domain

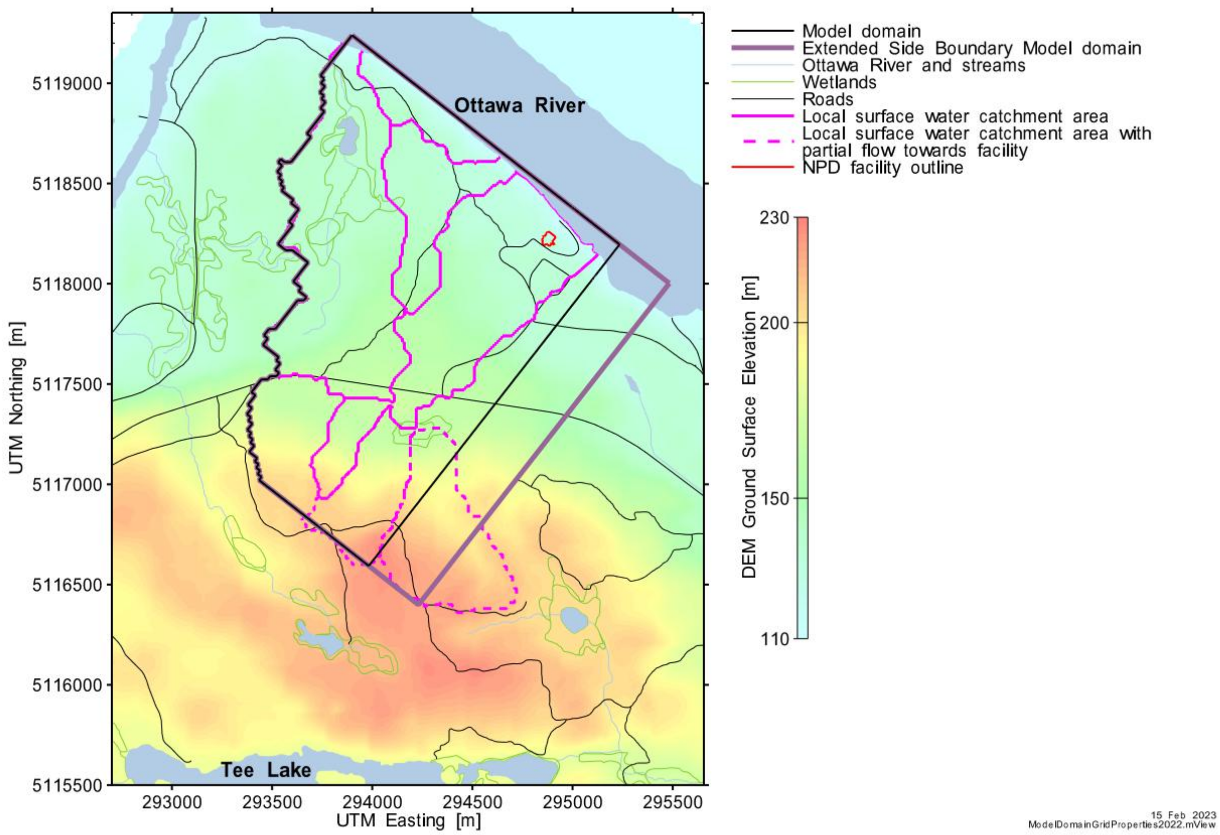

To show that the location of the boundary has minimal impact on the model results, the results of the calibration model are revisited. Figure 5-2 shows a cross plot of observed and measured water levels used for calibration, for both the calibrated model and the extended side boundary model. In addition, the tile drain flow for the extended side model is slightly reduced to 6.8 L/s (from 7.0 L/s in the calibrated model). The model calibration is very similar between the extended model and the calibrated model.

Figure 5-3 compares the water table head contours for the extended side boundary case compared to the calibrated model in plan view, and Figure 5-4 shows the same comparison in cross-sections near the facility. In general, head contours are very similar, with some differences at the eastern boundary. Of particular note is the similarity of the head contours in the vicinity of the facility, and the direction of flow in the extended eastern portion of the model, in which flow is generally directed parallel to the model boundary (head contours perpendicular to the boundary). Where the contours are not parallel to the model boundary, the water table is very flat.

Geosphere flows in the vicinity of the facility are reduced by approximately 3% when examining flows crossing the flow calculation (1) boundary (Section 4.2).

Given the limited impact of the eastern flow boundary location based on the above evidence, it can be confirmed that the location of the flow boundary in the calibrated model is reasonable.

Figure 5-2 Cross-plot of Modelled and Observed Water Levels – Comparison of Extended Model Boundary to Post-Calibration Model

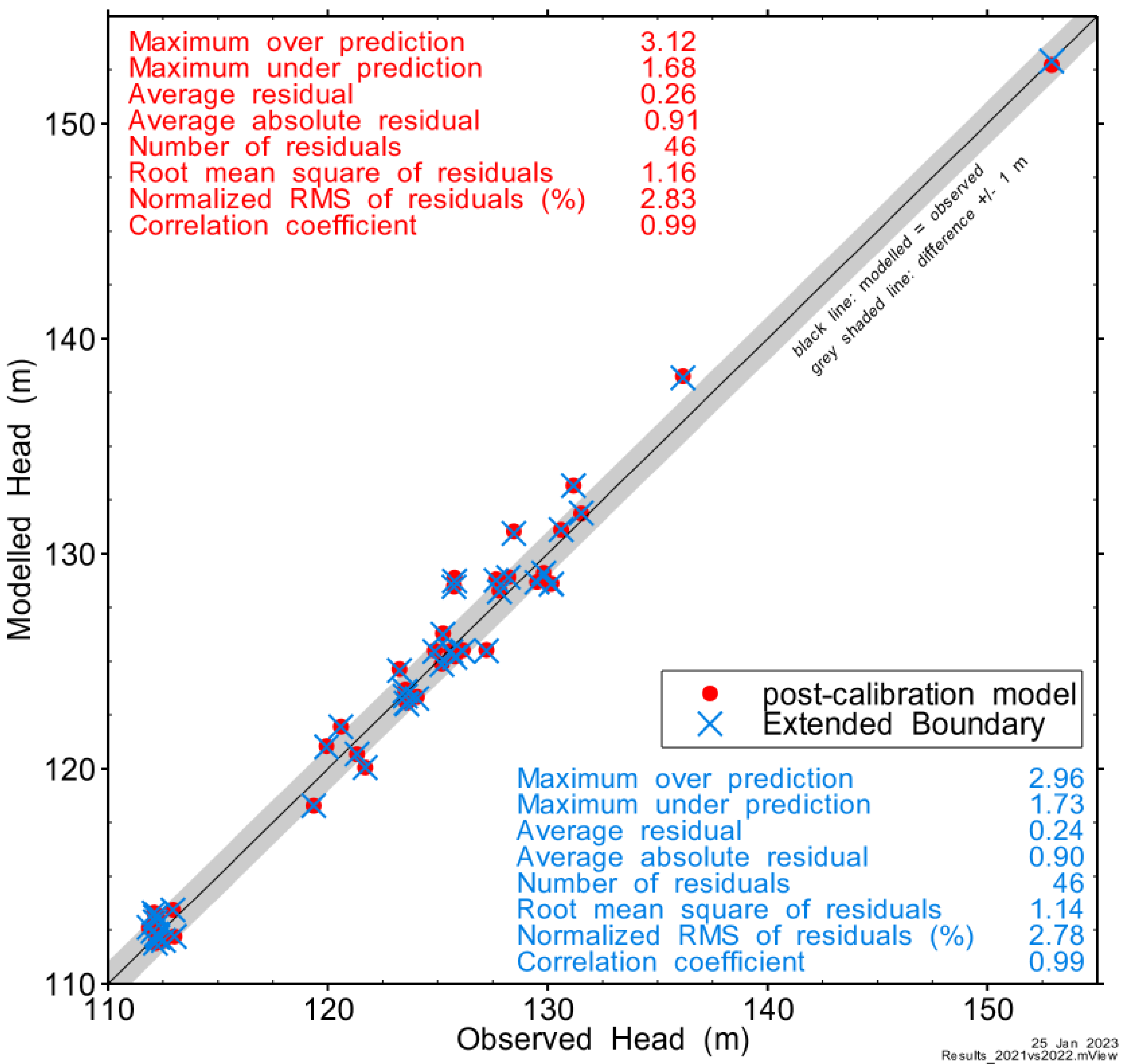

Figure 5-3 Plan View Showing Model Water Table Elevations and Velocities – Comparison of Extended Model Boundary to Post-Calibration Model

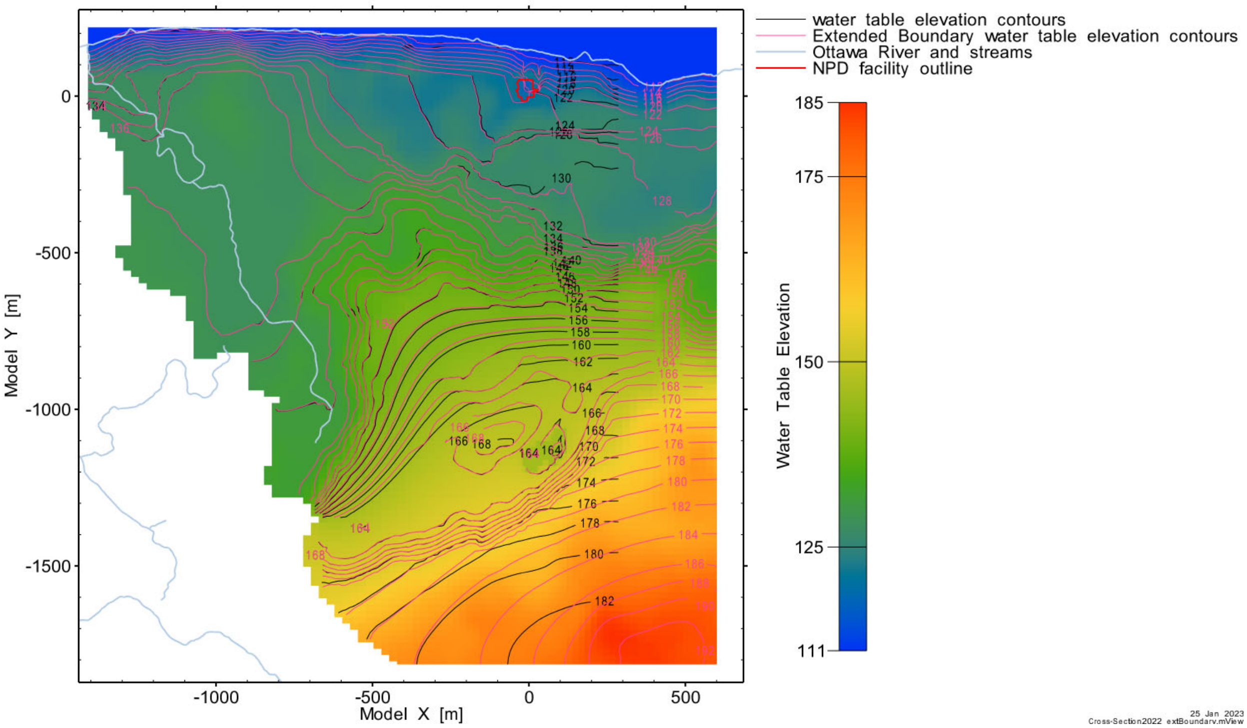

Figure 5-4 Cross-sections Showing Model Head Contours, Velocities and Water Table – Comparison of Extended Model Boundary to Post-Calibration Model

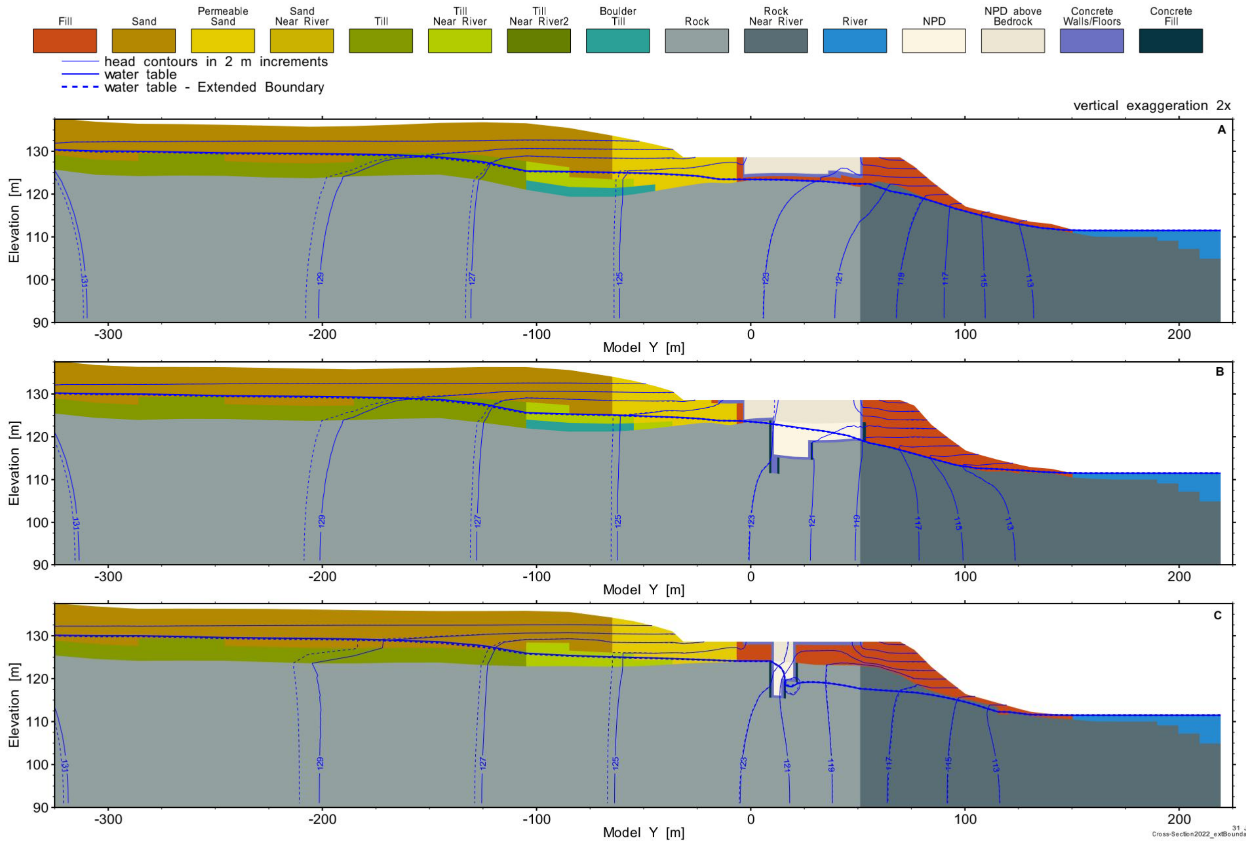

5.2 Fill Conductivity

The fill represents the primary overburden material between the facility and the river. However, the calibrated model is relatively insensitive to the fill hydraulic conductivity and the final calibrated value is at the upper range of expected values for this material (10^{-3} m/s). This suggests that the fill conductivity could be reduced with limited impact on model calibration. A series of cases with fill hydraulic conductivity across the expected range of fill conductivity (10^{-6} to 10^{-3} m/s) were simulated to investigate the impact of fill hydraulic conductivity on model results. A total of six simulations were conducted, with fill conductivity changing by half an order of magnitude: $5x10^{-4}$, 10^{-4}, $5x10^{-5}$, 10^{-5}, $5x10^{-6}$, and 10^{-6} m/s.

Modifying the fill conductivity only affects water levels in the vicinity of the fill, and consequently, as expected, has minimal impact on the overall calibration statistics. Figure 5-5 shows the cross-plot of the fill conductivity cases, compared to the comparable NES case. The outlier (BH16-02B) is also removed from the cross-plot and statistics. While reducing the fill conductivity increases the water table near the river (and low observed heads), it has a limited impact on the overall calibration statistics. Limiting calibration statistics to water levels below 125 m of observed head, as shown in Figure 5-6, the differences between the cases is apparent: below an approximate conductivity of $5x10^{-5}$ m/s, the change in root mean square

(RMS) increases substantially, with a 5% increase in RMS at 10^{-4} m/s, 9% at $5x10^{-5}$ m/s, 28% at 10^{-5} m/s and 70% at 10^{-6} m/s.

Figure 5-5 Cross-plot of Modelled and Observed Water Levels for Fill Hydraulic Conductivity Sensitivity Cases

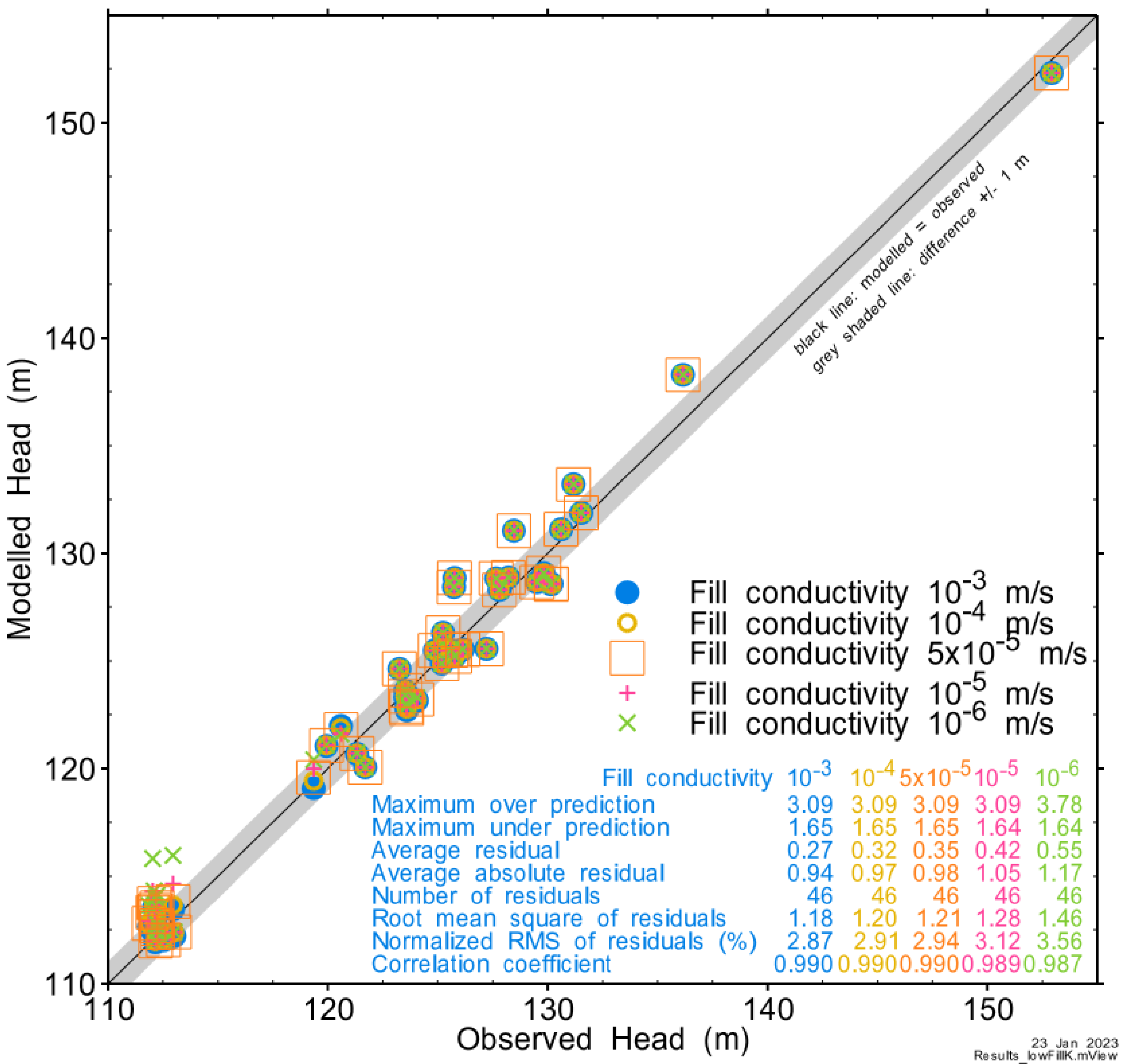

Figure 5-6 Lmited Cross-plot of Modelled and Observed Water Levels for Fill Hydraulic Conductivity Sensitivity Cases

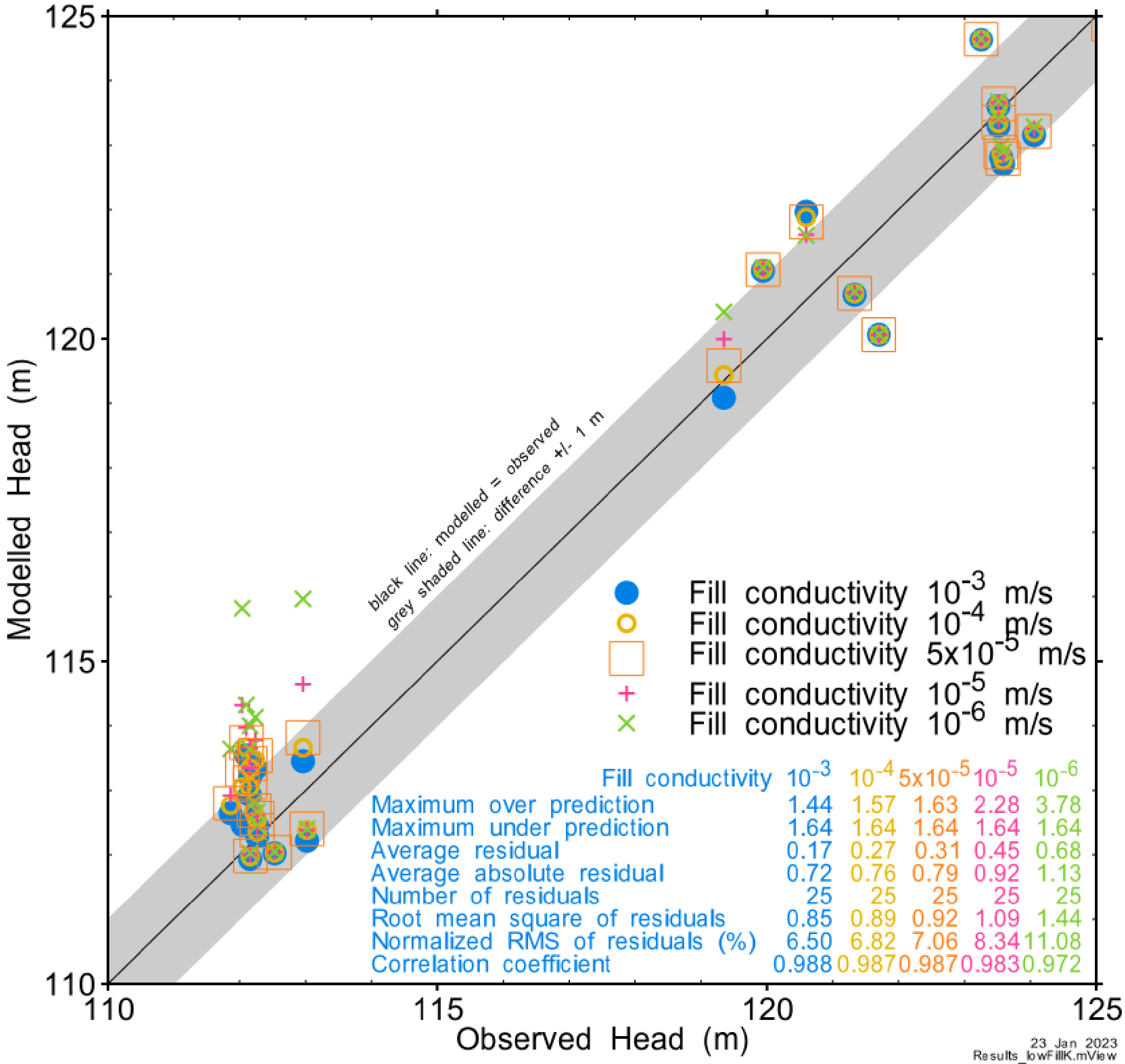

Figure 5-7 shows the water table for three of the cases, 10^{-4}, 10^{-5} and 10^{-6} m/s, compared to the NES case. At 10^{-5} and 10^{-6}, the water table is above ground surface at the base of the bluff and near the river, indicative that these cases are not reasonable representations of the groundwater system.

Based on these model results, it can be inferred that the fill hydraulic conductivity can be reduced to $5x10^{-5}$ m/s with limited impact on the model calibration. Such a decrease results in a marginal increase in the water table of the fill downgradient of the facility.

Figure 5-7 Cross-sections Showing Calibrated Model Head Contours, Velocities and Water Table

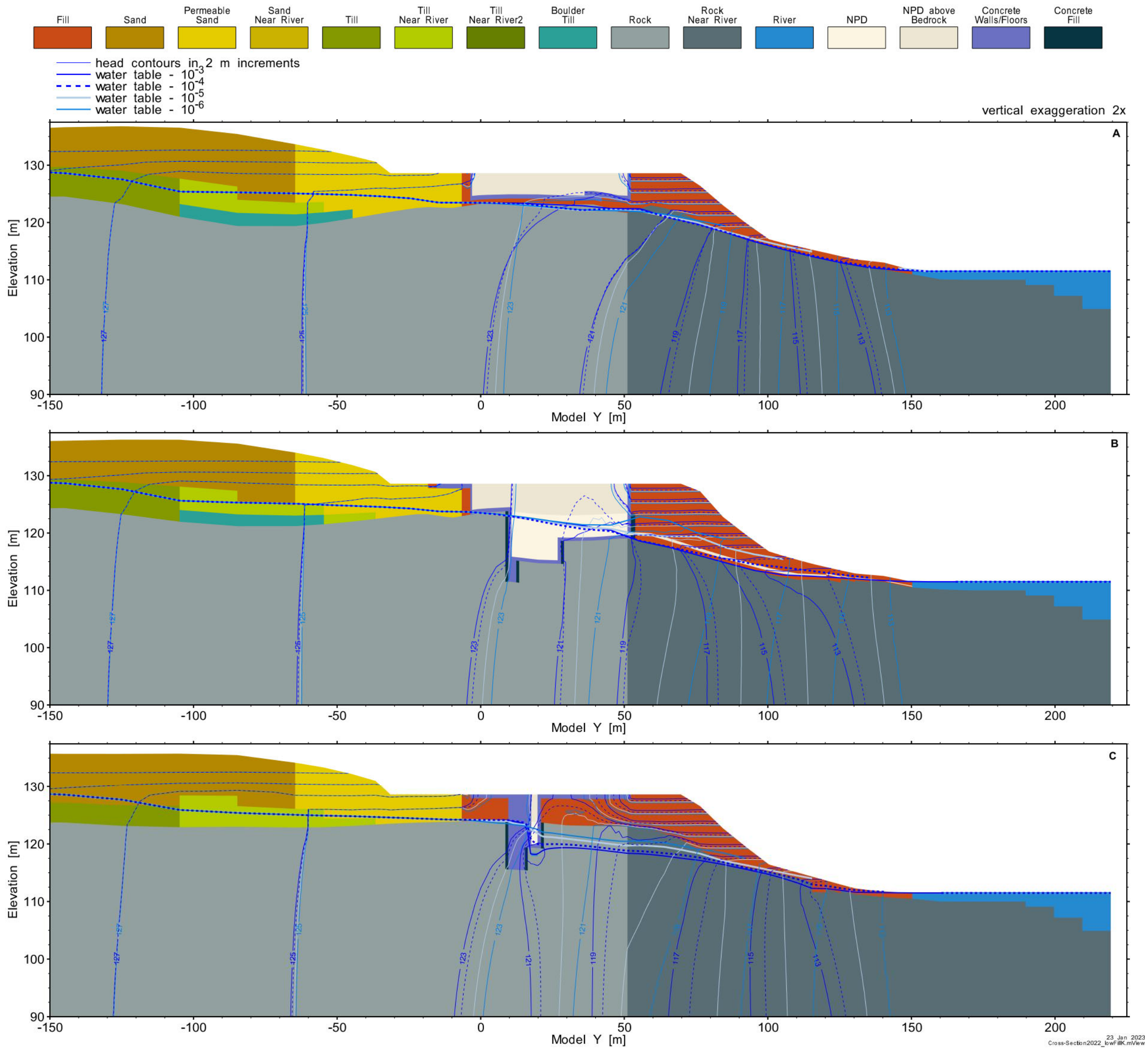

The effect of a fill hydraulic conductivity of 5x10^{-5} m/s on groundwater flows in the vicinity of the facility is small. Table 5-1 provides the groundwater flows, categorized by hydrogeologic material, for flows through the area surrounding the facility (calculation 1, as described in Section 4.2) and Figure 5-8 illustrates the changes in flow compared to the NES case. The table and illustration confirm the limited impact of fill hydraulic conductivity of 5x10^{-5} m/s on the geosphere flow system.

Table 5-2 provides a summary of the groundwater flows through the building itself (calculation 2, as - described in Section 4.2), categorized by elevation, for a fill hydraulic conductivity of 5x10^{-5} m/s. Building flows are reduced slightly in the lower bedrock, but increased slightly in the overburden and upper bedrock. The total flow through the building is increased by 7%.

Table 5-1 Low Fill Hydraulic Conductivity of 5x10^{-5} m/s : Groundwater Flows in m^3/s Through NPD Region (Calculation1)

m^3/s	Flow In	Flow Out	Difference
Fill	6.45E-06	2.11E-04	-2.05E-04
Sand	6.92E-03	7.38E-04	6.18E-03
Till	4.86E-05	2.34E-05	2.52E-05
Bedrock	2.22E-05	5.43E-05	-3.21E-05
Recharge	4.58E-04	-	-
Tile Drain 1	-	6.97E-03	-
Total	7.44E-03	8.00E-03	-5.61E-04

Figure 5-8 Histogram of Groundwater Flows Through NPD Region (Calculation1): Comparison of Low Fill Hydraulic Conductivity of 5x10^{-5} m/s Case to NES Case

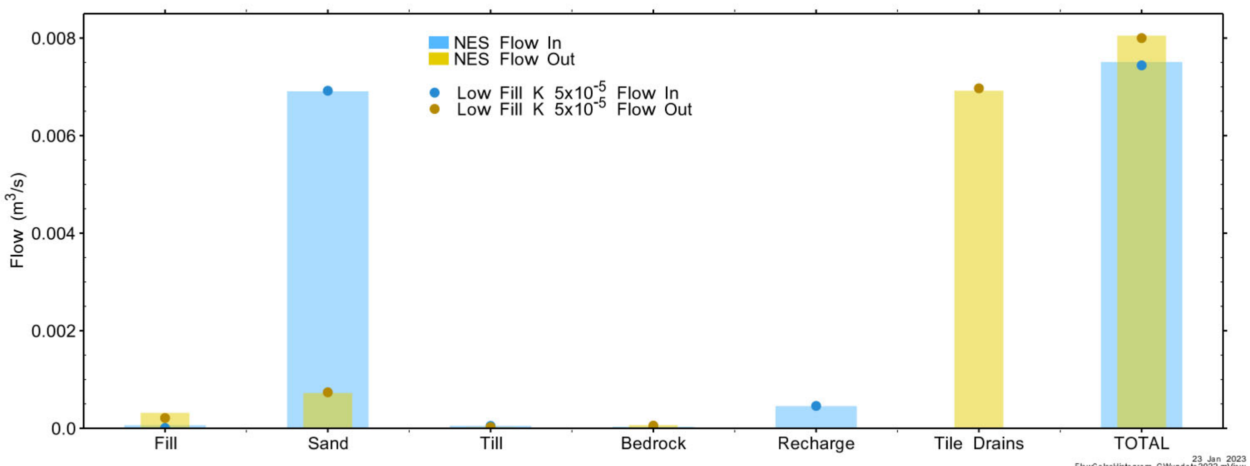

Table 5-2 Low Fill Hydraulic Conductivity of 5x10^{-5} m/s : Groundwater Flows in m^3/s Through NPD facility (Calculation2)

m^3/s	Flow In	Flow Out	Difference
Lower Bedrock (102-111 m)	6.53E-10	5.90E-10	6.36E-11
Middle Bedrock (111-120 m)	1.77E-09	3.78E-09	-2.02E-09
Upper Bedrock (120-122 m)	3.81E-09	3.31E-09	5.01E-10
Saturated Overburden (above 122 m)	5.74E-11	1.42E-10	-8.44E-11
Recharge	1.64E-09	-	1.64E-09
Total	7.93E-09	7.83E-09	9.94E-11

5.3 Tile Drain Flowrate

The tile drain flowrate has undergone substantial investigation over the course of this project, due to the high rates of flow relative to a simple water balance of the site. The model is currently calibrated to an average annual tile drain flow rate and an average annual recharge. Two sensitivity cases were considered with alternate tile drain flow rates, to evaluate the model calibration's sensitivity to small changes in this calibration target.

In these sensitivity cases, the model is recalibrated for a tile drain flow rate one standard deviation below the average (low tile drain rate case), 5.6 L/s, and one standard deviation above the average (high tile drain rate case), 8.4 L/s.

Both models obtained a successful calibration. Figure 5-9 shows a cross-plot of modelled water levels compared to observation water levels, with the target at BH16-02B removed. In addition to water levels, the expected tile drain flowrates were achieved by the model (5.6 L/s and 8.4 L/s).

Figure 5-9 Cross-plot of Modelled and Observed Water Levels for Tile Drain Flowrate Sensitivity Cases

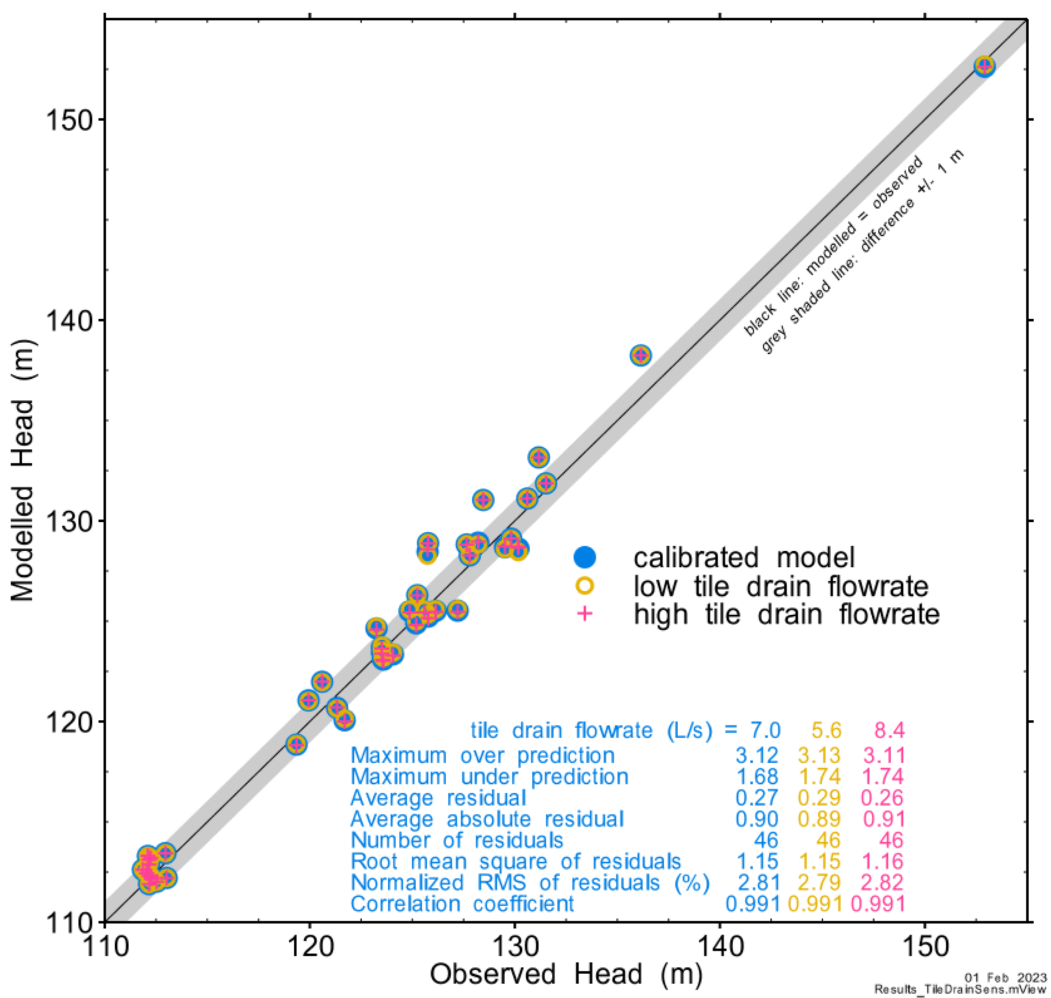

Figure 5-10 and Figure 5-11 shows the water table and head contours for the two cases, compared to the calibrated model, in both plan view and cross-section respectively.

Figure 5-10 Water Table for Tile Drain Flowrate Sensitivity Cases

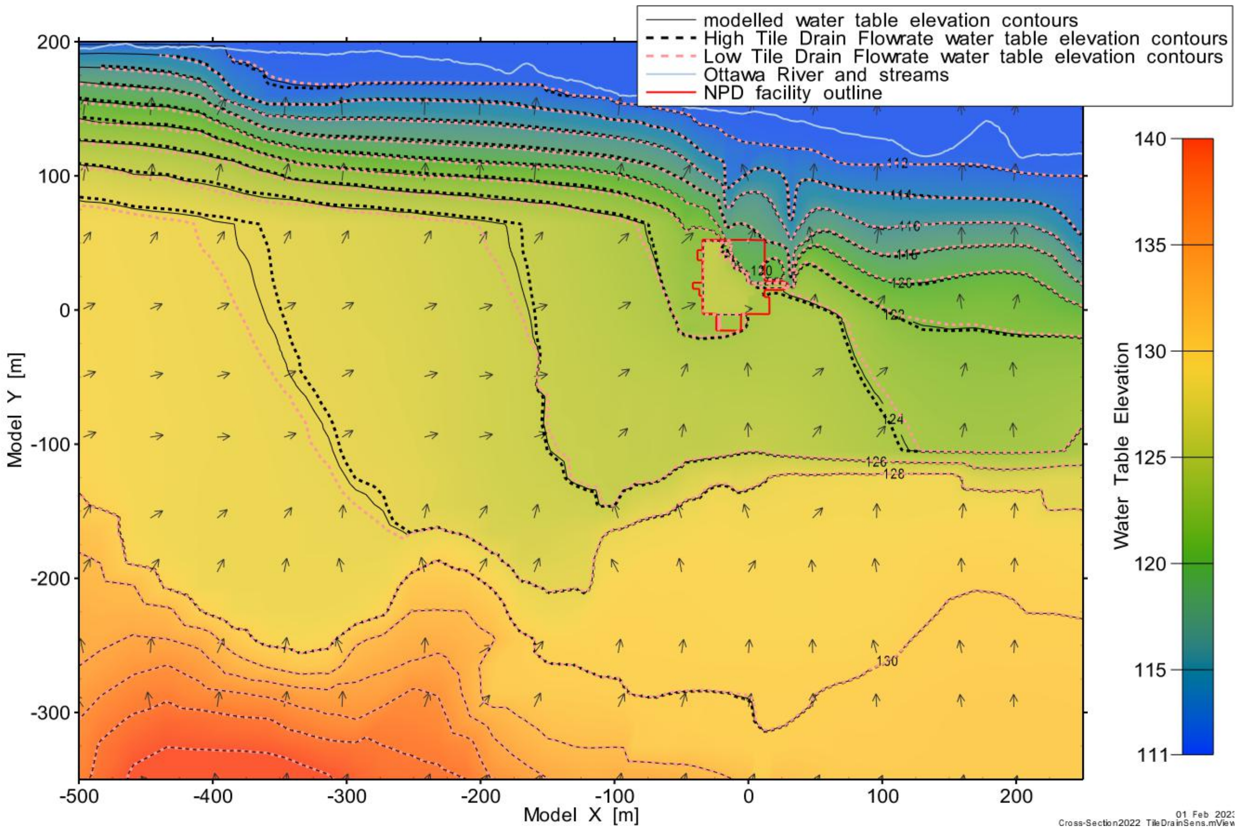

Figure 5-11 Cross-sections Showing Head Contours and Water Table for Tile Drain Flowrate Sensitivity Cases

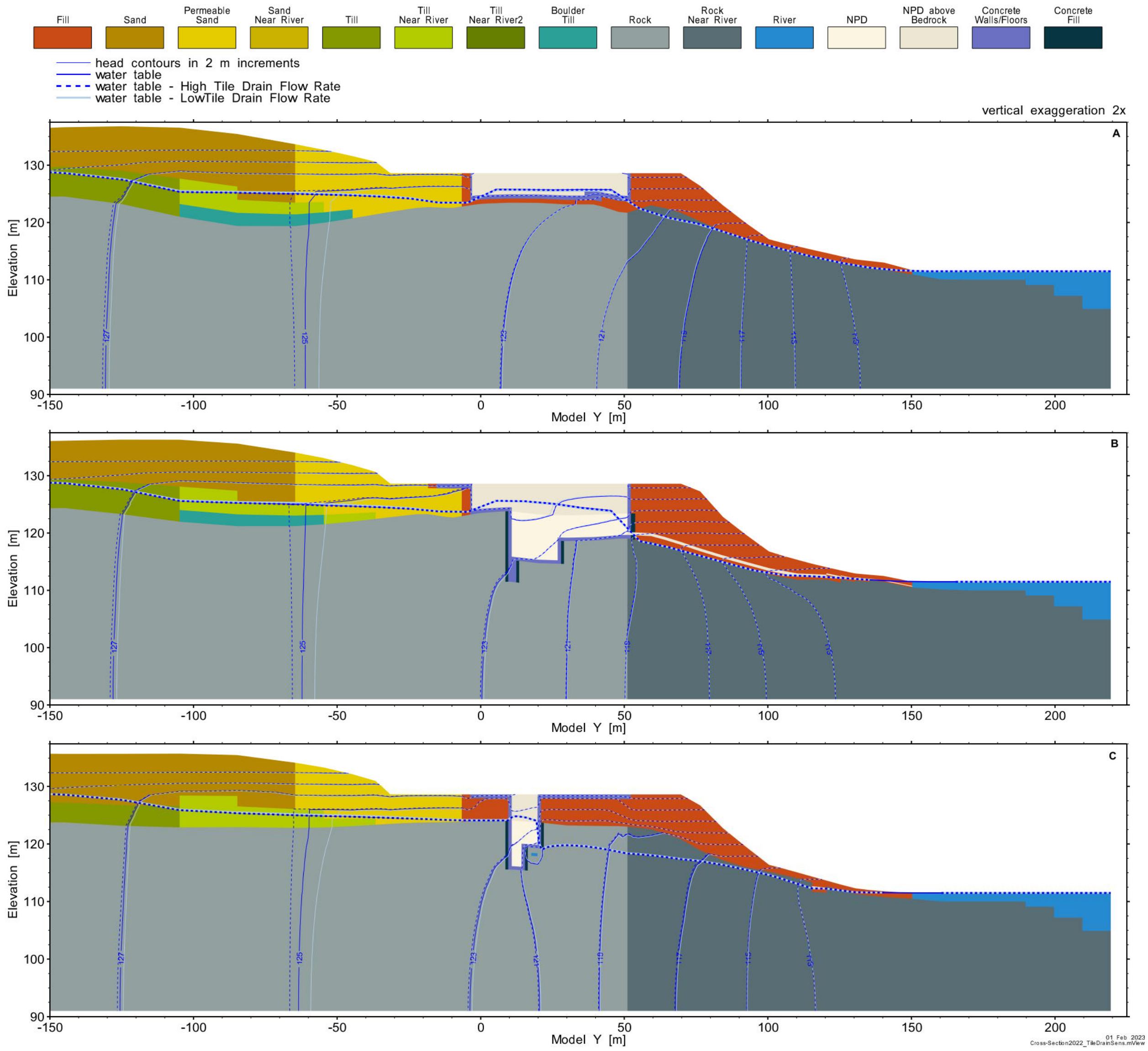

Table 5-3 shows the final calibrated hydraulic conductivities for the two cases, compared to the calibrated model. For the high tile drain flowrates, which represents a 20% increase in tile drain flow, only the sand and till near the river changed in magnitude, as highlighted in orange font in the table. The hydraulic conductivity of the permeable sand increased by approximately 20%, whereas the sand near the river and the till near the river 2 decreased by approximately 30%. These changes would funnel more water from the west towards the facility.

For the low tile drain flowrates, which represents a 20% decrease in tile drain flow, there was a similar change in hydraulic conductivities, with some minor changes to additional materials. Minor changes are small, less than 5%, and are represented in bold font in the table. More substantive changes are highlighted in orange font in the table, and the same parameters that changed for the high tile drain flowrate also changed for the low tile drain flowrate: the hydraulic conductivity of sand near the river and the till near the river 2 increased by approximately 40 and 30%, respectively, and the permeable sand hydraulic conductivity was reduced by approximately 20%. These changes reduce the amount of overburden water directed towards the facility from the west, as it allows water to more easily reach the river.

Table 5-3 Calibrated Material Hydraulic Conductivities and Parameter Sensitivity for Tile Drain Flowrate Sensitivity Cases

Calibrated Parameter	Calibrated Model		High Tile Drain Flowrate		Low Tile Drain Flowrate	
	Final Calibrated Value	Mean Sensitivity x 100	Final Calibrated Value	Mean Sensitivity x 100	Final Calibrated Value	Mean Sensitivity x 100
Sand Horizontal k (m/s)	1.0×10^{-3}	153	1.0×10^{-3}	173	1.0×10^{-3}	134
Sand Near River Horizontal k (m/s)	1.8×10^{-5}	122	**1.3×10^{-5}**	101	**2.5×10^{-5}**	127
Permeable Sand Horizontal k (m/s)	6.1×10^{-4}	90	**7.5×10^{-4}**	93	**4.7×10^{-4}**	78
Till Near River 2 k (m/s)	3.6×10^{-5}	28	**2.5×10^{-5}**	24	**4.6×10^{-5}**	30
Rock Near River k (m/s)	1.7×10^{-7}	17	1.7×10^{-7}	25	1.7×10^{-7}	14
Rock k (m/s)	5.0×10^{-8}	12	5.0×10^{-8}	11	**4.9×10^{-8}**	12
Till Near River k (m/s)	5.0×10^{-4}	9	5.0×10^{-4}	12	5.0×10^{-4}	8
Till k (m/s)	7.8×10^{-9}	5	7.8×10^{-9}	5	**7.7×10^{-9}**	5
Fill k (m/s)	1.0×10^{-3}	2	1.0×10^{-3}	2	1.0×10^{-3}	1
Sand Anisotropic Ratio	9.96	0.3	9.97	0.3	**10.0**	0.3
Boulder Till k (m/s)	3.9×10^{-5}	0.2	3.9×10^{-5}	0.2	**4.1×10^{-5}**	0.3

These sensitivity cases illustrate that changes to the tile drain flowrate, within a standard deviation of the mean, result in changes in the estimated overburden material properties. These changes to overburden hydraulic conductivity do not result in changes to the gradient or water table elevation downgradient from the facility.

6 CONCLUSIONS

A detailed numeric assessment of groundwater flows at the proposed disposal NPD facility in Rolphton, Ontario provides estimates of volumetric flow and groundwater velocity that comes in contact with the proposed decommissioned facility and surrounding engineered facilities. The numeric assessment was based on a FRAC3DVS numeric model with variably-saturated steady-state groundwater flow. The model reported here is an update to previous groundwater flow models.

The groundwater flow model was calibrated to July 2014, December 2018 and January 2019 water levels and a steady-state annual tile drain 1 flow rate of 7.0 L/s by modifying hydraulic conductivity of the geologic media. The groundwater model calibrated effectively to water elevations and the tile drain 1 flow rate, and was most sensitive to the fluvial sand and gravel (sand) hydraulic conductivity. The sand was divided into three units for the purposes of model calibration, in an effort to increase the capture zone of tile drain 1 to the west and south-west of the facility to obtain the high tile drain 1 flow rate previously unattainable by the groundwater flow model. While the horizontal sand units parallel to the river described in the model have not been characterized by drilling and well testing, it is consistent with the geological deposition of sediments at the site, the heterogeneity of sands observed at the site, and is currently the only mechanism in the groundwater model capable of increasing tile drain 1 flowrates near observed values. Model calibration was insensitive to bedrock conductivity, till conductivity (till and boulder till) and fill conductivity.

Calibrated conductivity values generally fell within the ranges of conductivity measurements available for the NPD site, although there is considerable heterogeneity in the measured conductivities, particularly in the sand. The availability of hydraulic conductivity measurements in the overburden increases confidence in the current groundwater model.

The current groundwater model calibration is only valid for the current hydrogeologic conceptualization, and represents a possible “best” parameter set for the conceptual model described (including parameter ranges) and the data available. It may be possible to obtain a similar calibration with an alternate conceptual model and/or additional data. The current calibrated model provides a reasonable description of the groundwater flow at the site, based on the data available, and is acceptable based on standard performance measures.

The improved model calibration achieved by the 2019 model update, relative to previous groundwater modelling, is a result of an improved conceptual hydrogeological model that is based on the 2019 site characterization work and that captures the spatial heterogeneity of the overburden and bedrock hydrogeological properties. The spatial heterogeneity of the overburden allows the capture area for the tile drain 1 to be increased to the west of the NPD facility, allowing the large volumes observed within tile drain 1. Previous groundwater models were unable to obtain these high tile drain 1 flow rates.

The 2022 groundwater model update was a relatively minor update to the 2019 model, with the inclusion of new data available, such as the deep section of tile drain 2 and a new cover design. The representation of groundwater flow at the site by the 2022 model update is a reasonable representation of groundwater flow at the site, and the data used to support the model is sufficient.

As expected, the tile drain system surrounding the facility channels groundwater towards the facility before discharging to the Ottawa River. The bulk of the groundwater flows through the overburden, including fill, just above the bedrock surface, and tile drain 1. Downgradient of the facility, where there is a steep elevation change, the water table drops below the bedrock surface.

A series of scenarios to support the Post SA calculations were conducted. Many of these scenarios are simulated under conditions representing different time intervals, with three time intervals considered: 0 to 100 years with current conditions, 100 to 1000 years with a degraded cap and degraded tile drains and 1000+ years with a degraded facility in addition to a degraded cap and degraded tile drains. From these scenarios, it is evident that:

- The facility hydraulic conductivity has negligible impact on groundwater flows in the geosphere adjacent to the facility, with the sand, fill and tile drain 1 dominating the flow response around the facility.
- Failure of the tile drains results in a slight decrease in geosphere flows adjacent to the facility, with geosphere flows dominated by overburden flows. The failure also results in a small increase in the very small amount of flow entering the facility, approximately a 35% increase in the NES Degraded Cap case, in comparison to the NES current conditions (0 to 100 years) case. Springs also develop along the steep bluff downgradient of the facility, resulting in flows of 2 L/s in the NES Degraded Cap and Degraded cases.
- Degradation of the cap and cover resulted in a small increase in recharge into the facility, responsible for an increase in water flow into the facility based on the NES Degraded Cap case, in comparison to the NES case. Note that the total flow into the facility is approximately 2.5 times greater than the NES case, approximately half of which is a result of tile drain failure and half from increased recharge.
- Flow within the building itself increased as the hydraulic conductivity of the building materials increased. The NES Degraded case saw a two orders of magnitudes increase in flow within the building, with only a 11% of the increase attributable to increased recharge.
- Increasing the fill conductivity had minimal impact on the groundwater flow system.
- Increasing bedrock conductivity had the effect of lowering the water table throughout the system. At the bedrock conductivities considered in this scenario, the water table is much lower than measured at observation wells, the tile drains have zero flow and no springs develop when the tile drains fail.
- The fault zone activation scenario had a more moderate increase in bedrock conductivities, and resulted in a more plausible geosphere flow system. Flows through the geosphere in the vicinity of the facility are reduced by approximately a third, with spring flows reduced to 0.8 L/s (from 2 L/s).
- An overburden well had limited impact on the geosphere flows, with a minor increase in flows through the building of 1-4%. The bedrock well had very localized drawdown, with a radius of influence of less than 50 m. The bedrock well resulted in increased flows through the building of approximately 25%.

- The cases considering the extreme degradation of concrete and grout confirmed the conclusions that changes to building materials do not impact the geosphere flow field. As expected, flows through the building are increased significantly under extreme degradation of concrete and grout.

Sensitivity of the groundwater model to model boundaries, fill conductivity and tile drain flowrate were also investigated:

- Extending the model boundary to the east had negligible impacts on the geosphere flow system in the vicinity of the facility, including metrics of the geosphere flow system.

- Fill hydraulic conductivity was a relatively insensitive parameter in the model calibration, and can be reduced to 5×10^{-5} m/s with limited impact on model calibration and geosphere flow results.

- The groundwater model can be successfully calibrated to a tile drain flow rate within one standard deviation of the mean annual tile drain flowrate with modified overburden hydraulic conductivity values to the west of the facility. The sand near river, permeable sand, and till near river 2 are the hydraulic conductivities that change, allowing either more or less water directed towards the facility from the west. Hydraulic conductivities for materials downgradient of the facility, as well as head gradients downgradient of the facility are unchanged from the calibrated model, indicating that transport downgradient of the facility would likely be unaffected by a change in the tile drain flowrate.

7 REFERENCES

Acsion Industries Incorporated. 2014. *Updated Hydrogeological Model of the Chalk River Laboratories Region, Revision 0.* Atomic Energy of Canada Limited Report Number 361101-10191-REPT-004.

Arcadis. 2018. *RFI #98 – Definition of Scoping Calculations for Grout: Grout, Scenarios, Model and Data Requirements*. Arcadis memo prepared for CNL dated November 26, 2018.

Calder, N. 2016. *Groundwater Modelling at the Site of the Proposed Decommissioned Rolphton Nuclear Power Demonstration (NPD) Reactor.* Arcadis technical report prepared for by Geofirma CNL.

Calder, N. 2017a. *Resaturation Modelling at the Site of the Proposed Decommissioned Rolphton Nuclear Power Demonstration (NPD) Reactor*. Arcadis technical report prepared by Geofirma for CNL.

Calder, N. 2017b. *Updated Groundwater Modelling at the Site of the Proposed Decommissioned Rolphton Nuclear Power Demonstration (NPD) Reactor*. Arcadis technical report prepared by Geofirma for CNL.

Calder, N. 2018. *Second Update to Groundwater Modelling at the Site of the Proposed Decommissioned Rolphton Nuclear Power Demonstration (NPD) Reactor.* Arcadis technical report prepared by Geofirma for CNL.

Calder, N. and R. Walsh. 2016. *CRL Gas Generation and Transport Model.* Prepared by Geofirma Engineering Ltd. for CNL. March.

Canadian General Electric Company Ltd. 1961. Design Manual 211.2 Buildings, Structures and Shielding – Waterproofing and Waterstops.

Canadian General Electric Company Ltd. 1962. *Final Hazards Report Part 1 for Nuclear Power Demonstration Generating Station.*

Canadian Nuclear Laboratories (CNL). 2018. *NPD Task Work Order 3 – Final Summary Report for Laboratory Testing Program on Fresh and Cured Properties of Bulk and Low pH Grout.* CNL No. 64-508120-REPT-005. Rev. 0. November.

Canadian Nuclear Laboratories (CNL). 2020. *Detailed Decommissioning Plan – Nuclear Power Demonstration Waste Facility.* CNL No. 64-508310-DDP-001. Rev. 2. March.

Canadian Nuclear Laboratories (CNL). 2022. *Nuclear Power Demonstration Effluent Monitoring Plan.* CNL No. 64-509200-PLA-001. Rev. 1. February.

Dixon, K., J. Harbour and M. Phifer. 2008. *Hydraulic and Physical Properties of Saltstone Grouts and Vault Concretes.* Savannah River National Laboratory Report SRNL-STI-2008-00421 prepared for the U.S. Department of Energy, Aiken, SC.

Drain All Ltd. 2017. *CCTV Inspection Report Tile Drain Sewer Lines.* Inspections conducted November 2016 and June 2017 for CNL.

Environment Canada. 1978. *Hydrological Atlas of Canada*. Supply and Service Canada, Ottawa.

Gadd, N R; Geological Survey of Canada, "A" Series Map 1132A, 1963, 1 sheet, https://doi.org/10.4095/107278

Garisto, F., A. D'Andrea, P. Gierszewski and T. Melnyk. 2004. *Third Case Study – Reference Data and Codes.* Ontario Power Generation Report OPG 06819-REP-01200-10107-R00. Toronto, Canada.

Golder Associates. 2017. *RFI 008 & RFI 014 Hydraulic Conductivity Tests Nuclear Power Demonstration (NPD) Site Deep River, ON.* Golder Report for CNL 1666131/6002.

Guo, R. 2004. *Application of Numerical Simulation in the Tunnel Sealing Experiment.* Ontario Power Generation Report OPG 06819-REP-01200-10137-R00. Toronto, Canada.

Gruntz, T., A. Shkarupin and L. Bellan. 2016. *Dilution Gauging - Fall 2016, CRL Memo CRL-509211-021-000*. November 3, 2016.

Hurtado, L.D., M.K. Knowles, V.A. Kelley, T.L. Jones, J.B. Ogintz and T.W. Pfeifle. 1997. *WIPP Shaft Seal System Parameters Recommended to Support Compliance Calculations. Sandia National Laboratories Report SAND97-1287*. Albuquerque, USA.

Hydro Electric Power Commission of Ontario. 1961. Nuclear Power Demonstration – 2 Generating Station Design Manual 158 Subsurface Drainage.

Killey, D. 2014. Current Groundwater Quality at NPD. *Canadian Nuclear Laboratories General Report 64-509247-REPT-001, Chalk River, Canada*.

Killey, D. and M.L. Benz. 2009. *The NPD Tile Drain System*. Memo to Rick Janzen, CNL File No. 64-10140-021-000. November 20.

Killey, R.W.D. and J.H. Munch. 1988. *Hydrogeologic Investigation of the NPD Landfill Site*. AECL report for Ontario Hydro, Chalk River, Canada.

Killey, R.W.D. and J.H. Munch. 1989. *Hydrogeologic Investigation of NPD Landfill Site #2*. AECL report, Chalk River, Canada.

Kinetrics Inc. 2018. *CNL NPD Concrete Core Tests*. Kinetrics report for CNL dated May 31, 2018.

Leverett, M.C. 1941. *Capillary Behaviour in Porous Solids.* Transactions of the AIME, 142, 159–172.

MacLarentech Inc. 1990. *Rolphton NPD Waste Management Facility Site Characterization and Facility Evaluation*. Report to Public Works Canada Project No. 703725.

McCrank, G. 2016. *Geologic Waste Management Facility Descriptive Geosphere Site Model Report: Phase 1*. CNL General Report for CRL Geologic Waste Management Facility 361101-10260-REPT-005, Revision 0.

NAGRA. 1994. *Report on Long-Term Safety of the L/ILW Repository at the Wellenberg Site*. Nagra Report NTB 94-06. Wettingen, Switzerland.

NAGRA. 2008. *Effects of Post-disposal Gas Generation in a Repository for Low- and Intermediate-level Waste sited in the Opalinus Clay of Northern Switzerland*. Nagra Technical Report TR-08-07. Wettingen, Switzerland.

Ontario Geological Survey 2010. *Surficial Geology of Southern Ontario*. Ontario Geological Survey, Miscellaneous Release--Data 128-REV.

Ontario Water Resources Commission and Quebec Water Board. 1971. *Ottawa River Basin, Water Quality and its Control in the Ottawa River*. Environment Canada, Water Quality Branch, Ottawa.

Penfold, J., K. Thatcher, N. Garisto, J. Avis and N. Calder. 2017. *Postclosure Safety Analysis of the In-Situ Decommissioning of the NPD*. Arcadis report prepared for Canadian Nuclear Laboratories, Richmond Hill, Canada.

Phifer, M.A., M.R. Millings and G.P. Flach. 2006. *Hydraulic Property Data Package for the E-Area and Z-Area Soils, Cementitious Materials, and Waste Zones.* Savannah River Site Report WSRC-STI-2006-00198 prepared for U.S. Department of Energy, Aiken, SC.

Pollock, D. 2016. *User's Guide for MODPATH Version 7; a Particle Tracking Model for MODFLOW.* U.S. Geological Survey Open-File Report 2016–1086, 35 p., http://dx.doi.org/10.3133/ofr20161086

Quintessa and Geofirma. 2011. *Postclosure Safety Assessment: Data*. Quintessa Ltd. and Geofirma Engineering Ltd. report for the Nuclear Waste Management Organization NWMO DGR-TR-2011-32 R000. Toronto, Canada.

Raven, K., S. Sterling and N. Calder. 2022. *2021 Updated Geosynthesis Nuclear Power Demonstration Closure Project Rolphton, Ontario.* Arcadis technical report prepared for CNL. CNL No. 64-5095410-REPT-010. Rev. 2. January.

RBEL (Raven Beck Environmental Ltd.). 1994. *Regional Hydrologic Characterization of the Chalk River Laboratories Property, Deep River, Ontario*. Siting Task Force Low-level Radioactive Waste Management Report Geo-Sci 12. STF Tech. Bib. No. 344.

Robertson, E. and P.J. Barry. 1985. *The Water and Energy Balances of Perch Lake (1969–1980).* Atmosphere-Ocean, 23:3, 238-253, DOI: 10.1080/07055900.1985.9649227.

Rockhold, M.L., M.J. Fayer and P.R. Heller. 1993. *Physical and Hydraulic Properties of Sediments and Engineered Materials Associated with Grouted Double-Shell Tank Waste Disposal at Hanford.* Report for the U.S. Department of Energy by Pacific Northwest Laboratory, Richland, Washington.

Russell, S.B. and G.R. Simmons. 2003. *Engineered Barrier System for a Deep Geologic Repository in Canada*. Proceedings, International High Level Radioactive Waste Management Conference. Las Vegas, USA.

Savage, D. and M. Stenhouse. 2002. *SFR 1 Vault Database*. SKI Report 02:53, Swedish Nuclear Power Inspectorate, Stockholm, Sweden, 2002.

Scheier, N. and D. Killey. 2009. *Modelling Groundwater Flow in the Vicinity of Waste Management Area A and the South Swamp*. AECL Memo 3613-121241-041-000, January 27, 2009.

Shkarupin, A. 2018. Email correspondence of Tile Drain Flow Measurements.

Sgro, N. 2023. *DRAFT 2022 Resaturation Modelling for the Proposed Decommissioned Rolphton Nuclear Power Demonstration (NPD) Reactor.* Arcadis technical report prepared by Geofirma for CNL.

Shkarupin, A. and L. Bellan. 2017. *Dilution Gauging - Spring 2017*. CRL Memo CRL- 509211-021-000, July 17, 2017.

Shkarupin, A. and A. Miller. 2016. *NPD Manhole 2 Flow Measurement.* CRL Memo CRL-S09211-021-000, January 28, 2016.

Sterling, S., R. Walsh, P. Pehme and K. Raven. 2019. *Geoscientific Characterization of the NPD Site Nuclear Power Demonstration Closure Project Rolphton, Ontario.* Geofirma technical report prepared for CNL.

Taylor, G.A. and M.A. Phifer. 2012. *Building 235-F Goldsim Fate and Transport Model.* Savannah River National Laboratory Report SRNL-STI-2012-00504 prepared for the U.S. Department of Energy, Aiken, SC.

Telmer, K. And J. Veizer. 2000. *Isotopic Constraints on the Transpiration, Evaporation, Energy, and Gross Primary Production Budgets of a Large Boreal Watershed: Ottawa River Basin, Canada.* Global Biogeochemical Cycles, Vol. 14, No. 1, pages 149-165.

Therrien, R., R.G. McLaren, E.A. Sudicky, S.M. Panday, and V. Guvanasen. 2010. *FRAC3DVS_OPG: A Three-dimensional Numerical Model Describing Subsurface Flow and Solute Transport. User's Guide*. Groundwater Simulations Group, University of Waterloo, Ontario, Canada.

United States Department of Agriculture (USDA). 1999. Rosetta Model. http://www.ars.usda.gov/News/docs.htm?docid=8953

Welter, D., J. White, R. Hunt and J. Doherty. 2015. *Approaches in Highly Parameterized Inversion: PEST++ Version 3, A Parameter ESTimation and Uncertainty Analysis Software Suite Optimized for Large Environmental Models*. U.S. Geological Survey, Reston, Virginia.

WIPP. 2009. *Waste Isolation Pilot Plant Hazardous Waste Facility Permit Renewal Application September 2009: Appendix A of Appendix I2, Material Specification Shaft Sealing System Compliance Submittal Design Report.* Waste Isolation Pilot Plant, U.S. Department of Energy, Carlsbad, USA.

Zhang, Y. 2019. *NPD Underground Structure Seismic Assessment Under DBE Loading.* Canadian Nuclear Laboratories Nuclear Power Demonstration Closure Project Report 64-20000-ASD-001 Rev 1, Chalk River, Canada.

APPENDIX A: WATER LEVEL MEASUREMENTS

APPENDIX A – WATER LEVEL MEASUREMENTS

BH ID	Easting (m)	Northing (m)	Screen Midpoint Elevation (m)	Killey and Munch (1988)	Killey and Munch (1989)		MacLarentech (1990)		Killey (2014)	Golder (2017)		Geofirma (2018)	
				1-May-88	31-Mar-89	15-Apr-90	1-Dec-89	Jan-90	Jul-14	18-Jan-17	18-Apr-17	12-Dec-18	16-Jan-19
NPD-1	294592.7	5118019.1	130.8	132.1	-	-	-	-	-	-	-	-	-
NPD-2	294561.0	5118052.0	131.0	131.4	-	-	-	-	131.8	-	-	-	-
NPD-4	294550.9	5118090.6	129.4	130.1	-	-	-	-	130.9	-	-	-	-
NPD-5-I	294674.2	5118084.8	124.5	127.0	-	-	-	-	-	-	-	-	-
NPD-5-II	294674.2	5118084.8	126.9	126.8	-	-	-	-	-	-	-	-	-
NPD-6	294640.9	5118103.8	125.7	127.1	-	-	-	-	-	-	-	-	-
NPD-7	294620.8	5118126.0	126.5	127.1	-	-	-	-	128.1	-	-	-	-
NPD-8	294571.6	5118152.5	127.3	127.5	-	-	-	-	128.7	-	-	-	-
NPD-9*	294525.8	5118471.9	127.5	-	128.5	130.4	-	-	130.4	-	-	-	-
NPD-10*	294544.8	5118521.6	128.8	-	129.6	131.6	-	-	130.4	-	-	-	-
NPD-11*	294486.1	5118492.0	126.2	-	126.8	129.3	-	-	128.5	-	-	-	-
NPD-12*	294501.4	5118445.9	127.6	-	128.3	130.4	-	-	129.8	-	-	-	-
NPD-13*	294535.3	5118551.2	124.9	-	125.0	127.1	-	-	126.0	-	-	-	-
NPD-14*	294444.8	5118443.8	127.8	-	128.4	131.0	-	-	130.1	-	-	-	-
MT-1	294570.5	5118005.4	129.5	-	-	-	130.8	130.1	131.4	-	-	-	-
MT-2	294688.5	5118093.8	119.7	-	-	-	124.6	124.5	127.9	-	-	-	-
MT-4	294927.7	5118080.5	124.3	-	-	-	128.0	127.7	-	-	-	-	-
MT-5	294805.5	5118194.2	121.0	-	-	-	123.9	123.7	125.4	123.8	124.1	125.0	-
MT-7	294888.9	5118285.8	121.2	-	-	-	dry	dry	121.6	-	-	-	-
MT-8	294929.2	5118305.7	112.4	-	-	-	113.0	112.9	113.2	-	113.4	112.5	-
MT-9	295021.2	5118144.6	121.4	-	-	-	121.5	dry	-	-	-	121.5	-
MT-10	295046.6	5117961.6	128.7	-	-	-	129.1	128.7	-	-	-	-	-
BH-07-01	294942.8	5118295.4	112.4	-	-	-	-	-	112.3	-	112.5	-	-
BH-08-01	294960.0	5118280.2	112.6	-	-	-	-	-	112.1	-	-	-	-
BH-09-01	294979.5	5118267.3	112.7	-	-	-	-	-	113.3	-	113.8	-	-
BH-10-01	294999.3	5118246.5	113.3	-	-	-	-	-	112.8	-	-	-	-
BH-11-01	294921.3	5118245.8	120.7	-	-	-	-	-	119.6	-	119.8	-	-
BH-12-01	294883.2	5118280.2	120.1	-	-	-	-	-	120.2	122.5	120.3	119.7	-
BH-13-01	294886.9	5118256.1	120.8	-	-	-	-	-	120.9	120.3	121.0	120.5	-
BH16-01	294881.0	5118149.0	123.0	-	-	-	-	-	-	123.9	124.2	123.0	-
BH16-02A	294875.0	5118175.0	105.8	-	-	-	-	-	-	120.7	122.8	-	-
BH16-02B	294878.0	5118179.0	115.0	-	-	-	-	-	-	117.8	122.8	118.1	-

BH ID	Easting (m)	Northing (m)	Screen Midpoint Elevation (m)	Killey and Munch (1988)	Killey and Munch (1989)		MacLarentech (1990)		Killey (2014)	Golder (2017)		Geofirma (2018)	
				1-May-88	31-Mar-89	15-Apr-90	1-Dec-89	Jan-90	Jul-14	18-Jan-17	18-Apr-17	12-Dec-18	16-Jan-19
BH16-03	294905.0	5118253.0	117.0	-	-	-	-	-	-	dry	117.4	-	-
BH16-04	-	-	-	-	-	-	-	-	-	dry	dry	-	-
BH18-01	294543	5117634.43	147.52	-	-	-	-	-	-	-	-	-	152.7
BH18-02	294689.2	5117698.3	132.66	-	-	-	-	-	-	-	-	-	135.9
BH18-03	294782.4	5118037.02	124.79	-	-	-	-	-	-	-	-	-	125.5
BH18-04	294679.1	5118194.71	120.67	-	-	-	-	-	-	-	-	-	125.0
BH18-09	294787.2	5118170.47	118.03	-	-	-	-	-	-	-	-	-	125.5
BH18-10	294751	5118176	115.47	-	-	-	-	-	-	-	-	-	124.6
MW18-05-1	294753.81	5118189.61	107.765	-	-	-	-	-	-	-	-	-	125.4
MW18-05-2	294753.81	5118189.61	101.14	-	-	-	-	-	-	-	-	-	125.9
MW18-05-3	294753.81	5118189.61	95.515	-	-	-	-	-	-	-	-	-	127.0
MW18-05-4	294753.81	5118189.61	86.015	-	-	-	-	-	-	-	-	-	126.7
MW18-05-5	294753.81	5118189.61	77.39	-	-	-	-	-	-	-	-	-	126.1
MW18-05-6	294753.81	5118189.61	67.765	-	-	-	-	-	-	-	-	-	127.0
MW18-05-7	294753.81	5118189.61	63.39	-	-	-	-	-	-	-	-	-	127.3
MW18-06-1	294920.48	5118148.12	118.15	-	-	-	-	-	-	-	-	-	123.3
MW18-06-2	294920.48	5118148.12	112.4	-	-	-	-	-	-	-	-	-	123.3
MW18-06-3	294920.48	5118148.12	108.9	-	-	-	-	-	-	-	-	-	123.8
MW18-06-4	294920.48	5118148.12	98.15	-	-	-	-	-	-	-	-	-	123.3
MW18-06-5	294920.48	5118148.12	93.15	-	-	-	-	-	-	-	-	-	123.3
MW18-06-6	294920.48	5118148.12	86	-	-	-	-	-	-	-	-	-	122.7
MW18-06-7	294920.48	5118148.12	81.7	-	-	-	-	-	-	-	-	-	122.7
MW18-07-1	294999.77	5118248.34	108.24	-	-	-	-	-	-	-	-	-	111.9
MW18-07-2	294999.77	5118248.34	101.69	-	-	-	-	-	-	-	-	-	112.0
MW18-07-3	294999.77	5118248.34	96.64	-	-	-	-	-	-	-	-	-	112.0
MW18-07-4	294999.77	5118248.34	91.59	-	-	-	-	-	-	-	-	-	112.0
MW18-07-5	294999.77	5118248.34	79.065	-	-	-	-	-	-	-	-	-	112.0
MW18-07-6	294999.77	5118248.34	73.24	-	-	-	-	-	-	-	-	-	111.8
MW18-07-7	294999.77	5118248.34	64.94	-	-	-	-	-	-	-	-	-	112.0
MW18-08-1	294926.79	5118325.57	108.79	-	-	-	-	-	-	-	-	-	111.9
MW18-08-2	294926.79	5118325.57	103.79	-	-	-	-	-	-	-	-	-	111.9
MW18-08-3	294926.79	5118325.57	100.69	-	-	-	-	-	-	-	-	-	112.0
MW18-08-4	294926.79	5118325.57	93.69	-	-	-	-	-	-	-	-	-	111.9

BH ID	Easting (m)	Northing (m)	Screen Midpoint Elevation (m)	Killey and Munch (1988)	Killey and Munch (1989)		MacLarentech (1990)		Killey (2014)	Golder (2017)		Geofirma (2018)	
				1-May-88	31-Mar-89	15-Apr-90	1-Dec-89	Jan-90	Jul-14	18-Jan-17	18-Apr-17	12-Dec-18	16-Jan-19
MW18-08-5	294926.79	5118325.57	77.94	-	-	-	-	-	-	-	-	-	111.9
MW18-08-6	294926.79	5118325.57	71.44	-	-	-	-	-	-	-	-	-	111.9
MW18-08-7	294926.79	5118325.57	61.79	-	-	-	-	-	-	-	-	-	111.9

* Screen midpoint and water elevations corrected for difference between borehole log ground surface and DEM ground surface. The DEM ground surface was used for consistency with the groundwater model.

APPENDIX B: DILUTION GAUGE TILE DRAIN MEASUREMENTS

APPENDIX B – DILUTION GAUGE TILE DRAIN 1 MEASUREMENTS

Date	Steady-State Method (L/s)	Steady -State Error	Integration Method (L/s)	Average* Flow Rate (L/s)	Measurement Location	Reference
Jul 31, 2001	9.3	±0.39	9.5	9.4	unknown	Killey and Benz (2009)
Jun 16, 2009	13.1	±0.27	13.3	13.2	MH2 to access hatch 10 m south of river shoreline	Killey and Benz (2009)
Jul 27, 2009	12.9	±0.34	12.3	12.6	MH2 to river	Killey and Benz (2009)
Oct 8, 2009	9.9	±1.36	9.5	9.5	MH2 to river	Killey and Benz (2009)
Jun 8, 2010	7.7	±0.53	7.8	7.8	unknown	Tile Drain 1 Summary 2010.xls
Oct 21, 2015	7.1	-	7.0	7.1	break point** to river	Shkarupin and Miller (2016)
Oct 7, 2016	6.1	-	6.1	6.1	break point** to river	Gruntz *et al.* (2016)
June 2017	-	-	-	30	Furnace room well to MH2	Shkarupin and Bellan (2017)
	-	-	-	24	MH2 to break point**	Shkarupin and Bellan (2017)
Feb 15, 2018	4.67	±0.18	-	4.67	MH2 to break point**	Shkarupin (2018)
Mar 15, 2018	4.32	±0.10	-	4.32	MH2 to break point**	Shkarupin (2018)
Apr 18, 2018	4.10	±0.30	-	4.10	MH2 to break point**	Shkarupin (2018)
May 15, 2018	4.98	±0.07	-	4.98	MH2 to break point**	Shkarupin (2018)
Jun 20, 2018	8.67	±0.29	-	8.67	MH2 to break point**	Shkarupin (2018)
Jul 17, 2018	-	-	-	10.6	MH2 to break point**	Email communication from Bonnie Bayne Mar 13, 2019
Aug 15, 2018	-	-	-	8.25	MH2 to break point**	Email communication from Bonnie Bayne Mar 13, 2019
Sep 18, 2018	-	-	-	6.25	MH2 to break point**	Email communication from Bonnie Bayne Mar 13, 2019
Oct 16, 2018	-	-	-	6.27	MH2 to break point**	Email communication from Bonnie Bayne Mar 13, 2019
May 29, 2019	13.29	±0.41	-	-	MH2 to break point**	NPD Tile Drain Monthly Flow Monitoring.xls
Jul 9, 2019	11.69	±0.34	-	-	MH2 to break point**	NPD Tile Drain Monthly Flow Monitoring.xls
Aug 15, 2019	8.17	±0.21	-	-	MH2 to break point**	NPD Tile Drain Monthly Flow Monitoring.xls
Sep 19, 2019	6.58	±0.12	-	-	MH2 to river	NPD Tile Drain Monthly Flow Monitoring.xls

Date	Steady-State Method (L/s)	Steady-State Error	Integration Method (L/s)	Average* Flow Rate (L/s)	Measurement Location	Reference
	6.33	±0.27	-	-	MH2 to river	NPD Tile Drain Monthly Flow Monitoring.xls
Oct 9, 2019	5.7	±0.19	-	-	MH2 to break point**	NPD Tile Drain Monthly Flow Monitoring.xls
Nov 26, 2019	4.21	±0.04	-	-	MH2 to break point**	NPD Tile Drain Monthly Flow Monitoring.xls
Dec 16, 2019	6.51	±0.38	-	-	MH2 to break point**	NPD Tile Drain Monthly Flow Monitoring.xls
Jan 28, 2020	3.51	±0.08	-	-	MH2 to break point**	NPD Tile Drain Monthly Flow Monitoring.xls
Feb 29, 2020	3.57	±0.07	-	-	MH2 to break point**	NPD Tile Drain Monthly Flow Monitoring.xls
	3.69	±0.12	-	-	Furnace room well to unknown	NPD Tile Drain Monthly Flow Monitoring.xls
May 28, 2020	9.12	±0.30	13.4	11.3	MH2 to break point**	CNL RFI – Tile Drain Summary-Updated (002).docx
Oct 14, 2020	7.4	±0.28			MH2 to break point**	Email communication from Bonnie Bayne Sept 13, 2021
Nov 17, 2020	6.82	±0.15			MH2 to break point**	Email communication from Bonnie Bayne Sept 13, 2021
Dec 21, 2020	6.16	±0.11			MH2 to break point**	Email communication from Bonnie Bayne Sept 13, 2021
Feb 24, 2021	4.49	±0.11			MH2 to break point**	Email communication from Bonnie Bayne Sept 13, 2021
Mar 23, 2021	4.29	±0.14			MH2 to break point**	Email communication from Bonnie Bayne Sept 13, 2021
Apr 20, 2021	4.86	±0.09			MH2 to break point**	Email communication from Bonnie Bayne Sept 13, 2021
May 26, 2021	5.78	±0.08			MH2 to break point**	Email communication from Bonnie Bayne Sept 13, 2021
Jun 23, 2021	6.14	±0.20			MH2 to break point**	Email communication from Bonnie Bayne Sept 13, 2021
Jul 27, 2021	5.09	±0.06			MH2 to break point**	Email communication from Bonnie Bayne Sept 13, 2021

* Average of steady-state and integrated flow methods

** Break point is located approximately halfway between MH2 and the river.

Flow measurements in rows highlighted light orange are suspect for the following reasons:

Oct 8, 2009 – The steady-state error is very high, suggesting poor test results.

Sep 18, 2018 and Oct 16, 2018 – Values are similar for these two months. With the expected seasonal flow pattern of tile drain 1 flow rates, it would be expected that the value in October would be less than September. Without additional data about these tests (e.g. steady-state error, comparison between steady-state or integration methods or alternative measurements), one or both of these measurements may be suspect.

Dec 16, 2019 – This measurement appears to be an overestimate when compared to the seasonal trend documented by ultrasonic flow measurements taken at the same time. All other measurements in this year coincide with the trend in the ultrasonic flow measurements.

May 28, 2020 – Steady-state and integration methods provide substantially different estimates, suggesting a poor test. The value is also inconsistent with the trend defined by ultrasonic flow measurements, with both methods (steady-state and integration) overestimating flow.

Flow measurements taken from the furnace room, highlighted in grey, have higher flowrates than similar measurements taken from MH2, particularly in June of 2017. The higher flowrate within the operational perforated tile drain (30 L/s), compared to 24 L/s in the originally unperforated pipe between MH2 and the river, may be entirely due to the dilution that occurs in the perforated tile drain. An addition of 25% more flow at the end of the measurement, relative to the injection point, is sufficient to explain the different flowrates measured in June 2017. The 24 L/s measurement is still high relative to previous measurements, likely related to the high rainfall event that occurred in the day prior to the measurement, as well as the uncharacteristically wet spring and early summer in 2017. A similar increase in February 2020 was not observed; this may be due to the overall low flow rates in the tile drain at this time, and indicative of minimal additional flow between the furnace room and MH2 at that time.

APPENDIX C: CALCULATION OF ANNUAL STEADY-STATE TILE DRAIN FLOW RATE

APPENDIX C – CALCULATION OF ANNUAL STEADY-STATE TILE DRAIN 1 FLOW RATE

In calculating an annual steady-state flow rate, two factors were considered:

(1) The seasonal shape of the tile drain 1 flow rates, obtained from both ultrasonic testing and monthly dilution gauge testing. Based on these measurements, peak tile drain 1 flow rates typically occur in June (2009, 2019 and 2020). The exception is in 2018, when the peak occurs later in mid-July.

(2) The impact of climatic factors on the peak flow rates. Data from 2019 and 2020 show that the peak flow rate can differ substantially, by almost a factor of 2 for these two years, and this can be explained with climatic factors.

The seasonal shape of the tile drain 1 flow rates between 2018, 2019 and 2020 are compared by normalizing the flow rates and plotting them by month, shown in Figure C-1. 2019 and 2020 have very similar shapes, with 2018 similar but delayed by approximately one month.

Figure C-1: Normalized Tile Drain 1 Flow Rates

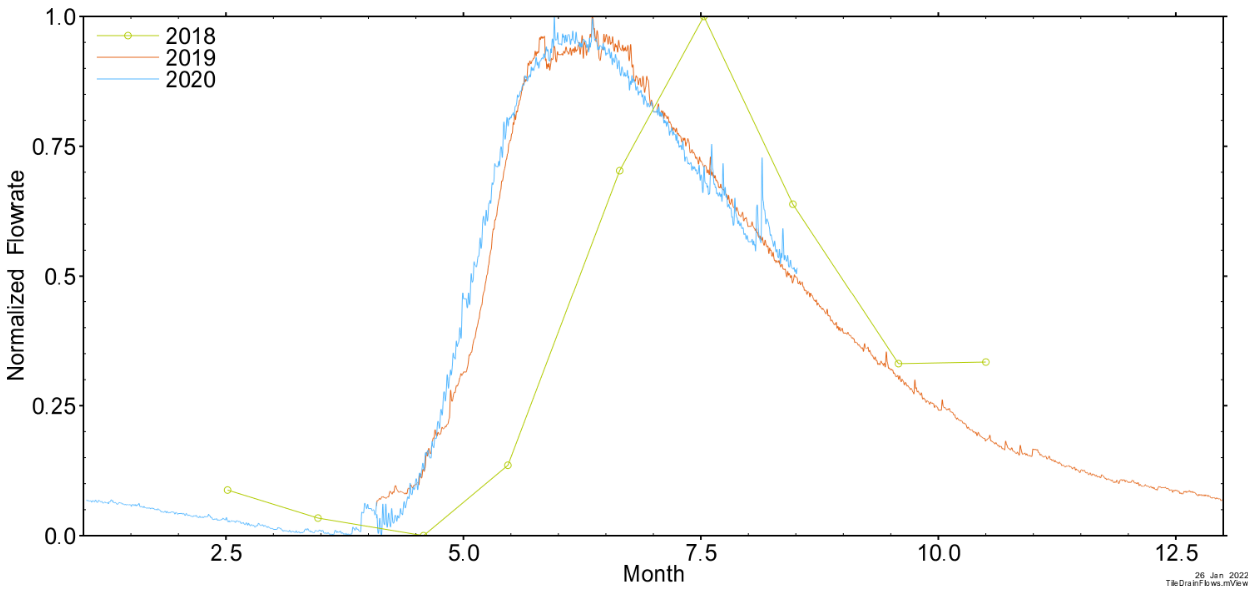

For each year with tile drain 1 flow measurements, the peak flow rate for that year was estimated based on the normalized flow rate at the time of the flow measurement and an assumed minimum flow rate of 4 L/s. The estimated peak flow rate was then compared to the total annual precipitation for that year, as shown in Figure C-2. Total precipitation was obtained from the Petawawa Hoffman Environment Canada weather station, instead of Chalk River, due to substantial missing data at the Chalk River station.

There is a strong correlation between total precipitation and tile drain 1 flow rate, with some exceptions. The exceptions are typically for years in which a single data point is used to estimate the peak flow rate. Using the 2018 normalization improves the estimate in some cases, e.g. the 2015 peak flow rate estimate of 22 L/s is reduced to 13.3 L/s using the 2018 normalization curve, putting it closer to the correlation of the other estimates. The correlation line was defined using only those cases where there was a measurement in June, which would be near the time of the expected peak flow rate, eliminating some of the uncertainty associated with which normalization curve is used. The data points used in the correlation line are highlighted with dark grey diamonds.

Figure C-2: Correlation Between Total Annual Precipitation and Peak Flow Rate

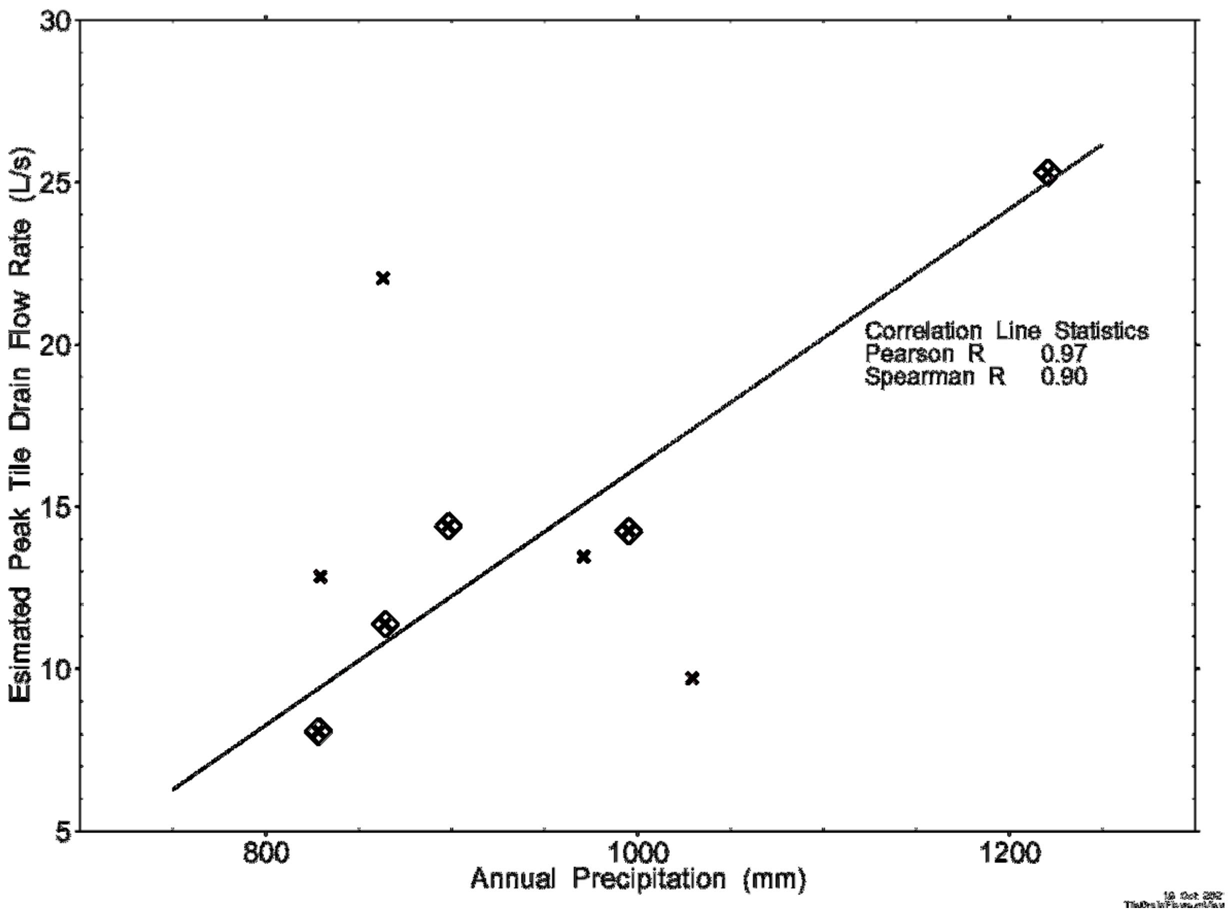

Peak flow estimates were then developed for 30 years using total annual precipitation and the correlation developed above. The steady-state average flow for each year is calculated by multiplying the normalized average for 2019 (0.32 both by arithmetic and integrated averages) by the estimated peak flow rate for the year.

Table C-1 provides the resulting estimates, and includes the measured data for years with measurements in June. There is a good correspondence between peak estimates and measured data, with the average difference between the peak and the measurement -1.3 L/s. Note the method may assume the measurement to occur slightly before or after the peak.

The average annual steady state value based on these estimates is 7.0 L/s ± 1.4. This compares to the arithmetic average of 7.5 L/s ± 4.1 for all dilution gauging tests between MH2 and the river, with those with potential test error removed.

Table C-1 Estimated Peak Tile Drain 1 Flow Rate and Average Annual Flow Rate for 30 years

Year	Annual Precipitation (mm)	Estimated Peak (L/s)	May/June Dilution Gauge Measurement (L/s)	Estimated Steady-State Average (L/s)
1994	789	7.8	-	5.2
1995	920	13.0	-	6.9
1996	943	14.0	-	7.2
1997	814	8.8	-	5.5
1998	909	12.6	-	6.7
1999	938	13.7	-	7.1
2000	897	12.1	-	6.6
2001	829	9.4	-	5.7
2002	782	7.6	-	5.1
2003	974	15.2	-	7.5
2004	801	8.3	-	5.4
2005	842	10.0	-	5.9
2006	1228	25.3	-	10.7
2007	962	14.7	-	7.4
2008	1081	19.4	-	8.9
2009	898	12.2	13.2	6.6
2010	828	9.4	7.8	5.7
2011	909	12.6	-	6.7
2012	851	10.3	-	6.0
2013	999	16.2	-	7.9
2014	885	11.6	-	6.4
2015	863	10.8	-	6.1
2016	971	15.1	-	7.5
2017	1221	25.0	24.0	10.7
2018	864	10.8	8.7	6.2
2019	995	16.0	13.3	7.8
2020	1029	17.4	-	8.2

Arcadis Canada Inc.

121 Granton Drive, Suite 12

Richmond Hill, ON L4B 3N4

Tel 905.764.9389

Arcadis.com